Title
Minimally Actuated Dynamic Climbing in the Sagittal Plane

Author
Birkmeyer, Paul Michael

Publication Date
2013

Peer reviewed|Thesis/dissertation

Minimally Actuated Dynamic Climbing in the Sagittal Plane

by

Paul Michael Birkmeyer

A dissertation submitted in partial satisfaction of the
requirements for the degree of
Doctor of Philosophy

in

Engineering - Electrical Engineering and Computer Sciences

in the

Graduate Division

of the

University of California, Berkeley

Committee in charge:

Professor Ronald S. Fearing, Chair
Professor Robert J. Full
Professor Pieter Abbeel

Spring 2013

Minimally Actuated Dynamic Climbing in the Sagittal Plane

Abstract

Minimally Actuated Dynamic Climbing in the Sagittal Plane

by

Paul Michael Birkmeyer

Doctor of Philosophy in Engineering - Electrical Engineering and Computer Sciences

University of California, Berkeley

Professor Ronald S. Fearing, Chair

This thesis explores the design of systems that can climb vertical surfaces with non-negligible dynamics in the sagittal plane. The development of a low-dimensional model addresses a lack of understanding of sagittal-plane dynamics during climbing in the space of reduced-order dynamic models of legged systems. Using a construction derived from the well-known and well-studied Spring-Loaded Inverted Pendulum (SLIP), we propose a two-legged system with both torsional and linear compliance driven by a position-controlled rotational actuator. Two simple foot models are considered to explore their effect on the dynamics and stability of the system. Results of the model indicate the existence of passively stable gaits during climbing as well as during inverted running and also suggest mechanical tuning parameters for physical climbing systems. A robotic platform capable of producing dynamic climbing behaviors is introduced. A reduced profile, sprawled posture, and improved internal mechanics allow the CLASH platform to be adapted to different climbing substrates. A passive claw engagement mechanism is proposed and tested with simulated steps to verify the design. With these mechanisms, CLASH becomes the first robotic platform capable of climbing loose cloth and climbs vertically at 15cm/s or 1.5 body-lengths per second. When climbing ferromagnetic surfaces, the system is capable of climbing at 1.8 body-lengths per second. To climb smooth, hard surfaces, a foot with a passively aligning ankle with a tendon-loaded gecko-inspired adhesive is designed and tested using simulated steps. With these engagement mechanisms, the system is able to climb at 1 body-length per second on acrylic with a 70° incline. A simple foot-impact model is created to explain the robot's inability to climb faster or up steeper inclines due to the sagittal-plane reaction forces created during rapid running.

To my two ladies, Alexis and Nina. And to any others that want to join our little clan.

Contents

List of Figures

List of Tables

Nomenclature

Symbols

Symbol	Description
$\mathbf{E_1} - \mathbf{E_2}$	Inertial coordinate frame
γ	Incline of surface relative to vertical ($\mathbf{E_2}$)
$\mathbf{e_1} - \mathbf{e_2}$	Coordinate frame at system center of mass rotated from $\mathbf{E_1} - \mathbf{E_2}$ by γ. $\mathbf{e_1}$ is normal to the surface and $\mathbf{e_2}$ is along the surface.
$\mathbf{r}$	Vector from origin of inertial coordinate frame to the center of mass
$\mathbf{p}$	Vector from origin of inertial coordinate frame to the foot in stance
$\mathbf{q}$	Vector from the foot in stance to the center of mass
$\mathbf{e}_\zeta$-$\mathbf{e}_\psi$	Coordinate frame at foot when in contact. $\mathbf{e}_\zeta$ is directed along the leg and $\mathbf{e}_\psi$ is orthogonal to the leg.
θ_i	Commanded rotational position of the i^{th} leg
$\dot{\theta}_i$	Commanded velocity of the i^{th} leg
$\theta_{release}$	Value of θ which dictates release of the controllable adhesive in CLASH
ψ	Angle from the surface to the leg, or from $\mathbf{p}$ to $\mathbf{q}$
$\mathbf{k}_\zeta$	Linear stiffness of Spring-Loaded Adhesive Pendulum model leg
$\mathbf{k}_\psi$	Torsional stiffness of Spring-Loaded Adhesive Pendulum model hip
$\mathbf{F}_\zeta$	Net force on the COM along leg, or along $\mathbf{e}_\zeta$
$\mathbf{F}_\psi$	Net force on the COM orthognal to the leg, or along $\mathbf{e}_\psi$
ζ_0	Nominal leg length
ζ	Instantaneous leg length
ϕ	Angle of foot retraction from surface
m	Body mass
$\mathbf{x} - \mathbf{y} - \mathbf{z}$	Coordinate frame defined on robots. X points in the anterior direction, y points to the left, and z points dorsally.

Acronyms and Abbreviations

Abbreviation	Description
CLASH	Climbing Autonomous Sprawled Hexapod
COM	Center of mass
CPG	Central pattern generator
CT-SLIP	Clock-Torqued Spring-Loaded Inverted Pendulum
DASH	Dynamic Autonomous Sprawled Hexapod
F-G	Full-Goldman
LLS	Lateral Leg Spring
LO	Lift-off
ODE	Ordinary differential equation
RCM	Remote center-of-motion
SCM	Smart Composite Microstructures
SLAP	Spring-Loaded Adhesive Pendulum
SLIP	Spring-Loaded Inverted Pendulum
TD	Touchdown

Acknowledgments

For all of his optimism, dedication, and guidance over the past six years, I want to first thank my advisor, Professor Ron Fearing. I am still amazed by his incredible ability to pull in ideas from disparate fields, bring them together in a few simple sketches and quickly get to the heart of any problem. He earns respect and credibility by spending his afternoons in the lab, and that makes one at least consider every crazy idea that comes out of all of the productive brainstorming sessions. I hope that will have the to privilege to work with him again in the future.

When I joined the lab, the incumbent graduate students displayed amazing patience and willingness to teach. Of all of the members of the lab, I would first like to thank Erik Steltz. He was always willing to take the time to give honest, sincere, thoughtful and selfless advice. The advice and mentorship I received from Erik has been and continues to be worth more to me than I can express here. Aaron Hoover taught me the ropes of SCM, helped me navigate some treacherous grad school waters, and never refused any of my nagging questions. Thanks for taking us to the jumping pillow that remains a highlight from my time in Boston. Stan Baek was always there to lighten the mood and his high jinks kept you on your toes, and I will always appreciate the game nights hosted by Bryan Schubert.

I would like to thank Professor Full for his always interesting and enlightening conversations about biology and helping to guide my career and research paths. His feedback on and vision for my work over the years has been truly invaluable, and my work has been better for it. I hope to stay in touch as career outside of grad school develops.

Thanks to Pieter Abbeel for his unhesitating willingness to be a part of my committee and to provide his input on this work and its applications beyond legged robots. I am also thankful that he has a good sense of humor as evidenced by his request for my t-shirt file rather than being upset by its existence.

I will miss the Biomimetic Millisystems Lab and all those with whom I currently share it. In addition to helping get our first papers out, getting through prelims, and working on more than one class together, Kevin Peterson and I learned ping pong the hard way at the hands of Erik, Aaron, Stan, and Jongho Lee. Andrew Gillies has been my sounding board for all things climbing, and without his willingness to and crank out experiments, I wouldn't be finishing now. Fernando Garcia Bermudez has been a great friend throughout my time at Berkeley, and he has always been willing to share his time, his knowledge, his opinion, and his code. And for those not mentioned explicitly, I have enjoyed all of our conversations and brainstorming sessions, and I hope you are more focused when cleaning your homes than you are when cleaning the lab.

Kaushik Jayaram, Jean-Michel Mongeau, Tom Libby, and Ardian Jusufi have all helped me to increase my understanding of how organisms work and how to construct studies to further that understanding. I am happy that I have been able to spend more time with Chen Li both on campus and the soccer pitch after he was so accommodating during my visit to Georgia Tech. I would like to thank Willi Mickelson for his support, understanding and constant positive attitude during his time at COINS for both my academic work and

personal life. Oren Milgrome has also been very helpful in creating amazingly complex pieces of hardware and still being able to get all of our public demos to work when at the last minute.

To Grey and PJ, your friendship has meant so much to Alexis and I over the years. I feel so fortunate to have met you both. I love the intelligent and funny conversations that we strike no matter how long it has been since we last were together. I am glad that we have at least a few more years where we can share this new phase in our lives together.

To the guys who convinced me to start a company while my wife was pregnant with our first child and I was trying to graduate, I owe you my sincere thanks. It is much easier including that previous sentence knowing now that I managed it all and will still graduate, but honestly I can't imagine a better group of guys to be doing this with.

My parents, Mike and Ann, my brother, Brian, and sister, Jenna, have been so important in supporting me at every step along the way leading up to this. Growing up with so much constant love and support gave me the confidence to take on such a challenge. And I am sure my mother would argue that all of the games we have played together were critical to my success. Jenna, thanks for reading and applying your sharp eye and unparalleled grammatical proficiency to this dissertation, and for supporting my use of hyphens. I think applying your edits was the first time I ever experienced happiness when revising a document like this. I would also like to thank my newest parents, Ron and Carole, for their unwavering support and valuable perspective in both our personal and professional lives.

And finally, I would like to thank my love Alexis with all of the gratitude these words can possibly contain. She has been my best friend and my most trusted advisor throughout these six years in graduate school and for the six years before that. Her efforts and sacrifices in the last four months have been beyond anything anyone could ask for, and without them I wouldn't be finishing now. She brought us our beautiful baby girl Nina, whose sweet smiles and disposition have been simultaneously distracting and fulfilling. I can't wait to see what little person is behind those sweet smiles.

Chapter 1

Introduction and Previous Work

The appeal of small, highly mobile robots is undeniable. Their size makes them easily transported, decreases the cost of individual units, and increases their mobility compared to larger units. The size of the systems allows them to navigate collapsed buildings or mines in the pursuit of survivors or to be used as real-time sensing platforms in dangerous remote-monitoring missions. The lowered cost enables large quantities of systems to be created and deployed to enable large-scale reconfigurable mobile sensor networks, the creation of groups of robots leveraging swarm algorithms, or the distribution as a tool for other academic research or education.

Never before has the potential for the development of these systems been so accessible. With consumer electronics driving down the size of sensors and processing units, increasing computational power, improving manufacturing of small-scale components, and refining sensor accuracy and precision, the advent of capable meso-scale robots seems imminent. Yet even equipped with the most advanced modern processors and sensing suites, the utility of a such a robot is limited without the ability to move in the world and physically interact with it.

For mobile robots, one of the most challenging interactions is trying to move quickly and efficiently through an unstructured environment. Traditionally, robots require many degrees of freedom to move through their environment with a satisfactory degree of confidence and stability. This, in turn, requires more actuators and sensors, as well as increased computational power and larger batteries to drive it all. To make robots on the order of 10 cm long, the challenge becomes how to generate high-performance locomotion given the significant space constraints which limit the number and size of onboard actuators, electronics, and batteries. As the scale of mobile robots decreases, the presence of obstacles which cannot simply be stepped over increases, driving the need to create systems capable of not only running but also climbing.

Although engineering is a significant challenge with small systems, there are reasons for decreasing the scale of mobile robots. Meso-scale robots can leverage physical scaling laws that control the interaction between forces acting on the system. Inertial forces scale with robot volume, or proportionally to L^3 where L is some characteristic dimension, while

surface forces like Van der Waal's, capillary and electrostatic forces go as L^2. Thus, the ratio of available adhesion, a surface force, to the weight is proportional to L^{-1}. By making a robotic platform smaller, the available adhesion should increase faster than the demands on the adhesive and make sustainable grasps more likely.

By looking to nature, we can see many examples of small systems capable of not only running stably over rough terrain at high velocities, but also climbing [3, 28, 42]. This climbing agility is one area in which animals have a significant advantage over their robotic counterparts. There are many terrestrial robots that are capable of traversing obstacles on the order of their own body height [8, 31, 58, 69], but anything larger than that often requires a system capable of climbing. While there are many robots capable of climbing, very few can climb as quickly and robustly as animals and even fewer can rapidly climb surfaces which are difficult to engage, and none can yet match the agility and adaptability of animals.

The challenge of creating robots that are as agile and elegant as biological organisms is extremely daunting. Animals such as the cockroach or gecko have dozens of degrees of freedom, refined sensing abilities, and highly-specialized morphologies that have evolved over millennia to produce gaits that are efficient, fast, and robust. However, work has been done to reduce the complexity of the roboticists' design problem by distilling the essence of animals' locomotion to reduced-order models. These simple yet elegant models are created to capture the fundamental mechanisms that produce the dynamics that we observe in the organisms. In general, these models reduce multilegged stance to a single, equivalent leg stance that embodies the stiffnesses and other properties of the legs.

Once these underlying mechanics are codified into these reduced-order models, the analysis of the models can inform the design of dynamic robots. Many robots have either been directly modeled after these reduced-order models [16, 17, 54], or the models have been heavily leveraged in the dynamic tuning of existing robots to improve dynamic performance [8, 21, 31, 37, 44, 69].

1.1 Previous Work

In the quest to create a minimally-actuated all-terrain robot that can rapidly climb surfaces, it is necessary to understand both the requisite dynamics for robust dynamic climbing as well as how to construct such a physical system. Because this work is influenced by and contributes to both of these areas, we first provide an overview of recent climbing robots followed by a summary of the work done in biological locomotion templates.

1.2 Mobile Robots

1.2.1 Modes of Engagement

To create a system capable of climbing vertical surfaces, not only must the system be able to perform work against gravity, but it must first be able to gain purchase on the climbing

surface to generate the forces required to perform that work. Given the long history of climbing robots, there are many examples of different engagement mechanisms that have been employed to climb different substrates.

Many engagement methods are inspired by the wide range of engagement modes exhibited by natural organisms. There are systems which use large engineered holds that find stable configurations using mass shifting similar to human rock climbers [11, 12]. Systems such as Spinybot [2, 43], RiSE [79], Mini-Whegs [18], and DROP [56] use claw mechanisms to grasp hard surfaces with small asperities. An omnidirectional microspine gripper was recently created that leverages the spine mechanisms of Spinybot and RiSE to create a robust, controllable grip on rough surfaces [60]. Other systems use penetration to achieve engagement [34, 64]. To grasp smooth surfaces, many robots use various forms of gecko-inspired adhesives. Stickybot [32, 45], Waalbot [59], and Geckobot [82] use soft elastomer adhesives to climb smooth surfaces.

When engineers do not consider only those mechanisms used by natural organisms, they are capable of devising creative engagement solutions. Often these solutions are reliable but can be restricted to specific classes of surfaces and require more power than the mechanisms derived from the biologically-inspired solutions. If navigating certain metals, magnetic attachments can be used [5, 35]. Suction cups [13, 68] and Bernoulli grippers [41] can also be used on relatively smooth surfaces, but the power requirements of such mechanisms is generally greater than passive mechanisms. A system which uses magnetorheological fluid to sustain shear and normal stress is capable of adhering to a range of surfaces [84]. Other robots use electrostatic adhesive technologies to generate the adhesion required for climbing [63, 86].

1.2.2 Dynamic Climbing Robots

Most of the systems described above are considered quasi-static climbers. In general, a system is considered to be running or climbing dynamically if the system exhibits either significant kinetic energy, loss of static stability during a stride, or both. While this definition is inexact, climbing systems that exhibit such behavior have been shown to exhibit increased climbing efficiency as well as robustness to perturbations not seen in quasi-static climbing systems [3, 54, 55, 65].

The first robot demonstrated to climb dynamically was DynoClimber [16]. Modeled after the Full-Goldman (F-G) template, as described in Section 1.3, Dynoclimber climbs using simple hooks that engage a carpeted wall. The robot provides a physical realization to support the stability claims derived from the analysis of the F-G model. Using a novel self-exciting control algorithm, DynoClimber is able to climb at 66 cm/s or 1.5 body-lengths/s [54] using one motor for each of two legs.

ROCR is another robot designed to climb carpeted vertical walls, but it leverages a massive swinging tail to climb in a novel manner [40]. A single motor swings the tail, enabling the robot to rotate about one foot and dynamically ascend the wall with high efficiency and high speed (15.7 cm/s, 0.34 body-lengths/s) [65]. RiSE v3 is capable of climbing vertical

telephone poles at speeds of 22 cm/s (0.33 body-lengths/s) using several clever design aspects including variable gear ratio cranks and variable leg-length linkages [34].

Other robots are designed to climb between vertical walls. DSAC and DTAR both climb by oscillating a mass side-to-side using a single actuator to create vertical climbing [20, 19]. DTAR is designed to climb vertical tubes and DSAC is designed to climb between two parallel vertical plates. Both robots require constant motion to ascend or even maintain vertical altitude. This is also true of ParkourBot, a system which bounces side-to-side between verticals using spring-loaded legs to ascend [21].

While all of these systems exhibit dynamic climbing gaits as defined at the beginning of this section, they are designed so that there is no actuation or dynamics in the sagittal plane. DTAR has some sagittal-plane dynamics, but as it is climbing in a symmetric tube, the system cannot fail by falling away from the surface [19]. The presence or effect of sagittal dynamics in RiSE v3 is unclear, though the system has eight actuators to achieve climbing on wooden poles [34].

1.3 Reduced-Order Models for Legged Locomotion

As an engineer looking to create a legged robot, the wealth of examples of highly mobile animals in the natural world from which to draw inspiration can be overwhelming. From basilisk lizards capable of running on the surface of water, to geckos capable of running up vertical glass or walking on inverted surfaces, to cockroaches and cheetahs that can run rapidly across horizontal surfaces, the range of behaviors and operating environments exhibited by natural organisms is immense. For the engineer, while these systems are inspiring in their performance, the systems themselves are impossible or impractical to recreate. The high-power density and sheer number of muscles and actuators used as well as the sensorimotor system which controls it are either impossible or infeasible to recreate synthetically. Thus, the challenge then becomes how to look past the range of morphologies, body sizes, and operating environments to understand the unifying principles which make these organisms so effective and efficient when running and climbing.

This distinction between bioinspiration and biomimicry is important, as bioinspiration removes the need to recreate the complexity of these systems which have evolved over millions of years. To this end, biologists have discovered locomotion dynamics that are common to a range of animals despite their incredibly different instantiations. This has led to better understanding of the efficiencies and improvements that have come as a result of millions of years of evolution. This knowledge can now be conferred to dynamic models, physical robotic systems, and even back to subsequent biological studies [25].

1.3.1 Rigid Inverted Pendulum Model

Before exploring existing climbing models, it is worth exploring the various models for horizontal surface locomotion. The simplest model that exists for horizontal ground loco-

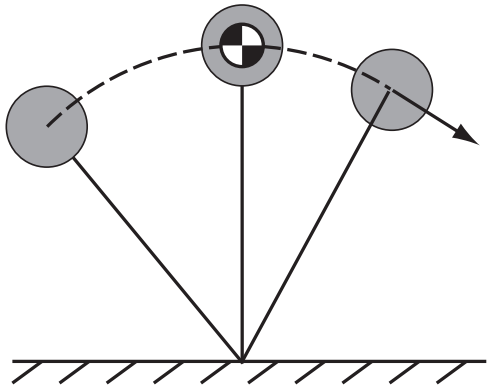

Figure 1.1: Rigid inverted pendulum model

motion is a rigid inverted pendulum model which addresses sagittal-plane dynamics [14]. Shown in Figure 1.1, the body is modeled as a point mass on top of a massless rigid leg with an ankle modeled as a pin joint. Kinetic energy is exchanged for potential energy during the first half of the stance, and returns to kinetic energy in the latter half. While the model doesn't describe key aspects of walking animal locomotion data, it has been leveraged with great success in several engineered systems, including passive-dynamic walkers [49].

1.3.2 The Spring-Loaded Inverted Pendulum (SLIP)

The SLIP model, shown in Figure 1.2, is an evolution of the rigid inverted pendulum model that explains sagittal-plane dynamics on a horizontal surface. Unlike the rigid inverted pendulum, it has been verified to model the sagittal-plane motions of a wide range of animals [9,23,36]. The addition of compliance creates the possibility of an aerial phase in addition to the stance phase. This creates a hybrid dynamical system in which the dynamics are defined by two distinct sets of differential equations, one for stance and one for the ballistic aerial phase determined by the legs touchdown (TD) and liftoff (LO) events. The stability of the SLIP model has been established by multiple analyses investigated using numerical methods and return maps [26, 27, 77]. This model has received much attention for its simplicity and dynamic properties in addition to its descriptive power and utility in informing the design of numerous running and hopping robots [1, 8, 15, 31, 37, 44].

1.3.3 Clock-Torqued SLIP (CT-SLIP)

A recent evolution of the SLIP model is the clock-torqued SLIP model [73]. Here, the SLIP model is modified to include a hip actuator with intra-stride control parameters as well as damped legs. These additions allow the model to explain the dynamic stability of a SLIP-like system over a wider range of relevant body parameters, including transitioning from rest to steady state. The inclusion of an actuator to the sagittal dynamics of the SLIP

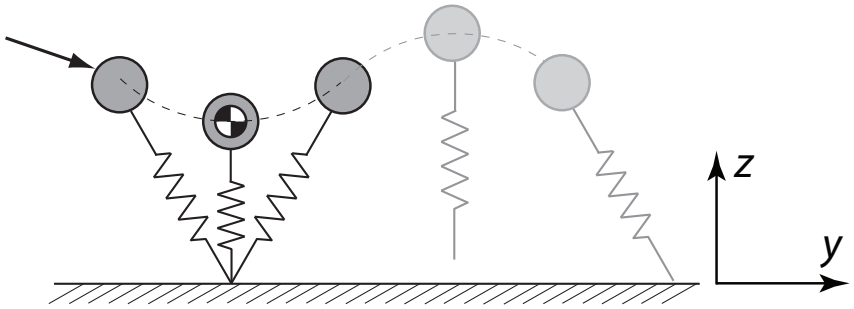

Figure 1.2: Spring-Loaded Inverted Pendulum model

model is a distinctive addition from previous work and one which is leveraged in the climbing model presented in Chapter 2. It is this actuator which enables the system to add energy into the system during locomotion - a necessity for climbing.

1.3.4 The Lateral Leg Spring (LLS)

Where the aforementioned models deal with sagittal-plane dynamics, animals exhibit significant lateral dynamics during locomotion that are not captured by the SLIP models [71, 72]. The LLS model addresses these horizontal plane dynamics through a construction shown in Figure 1.3. Here, the legs are oriented out from the body laterally, and the system bounces from side-to-side, planting one foot until liftoff then switching immediately to the opposite foot. Stability analysis reveals partial asymptotic stability. More recent work has incorporated yaw moments and an algorithm to control heading [51], as well as analyzing the stability of lateral dynamics on inclines using linear leg actuation [70].

1.3.5 Full-Goldman Model

The first template created to understand dynamic climbing, the Full-Goldman model considers the dynamics of a climbing system in the plane of the surface [3, 28]. Spurred by the similarity between the dynamics observed in geckos and cockroaches running on vertical surfaces, the F-G model was hypothesized as a template to capture the common dynamics in the plane of the surface. DynoClimber was modeled after the F-G template, providing a physical anchor that demonstrated that stability predicted by the F-G template is preserved when embodied in a physical system [16, 17].

The F-G model is the only previously-existing model to examine dynamic climbing stability, but it does not consider sagittal-plane dynamics that result from a non-planar system. To create a system that preserves horizontal locomotion performance gained from sagittal dynamics but gains the ability to climb quickly and robustly, the understanding of sagittal-plane dynamics while climbing needs to be improved.

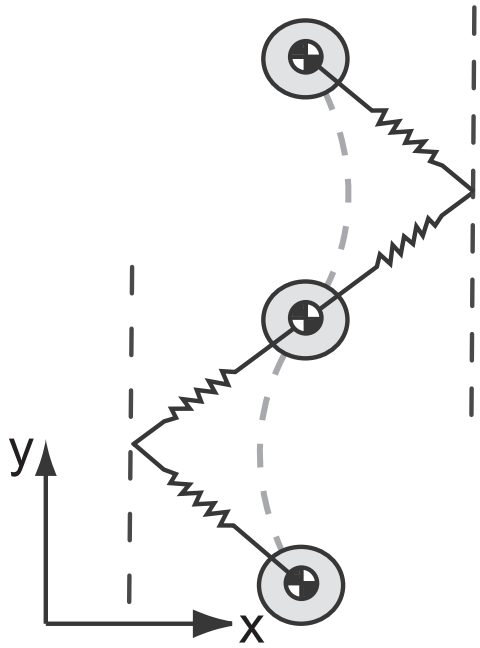

Figure 1.3: Lateral Leg Spring model

The goal of the work presented in this dissertation is to demonstrate both a theoretical and physical path toward high-performance climbing. To support the former, in Chapter 2 we present a new reduced-order model that is the first to address the dynamics and stability of a SLIP-like legged system on inclined, vertical, and inverted surfaces. We examine the ground reaction forces and COM dynamics of such a system, the loads required by the adhesives, and consider the system's stability to perturbations.

In Chapter 3 we present a robot transmission which serves as the foundation for rapid climbing of cloth and smooth hard surfaces in Chapters 4 and 5, respectively. In Chapter 4, we present a passive spine foot mechanism that is capable of sustaining tensile normal loads through a stroke but can easily disengage at the appropriate retraction angle. This allows the robot to climb loose and supported cloth at high speeds. In Chapter 5, we introduce a new leg and ankle design which allows for rapid passive engagement of a gecko-inspired adhesive to enable rapid climbing of near-vertical hard smooth surfaces. Appendix A shows the same robot platform adapted to rapidly climbing ferromagnetic surfaces. We summarize the contributions in Chapter 6 and suggest opportunities to further the understanding of sagittal-plane dynamics while climbing and develop more robust all-terrain robots.

1.4 Contributions

This work makes the following contributions:

- **Spring-Loaded Adhesive Pendulum - a reduced-order dynamic climbing model** - A simple model that predicts qualitatively similar dynamics to those seen in animals. Climbing performance is examined as a function of system parameters. System stability is analyzed and found to be stable over a range of speeds and stiffnesses. The model is also used to predict high-performance running on inverted surfaces. Two different adhesive foot models are used in the analysis.

- **CLASH - A lightweight, low-profile minimally-actuated climbing platform** - The design and kinematics of a lightweight, low-profile robotic platform driven by a single DC motor to produce a sprawled alternating tripod gait for climbing applications. The design improves body dynamics, mass distribution, and modularity to serve as the platform for subsequent climbing experiments.

- **Rapid vertical climbing of loose cloth** - The design and implementation of a robot capable of climbing loose vertical cloth. A passive claw-based engagement mechanism is presented, and experimental data of its performance are provided. The system is capable of climbing loose cloth at 1.5 body-lengths per second, making it one of the fastest climbing robots in existence.

- **Dynamic climbing of near-vertical hard surfaces** - The design and implementation of a remote-center-of-motion ankle and tendon foot design which enables dynamic climbing of near-vertical hard surfaces. Measurements of the foot performance are provided. The system can climb acrylic at 75 degrees above vertical and is the first to dynamically climb hard smooth surfaces. A simple dynamic impact model is introduced to improve understanding of performance limitations.

Chapter 2

Dynamic Climbing Model

To improve our understanding of dynamic climbing of a legged system, we developed the first low-dimensional model that provides insight into the challenges associated with sagittal-plane dynamics during climbing. The model presented in this chapter leverages a construction similar to that seen in SLIP and CT-SLIP, yet demonstrates ground reaction forces qualitatively similar to those observed in climbing geckos and cockroaches when rapidly climbing [3, 28]. The model provides the framework for analysis of basic requirements of adhesives for climbing, and also exhibits passive stabilization. The adhesive models generated for this model also allow for the first look at the dynamics required for running on an inverted surface. Two different foot models are considered. The first is modeled after the adhesives found in geckos and gecko-inspired synthetic adhesives [7, 29, 33, 50, 53, 61], and the second is defined to be a generalized controllable adhesive.

2.1 Spring-Loaded Adhesive Pendulum (SLAP) Model: Definition

The Spring-Loaded Adhesive Pendulum, or SLAP, model seen in Figure 2.1 consists of a two degree-of-freedom mass with two legs attached to a hip located at the COM of the body. As a result, the pitch angle of the system is not considered for this initial climbing model. More detailed models incorporating tails or multiple hips capable of producing moments are important to the complete understanding of dynamic climbing but should be considered once the dynamics of this simpler model are better understood. The system climbs a surface with angle γ from vertical. We assume that the legs and feet are massless, a practice that is well established in other legged dynamic models [9, 10, 28, 51, 70, 71, 72, 73]. This assumption is derived from the fact that individual leg masses in cockroaches represent less than 2% of the total system mass, but it has the added benefit of reducing the dimension of the model. Previous studies of rapidly-climbing cockroaches have suggested that the stance tripods of the animal can be well-represented by a single effective leg [23, 24], and this model follows the standard practice of approximating multiple-leg stances as one such effective

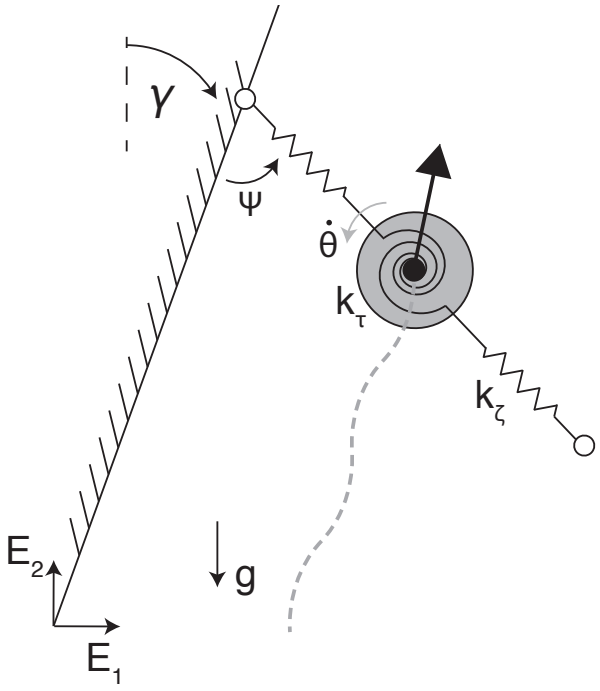

Figure 2.1: Diagram of Spring-Loaded Adhesive Pendulum model

leg [10, 16, 17, 71, 72, 73].

We define a global coordinate system, $\mathbf{E_1}$ and $\mathbf{E_2}$, to be fixed at the base of the climbing surface, and this is used to define the gravitational field. As seen in Figure 2.2, the COM position is defined by $\mathbf{r}$ in the inertial frame. A local coordinate frame, $\mathbf{e_1}$ and $\mathbf{e_2}$, is fixed at the COM of the system and is parallel with the climbing surface, which is rotated from $\mathbf{E_2}$ by angle γ. The $\mathbf{e_1}$-$\mathbf{e_2}$ frame is used to decompose fore-aft and normal phenomena. The $\mathbf{e}_{\zeta,\mathbf{i}}$-$\mathbf{e}_{\psi,\mathbf{i}}$ frame offers a convenient coordinate system for describing the linear and torsional forces that the system experiences due to the leg and hip forces for the i^{th} leg. The commanded position of the i^{th} leg is θ_i and is defined clockwise from $\mathbf{e_2}$.

A single cycle of a foot consists of a touchdown event (TD), stance phase, liftoff event (LO), and flight phase. The massless feet make contact with the surface without impact, and the foot acts as a frictionless pin joint during stance. Because the system must be able to generate normal forces that accelerate the system toward the surface, foot liftoff is not strictly defined as when the leg length reaches nominal length, as in SLIP and LLS [9, 71, 72]. Instead, the LO events are defined according to the engagement mechanism that the model uses, as explained in Section 2.3.

A rotational actuator is placed at the hip so that the model will be able to perform work to climb in the presence of gravity. While the CT-SLIP uses a proportional-derivative motor controller and a rigidly coupled leg [73], this model uses a functionally similar torsional spring in series with the output. For these studies, damping is not considered and the rotational

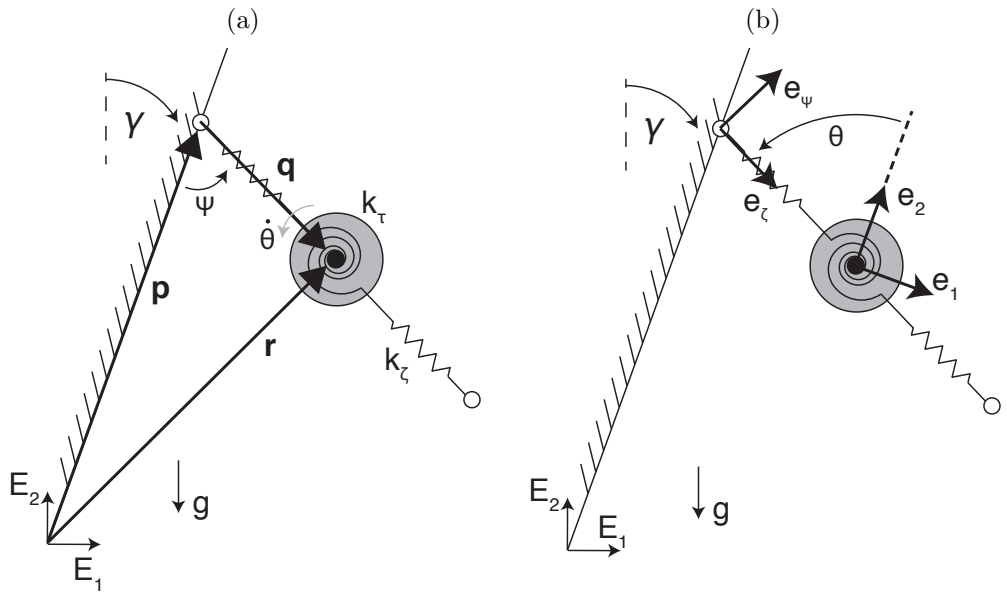

Figure 2.2: Notations used in the SLAP system.

Table 2.1: SLAP Parameter Definitions

k_ζ	Linear leg stiffness
k_τ	Torsional hip stiffness
$\dot{\theta}$	Rotational velocity
γ	Surface incline
ψ	Leg angle from surface
θ_i	Desired leg angle

speed is held constant throughout a single simulation, though future studies could implement the Buehler-clock controller used in the CT-SLIP model without fundamental modifications.

2.2 Body Dynamics

The change in dynamics associated with the transition of the system to stance and aerial phases results in a hybrid dynamical system with different states for foot one or foot two in stance, both in stance, or neither in stance. In all instances, the COM translations are given by Newton's second law:

$$\ddot{\mathbf{r}} = \sum_{i=1}^{2} \mathbf{F}_i - g\,\mathbf{E_2} \tag{2.1}$$

where $\mathbf{F}_i$ is the net ground reaction forces of the i^{th} foot and g is the gravitational constant.

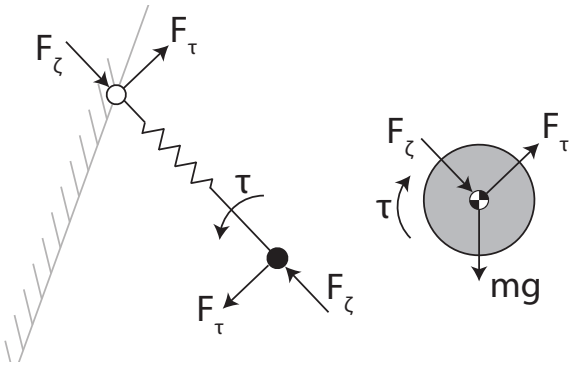

Figure 2.3: Free body diagram of the forces acting on the leg and the COM.

The free body diagram in Figure 2.3 shows the ground reaction forces on the COM when a single foot is in stance. The leg is assumed to be linearly compliant but torsionally rigid to decouple the linear and tangential components. The force $\mathbf{F}_\zeta$ along the foot-hip vector $\mathbf{e}_\zeta$ is created by a passive linear spring. $\mathbf{F}_\zeta$ is defined as

$$\mathbf{F}_\zeta = k_\zeta(\zeta_0 - \zeta) \cdot \mathbf{e}_\zeta \tag{2.2}$$

where k_ζ is the linear spring constant, ζ_0 is the nominal leg length, and the actual leg length ζ is defined as

$$\zeta = |\mathbf{q}| = \mathbf{r} \cdot \mathbf{e}_\zeta = \frac{\mathbf{r} \cdot \mathbf{e}_1}{\sin\psi} \tag{2.3}$$

where

$$\psi = \pi - \tan^{-1} \frac{\mathbf{r} \cdot \mathbf{e}_1}{(\mathbf{r} - \mathbf{q}) \cdot \mathbf{e}_2} \tag{2.4}$$

The force $\mathbf{F}_\tau$ created by the hip torque is tangential to the leg along $\mathbf{e}_\psi$. The torque is generated by a difference between the desired leg angle dictated by the actuator angle output at the hip and the actual angle created by the leg. The force on the COM resulting from the hip torque $\mathbf{F}_\tau$ is defined as

$$\mathbf{F}_\tau = \frac{\tau}{\zeta}\mathbf{e}_\psi = \frac{\tau}{\zeta}(\sin\psi\ \mathbf{e}_1 + \cos\psi\ \mathbf{e}_2) \tag{2.5}$$

where

$$\tau = k_\tau(\theta_i - \psi) \tag{2.6}$$

Thus, for a single foot in contact, the resultant force acting on the COM is defined as

$$\sum_{i=1}^{2}(\mathbf{F}_{\tau,i}\ \mathbf{e}_{\psi,i} + \mathbf{F}_{\zeta,i}\ \mathbf{e}_{\zeta,i}) - g\,\mathbf{E_2} \tag{2.7}$$

where $\mathbf{F}_i$ is zero if the i^{th} foot is not in contact.

(a) Frictional contact

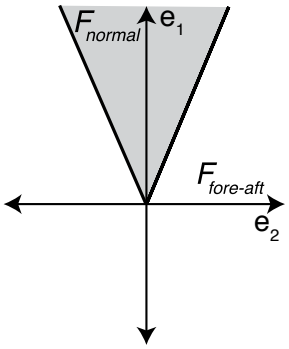

(b) Magnet with frictional contact

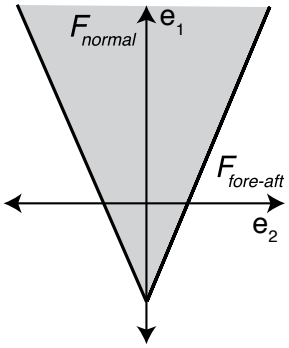

(c) Shear-induced gecko adhesive contact

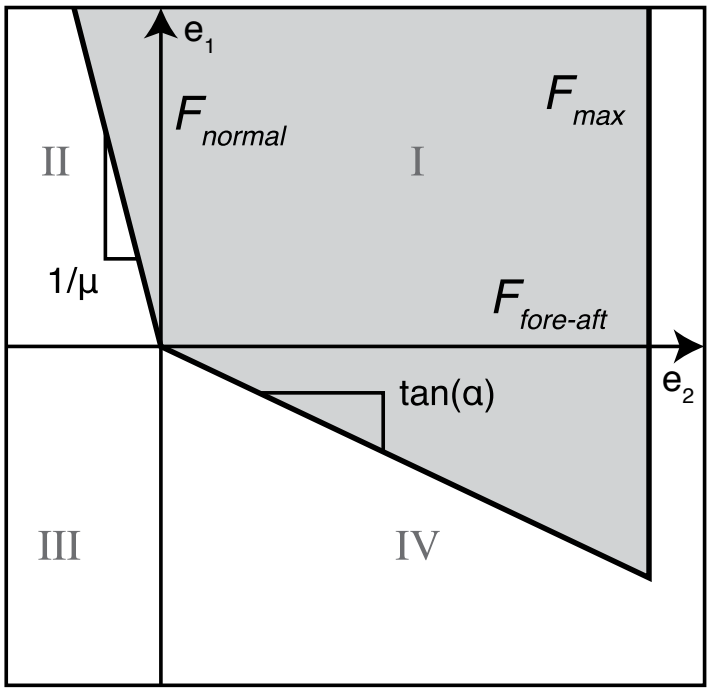

Figure 2.4: Comparison of stable regions for feet with frictional contacts (a), magnetic feet with frictional contacts (b), and the shear-induced adhesive foot model (c). The anisotropic gecko-inspired adhesive is capable of generating large shear forces and adhesive normal forces when pulling down and towards the rear of the system, but can generate only friction in the opposite direction. The maximum fore-aft force in quadrant I and IV is determined by the maximum shear stress of the material. Table 2.2 defines the limits in the four quadrants.

2.3 Foot Models

We propose two different foot models that enable the SLAP to climb inclined, vertical, and inverted surfaces. For both models, when the foot is engaged with the surface, they function identically - as a frictionless pin joint fixed to the wall. Also, TD is defined identically for both feet models as

$$\mathbf{r} \cdot \mathbf{e}_1 - \zeta_0 \sin\psi = \mathbf{r} \cdot \mathbf{e}_1 + \zeta_0 \cos\psi = 0 \tag{2.8}$$

Instead, it is the conditions that define LO from the surface for each foot that characterize and distinguish them.

One model, referred to as the force-based LO model, has a defined space of ground reaction forces possible that allow for stable grasping of the surface. If the ground reaction

Quadrant	Normal Force $\mathbf{F} \cdot \mathbf{e_1}$	Fore-Aft Force $\mathbf{F} \cdot \mathbf{e_2}$	**LO Condition**
III	< 0	< 0	Always
IV	< 0	> 0	$\mathbf{F} \cdot \mathbf{e_2} < -\tan\alpha\, \mathbf{F} \cdot \mathbf{e_1}$
II	> 0	< 0	$\mathbf{F} \cdot \mathbf{e_2} > \mu\, \mathbf{F} \cdot \mathbf{e_1}$
I	> 0	> 0	$\mathbf{F} \cdot \mathbf{e_2} > \mathbf{F}_{max}$

Table 2.2: Lift-off conditions for the gecko-inspired adhesive model.

forces required of the foot during stance ever leave the space of acceptable ground reaction forces, the adhesive fails and the foot releases from the surface. In particular, we consider the space of stable forces of a generalized gecko-inspired adhesive [7, 45, 52, 81], shown in Figure 2.4. Here, a positive fore-aft force ($\mathbf{F_i} \cdot \mathbf{e_2} > 0$) allows the adhesive to sustain a tensile normal force ($\mathbf{F_i} \cdot \mathbf{e_1} < 0$) that is linearly dependent upon the fore-aft force. A negative fore-aft force is only permitted in the presence of a compressive normal force, and here the limitation is that which is imposed by friction. Thus, if the ground reaction forces required by the foot ever leave the shaded region in Figure 2.4, the adhesive will fail and the foot will instantaneously return to the angle dictated by θ_i. Note that the failure mode in quadrant I and II is sliding rather than vertical liftoff, but that the model treats it similarly to liftoff. When the foot fails in quadrant III or IV, the foot lifts from the surface and goes to the commanded position given by θ_i instantaneously because the foot is massless. When the foot slides in quadrant I and II, the model assumes no kinetic friction and thus goes to the commanded position given by θ_i instantaneously as well. Also, the area of the foot is assumed to be such that maximum shear stress of the adhesive is never reached during stance. Given the forces exhibited by the SLAP model in Section 2.5 and the forces which the gecko-inspired adhesive in Chapter 5 is capable of sustaining, this assumption is justified. Table 2.2 summarizes the conditions for failure used for the gecko-inspired adhesive model. This model takes $\tan\alpha$ as an input, which in turn defines the maximum tensile normal load the adhesive can bear given a shear load before failing.

The second foot model considered is referred to as the clock-driven LO model. This model is a generalization of an adhesive that can be switched on and off by the system, such as an electrostatic adhesive [47, 63, 86] or a foot with the ability to generate internal forces that aid in grasping and releasing [45, 46]. For this work, we considered the switching event of the adhesive to be a function of the output angle of the rotational actuator θ_i rather than other conditions such as ψ_i or the COM motion. If the system is operating as one driven by a central pattern generator (CPG) [22, 48, 73], then having the control of the foot dictated by such a CPG suggests that control should rely upon the phase of the system, given here as θ_i. Further studies could incorporate additional control strategies to the CPG given such additional state feedback [39,67]. Using a clock-based LO, the foot releases the surface when the rotational hip input reaches the predefined angle ($\theta_i = \theta_{release}$), which is not necessarily equivalent to the actual angle of the leg due to the torsional hip.

Table 2.3: Properties of Model Robot

m, mass	$0.019\,kg$
ζ_0, Nominal Leg Length	$0.025\,m$
$\dot{\theta}$, Angular Velocity	$2\pi\{1-16\}\,radians/s$
k_ζ, Linear Stiffness	$18\frac{N}{m \cdot tripod}$
k_τ, Torsional Stiffness	$9 \cdot 10^{-2}\frac{N \cdot m}{radian \cdot tripod}$

2.4 Simulation Methods

The inclusion of hip actuation and gravitational force in the model breaks conservation of energy and angular momentum about the foot and makes analytical solutions to the dynamics of the system impractical. Therefore, numerical simulations are performed using the conventions described above within the MATLAB Simulink environment using the *ode45* Runge-Kutta solver with variable time steps.

The parameters given as inputs to the model include body mass m, uncompressed leg length ζ_0, linear leg stiffness k_ζ, torsional stiffness k_τ, initial displacement and velocity of COM along $\mathbf{e}_\zeta$, and initial fore-aft velocity along $\mathbf{e}_\psi$. For the gecko-inspired adhesive foot model, the maximum shear-to-normal ratio $\tan(\alpha)$ is given, and for the clock-driven release model, the rotational output angle at which the foot is released, $\theta_{release}$, is given.

The parameters used to test this system were based on the robot design featured in Chapter 4 and can be found in Table 2.3. Mass and uncompressed leg length remain constant through trials and are set as $m = 0.019$ kg and $\zeta_0 = 0.025$ m, respectively. While the mass and leg length are dependent upon the specific realizations of the design presented in Chapter 3, there are engineering constraints associated with building robots at the scale of this work that bind these relatively tightly and thus will not vary significantly from these values as the design changes. Rotational speeds $\dot{\theta}$ were varied from 1Hz up to 16 Hz, the maximum realizable with the physical system presented in Chapter 3. Torsional hip stiffness of the model robot was calculated using the measured leg deflection under static load of the robot when the leg is at mid-stance. Similarly, the linear stiffness was experimentally found at mid-stance. Because the system dynamics are expected to be sensitive to these stiffnesses, and because these stiffnesses are easily modified through variation of leg material or morphology, a wide range of stiffnesses were tested in numerical simulations. Unless otherwise noted, stiffnesses k_ζ and k_τ spanning three orders of magnitude and centered roughly at the values presented in Table 2.3 are used for the simulations. Unless otherwise noted, k_ζ from $0.1\frac{N}{m}$ per tripod up to $100\frac{N}{m}$ per tripod and k_τ from $0.005\frac{Nm}{radian}$ per tripod up to $5\frac{Nm}{radian}$ were used.

2.5 Results

The requirement of the feet models to generate tensile normal forces led us to create the two considered foot models which rely upon ground reaction forces or rotational output

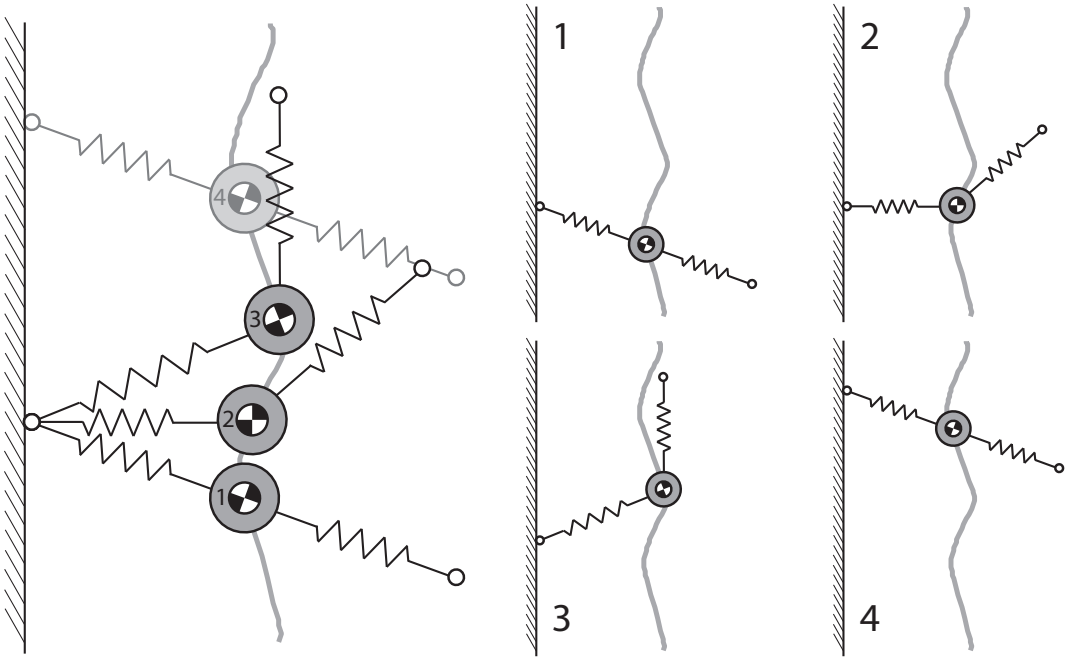

Figure 2.5: A stride of the SLAP model climbing a vertical surface ($\gamma = 0$). (1) The system at touchdown. (2) The system at mid-stance. The unloaded foot continues to follow the prescribed foot trajectory while the foot in stance deflects under load. (3) The system at liftoff. The loaded foot has continued to deflect during stance. (4) The system at the next touchdown. The system is in an aerial phase between (3) and (4).

angle position to define LO events. This differs from previous dynamical models that have LO when the ground reaction forces go to zero. While the inclusion of tensile forces was necessary to produce the desired climbing behavior, the breaking of symmetry that results was predicted to create quasi-periodic, chaotic gaits [30, 73]. As will be seen in this section, this was in fact the case. Although many gaits are practically stable in the sense that they reject perturbations to converge to some quasi-periodic behavior, finding fixed points of the system for a set of parameters that results in chaotic gaits is often impractical or impossible. Therefore, initial conditions are chosen based on fixed points for similar gaits that do converge. While this generates a conservative determination of which parameters yield stable gaits, it only fails to consider those parameters which are incapable of rejecting perturbations from their own steady state gait or those for which the chosen initial conditions lie outside of the basin of attraction for that system. To reduce the frequency of this latter occurrence, a range of initial conditions was tested for each parameter combination to determine if any resulted in successful climbing.

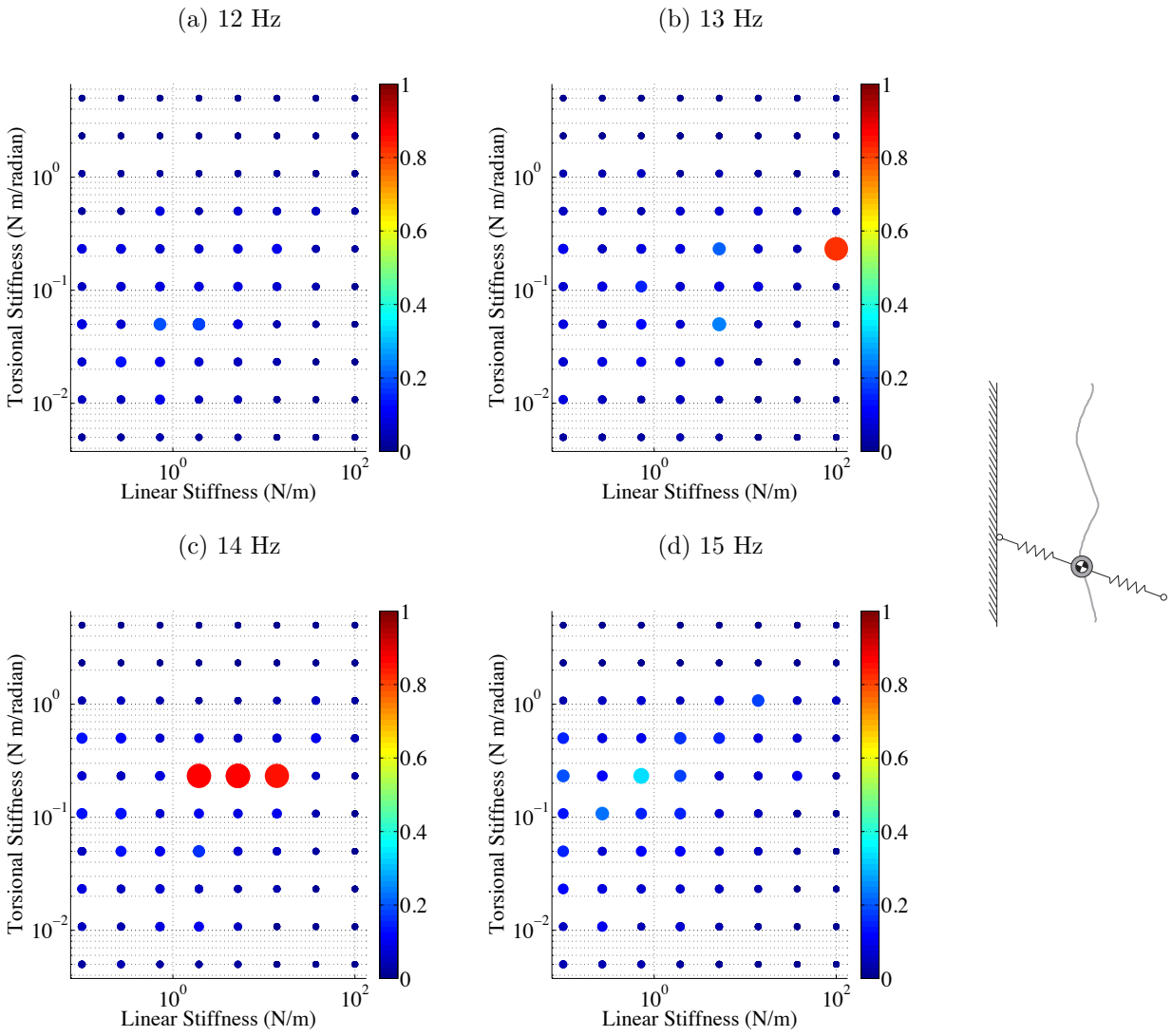

Figure 2.6: Normalized climbing speed of model on a vertical surface using the gecko-inspired adhesive model where $\tan\alpha = 0.4$. Successful climbing gaits were only observed for $\dot{\theta}$ above $2\pi \cdot 12 \frac{radian}{s}$. Velocities are normalized by the product of the angular velocity of the legs and the leg length. Larger, warmer dots indicate a faster normalized average climbing velocity. $\tan\alpha = 0.4$ yields few parameters which result in successful climbing.

2.6 Gecko-Inspired Foot Model

In this section, the SLAP model is simulated with the force-based release foot model configured to mimic the performance currently achievable by the gecko-inspired synthetic adhesive from [6], which can sustain an adhesive normal load of up to 0.4N in the presence of a shear load of 1N. Thus, for these trials, unless otherwise noted, $\tan\alpha = 0.4$.

An adhesive with $\tan\alpha = 0.4$ produces very few trials capable of rapidly climbing a vertical surface given the search methods outlined in Section 2.5. The average climbing velocity achieved for each configuration over a range of linear stiffness k_ζ, torsional stiffness k_τ, and angular velocities $\dot{\theta}$ on a vertical surface is presented in Figure 2.6. The velocity of the system is normalized to the maximum fore-aft leg velocity during the stride, $\dot{\theta} \cdot \zeta_0$. The larger, warmer-colored dots indicate successful parameter combinations that create gaits with fore-aft velocities approaching $\dot{\theta} \cdot \zeta_0$. The small, cooler dots are typically gaits that fail by falling off of the climbing surface or having the COM hit the surface. Leg frequencies from 1Hz to 16Hz were considered, but only the higher frequencies shown in Figure 2.6 resulted in stable gaits.

As previously mentioned, gaits of the SLAP model can be practically stable but exhibit chaotic behavior. To demonstrate this, we define the stride-to-stride Poincaré return map $\mathbf{P}$ which evolves the system from the one leg touchdown until the next touchdown of the same leg. The return map $\mathbf{P}$ effectively fixes one dimension of the system, allowing the system state to be entirely described by the system fore-aft velocity, normal velocity, and the leg angle at TD. By examining the intersection of the system state with this section, we can observe the evolution of the state at TD as shown in Figure 2.7. Here, $k_\zeta = 1.9307\frac{N}{m}$, $k_\tau = 0.2321\frac{Nm}{radian}$, and $\dot{\theta} = 2\pi \cdot 14\frac{radian}{s}$. Over a 20-second simulation and 300 TD events, the system exhibits an initial transients but doesn't converge to a fixed point, instead behaving as a chaotic attractor.

Despite a prevalence of chaotic attractors, there are still system parameters which exhibit convergent, stable gaits. When k_ζ is changed from $1.9307\frac{N}{m}$ to $5.1795\frac{N}{m}$, the system converges to a period-1 gait as shown in Figure 2.8. In this case, the stability of system is amenable to the well-established practice of finding the Jacobian of the Poincaré map from which the eigenvalues can then be computed [20, 51, 57, 72, 73]. The rate of convergence can be found by considering the magnitude of the maximum eigenvalue as this is associated with the eigenvector which will be slowest to converge in the system.

For the system presented in Figure 2.8, the fixed point of the system is found numerically by allowing the system to evolve until the intersection of the state evolution with the Poincaré section are within 0.1% of each other for four consecutive intersections. The average of the final four states is then used as the fixed point of the system around which $\mathbf{P}$ is linearized. The normal velocity, fore-aft velocity, and the angle of the leg at TD are individually perturbed by 2% of the fixed point values. The resultant evolution of the state to each perturbation is then used to compute the Jacobian of the return map about the fixed point. The eigenvalues of the linearized map $\mathbf{DP}$ are approximated by finite-differencing methods similar to those seen in [74, 75, 76]. For this parameter set, the maximum eigenvalue $|\lambda_{max}|$ is numerically found to be 0.1872, well under the $|\lambda_{max}| \geq 1$ threshold which indicates an unstable fixed point.

Examining high-speed gaits shows a smooth, undulatory COM translation as seen in Figure 2.9. Here, the system exhibits a transient due to an initial condition perturbed from the fixed point, similar to that used in the computation of the eigenvalues of the linearized

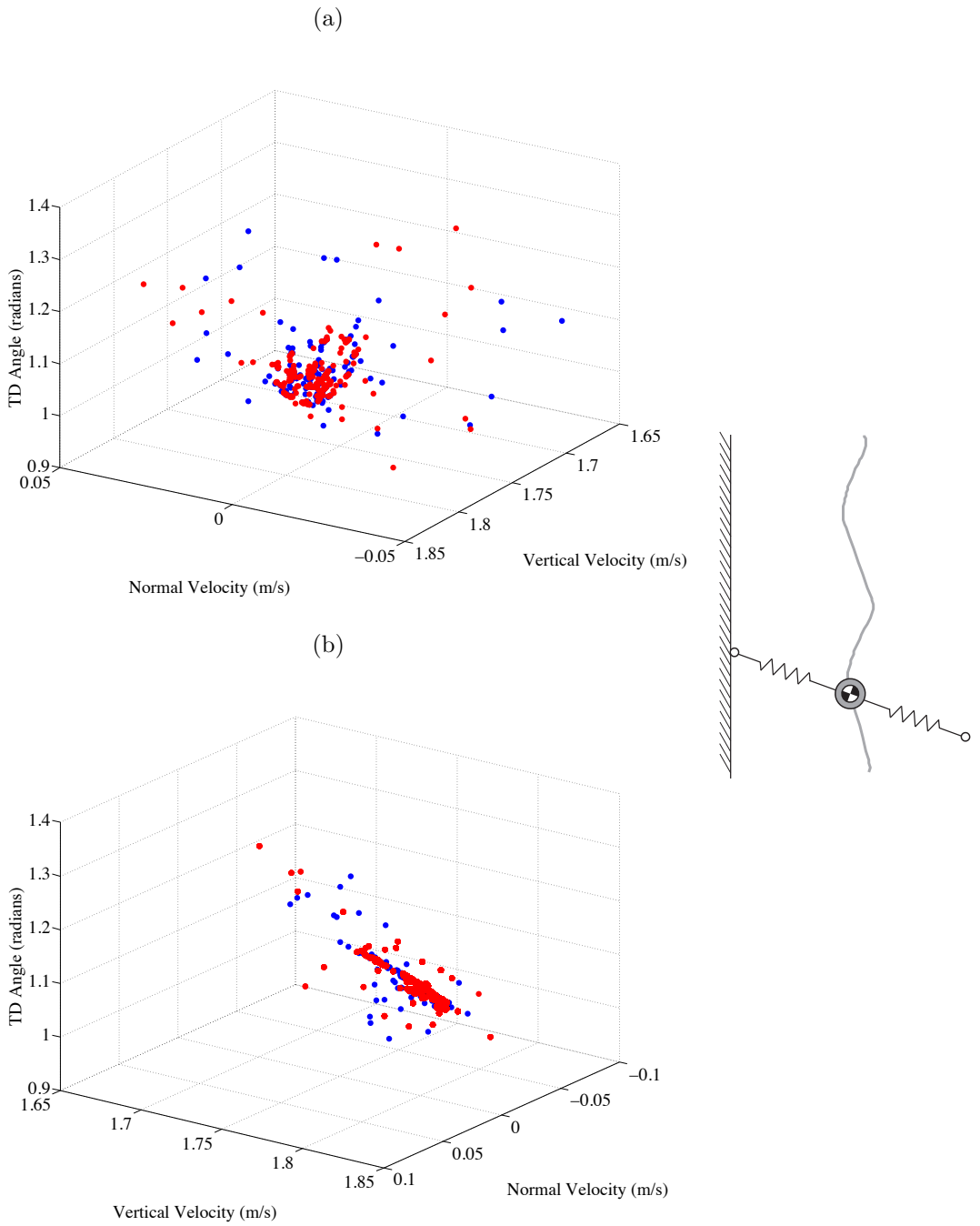

Figure 2.7: System state at TD events on a vertical surface with the gecko-inspired adhesive model exhibiting a chaotic attractor. The axes are chosen to be the TD leg angle ψ, the normal velocity at TD, and the fore-aft velocity at TD as the system dynamics at TD are fully defined by these values. (a) and (b) show two perspectives of the chaotic attractor whose states remain in a roughly planar space of states in the TD state space. Red dots indicate the state at TD of foot one, and blue dots indicate foot two.

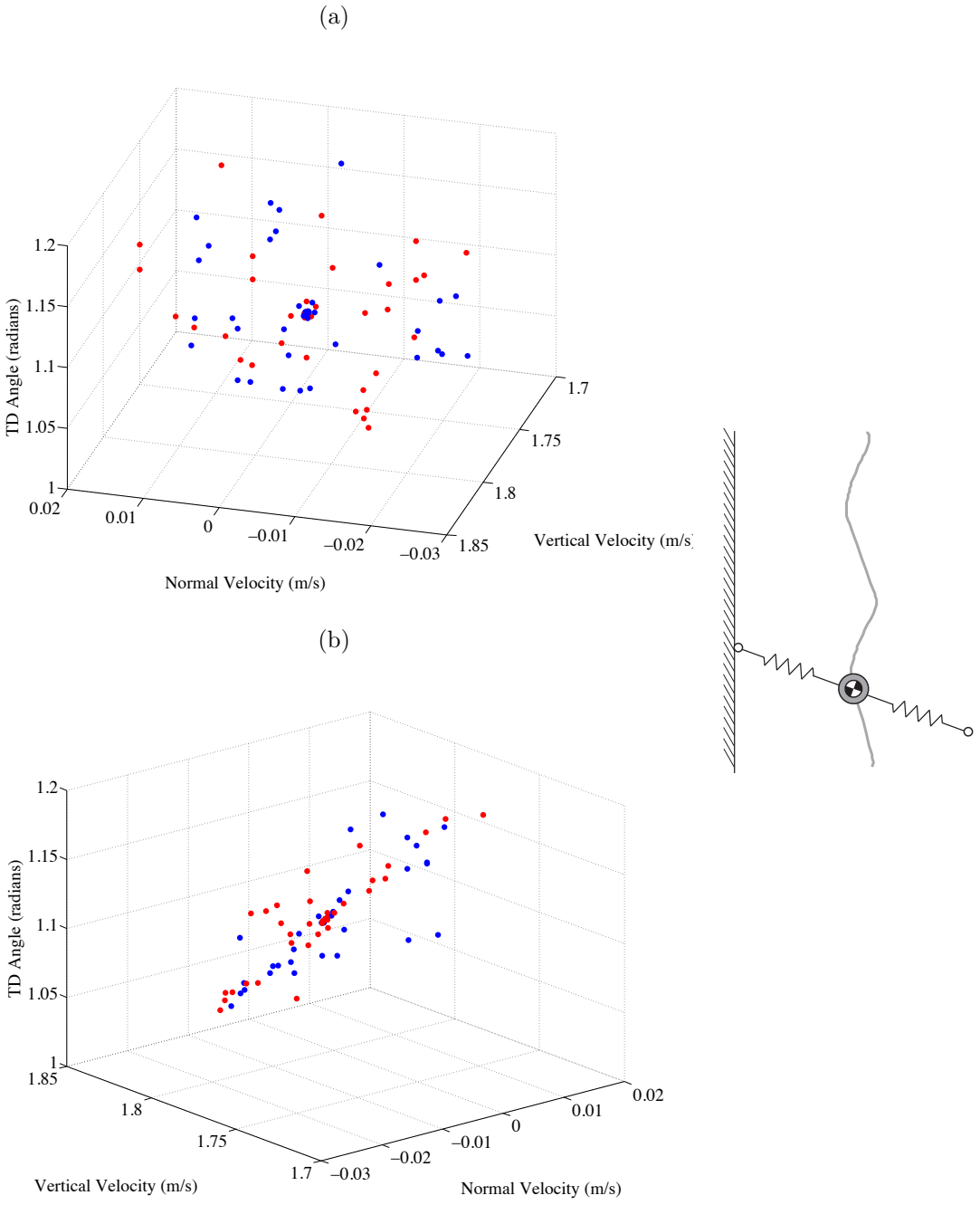

Figure 2.8: System states at TD events on a vertical surface with the gecko-inspired adhesive model which demonstrates convergence to a periodic gait. Unlike the gait shown in Figure 2.7, this gait converges to a fixed point in the space of states at TD. (a) and (b) show two perspectives of the states at TD to better convergence. Red dots indicate the state at TD of foot one, and blue dots indicate foot two.

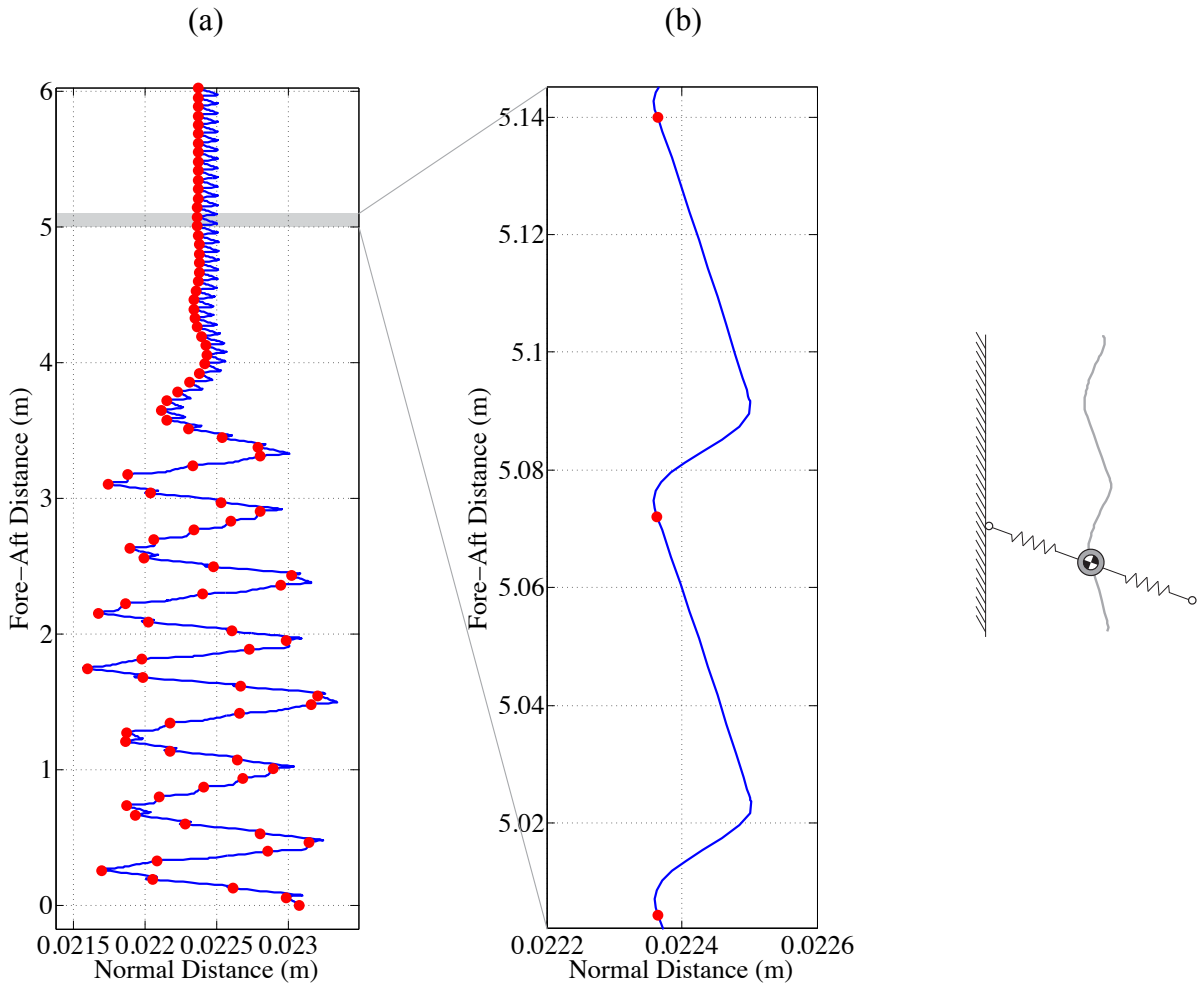

Figure 2.9: The COM translation of the system on a vertical surface ($\gamma = 0$) with the gecko-inspired adhesive foot model. The normal axis is magnified to better show normal motion. (a) Initial conditions produce a significant transient in the COM that stabilizes. (b) A closer look at the the COM translation of the system. Red dots show the state of the system at TD events.

Poincaré map. Figure 2.10 shows the ground reaction forces that this gait produces. In this stable gait, the TD initiates a compressive force away from the wall while the leg produces a positive, forward fore-aft force. The fore-aft force saturates before mid-stance, but the normal forces become tensile and accelerate the body back towards the wall. When the leg is behind the hip, the normal load on the adhesive exceeds the available adhesion and causes disengagement of the adhesive.

We note that the shape of the ground reaction forces here are qualitatively similar to those

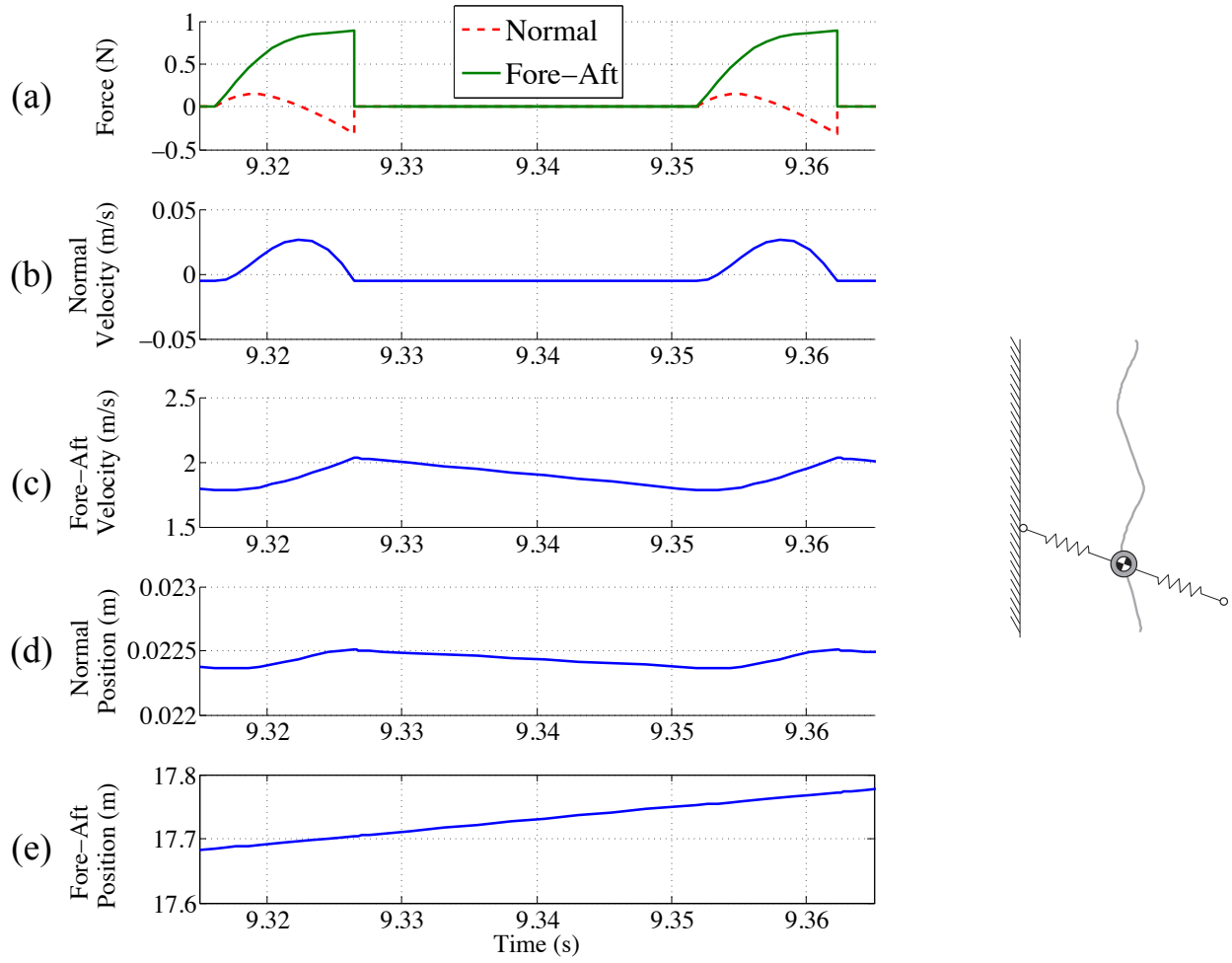

Figure 2.10: The ground reaction forces (a), normal and fore-aft velocities (b, c), and normal and fore-aft positions (d, e) of the model using the gecko-inspired adhesive climbing a vertical surface. (a) Fore-aft forces are green and normal forces are red. Negative normal forces indicate pulling towards the surface. The rapid fall in forces is due to overloading of the adhesive which results in the foot releasing the surface. (b) shows that the system is traveling towards the wall at TD. (c) shows fore-aft deceleration during flight.

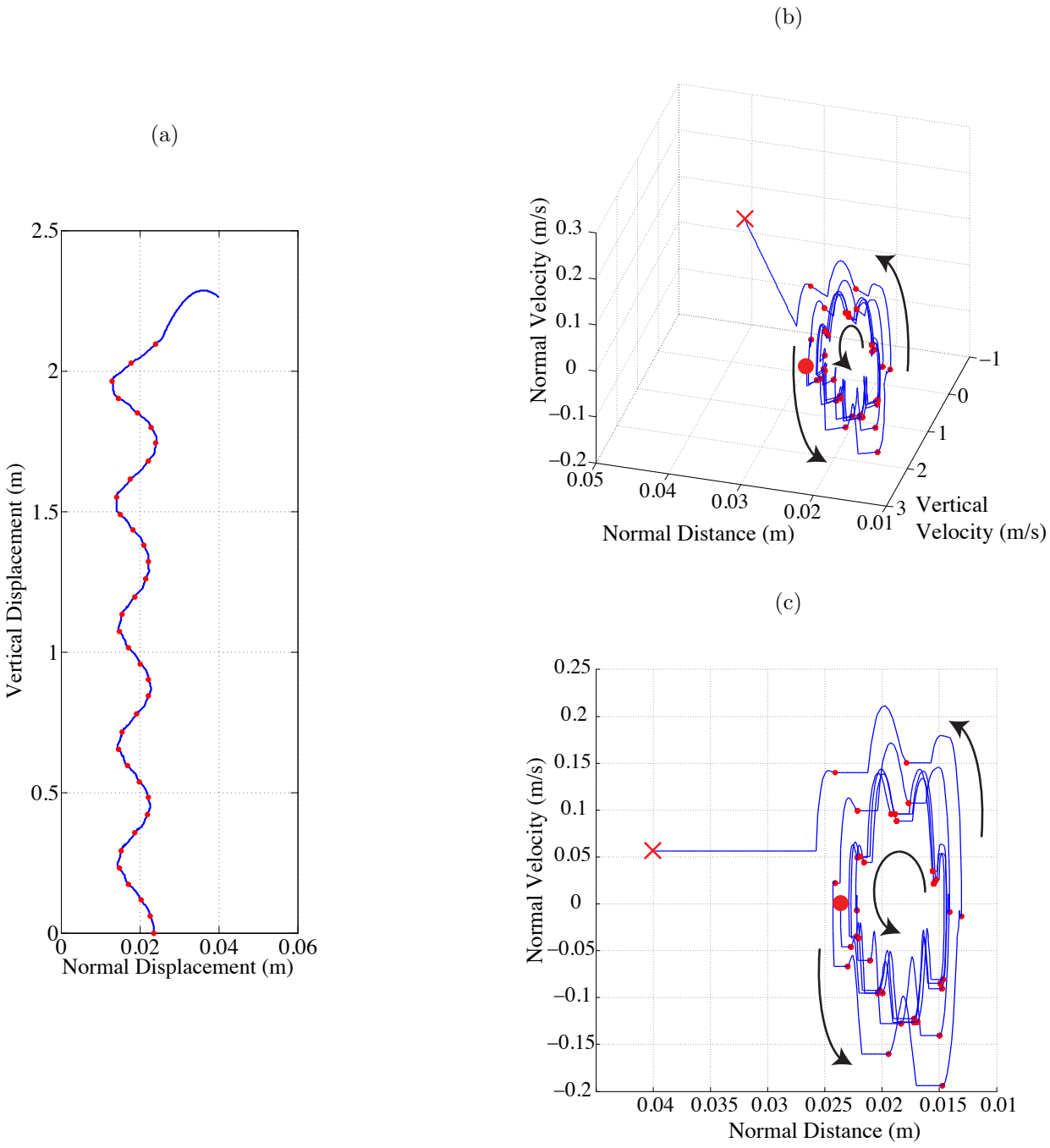

Figure 2.11: (a) The COM of the system from a failed vertical climb. The simulation stops when it determines the system has failed irrecoverably. (b) The state evolution of failed climb. Small red dots mark TD events as in (a). The state starts at the large red dot and continues along the path until the red cross when the simulation stops due to failure. (c) The normal velocity and normal displacement at touchdown shows the unstable nature of the gait.

observed in rapidly climbing geckos [3]. The fore-aft force is always positive, accelerating the COM upward during stance. Before mid-stance, both the fore-aft force of the model and the gecko saturate before dropping to zero. The normal force has twice the frequency of the fore-aft force and begins by accelerating the system away from the surface. In the latter half of the stride, the ground reaction forces accelerate the system back toward the surface. Several limitations in the model, as discussed in Section 2.8, create a duty factor significantly lower than measured in the organism. This, in turn, requires a larger shear force relative to the system body weight. The model is also less elegant than the organisms, generating significantly larger normal forces during stance.

Trials that fail often do so in a manner similar to that in Figure 2.11. In this plot of the state at TD, the system appears to settle from its initial condition toward an attractor similar to that seen in Figure 2.7 or Figure 2.8. Note that the plot in Figure 2.11 uses normal distance rather than leg angle at TD to improve visualization. Rather than settling to a stable point or into a chaotic attractor as in those examples, the system behaves as a saddle point and becomes unstable after the initial transient. The rotational input creates an unstable growth of normal kinetic energy at touchdown over time. There is an exchange of normal velocity at touchdown with normal distance from the surface at a frequency slower than the leg frequency. Eventually the velocity of the system away from the surface is such that a single stance cannot accelerate it back to the surface, causing the system to fail.

If we allow the gecko adhesive to have a value of $\tan\alpha > 0.4$, then the space of stiffnesses k_ζ and k_τ and angular velocity $\dot{\theta}$ that result in successful climbs increases significantly. Figure 2.12 demonstrates the effect of increasing $\tan\alpha$ to 0.5, 0.6, and 0.7. The ground reaction forces and stability of these systems are largely the same as those shown above for $\tan\alpha = 0.4$. It is not an unreasonable to assume these adhesive properties are possible, as there exist gecko-inspired adhesive feet capable of achieving shear-to-normal ratios of nearly 1:0.6 [32] and geckos themselves exhibit a ratio of 1:1 [4].

Relaxing the adhesive load required for climbing by using an incline of $\gamma = -5°$ as seen in Figure 2.13g resulted in significantly more stable gaits for $\tan\alpha = 0.4$. Figure 2.13 shows the climbing performance of the system when tested over a range of running frequencies $\dot{\theta}$, linear stiffnesses k_ζ, and torsional stiffnesses k_τ. The velocity of the system is normalized to the maximum fore-aft leg velocity during the stride, $\dot{\theta}\cdot\zeta_0$. Viewed in this manner, one can see that the performance improves nonlinearly with running frequency, performing significantly worse at slower frequencies and quickly saturating at a normalized velocity around 0.8 at higher rotational velocities.

Examining high-speed gaits on this incline shows a smooth, undulatory COM translation as seen in Figure 2.14. Figure 2.15 shows the ground reaction forces that this gait produces. While these forces are very similar to those shown in Figure 2.10, this gait is highlighted because of the interesting behavior at the end of the stroke when the normal load causes the adhesive to disengage. Because of the assumption that the foot is massless, the foot then 'bounces' and instantaneously moves to the position dictated by the rotational output θ, creating a sort of stick-slip behavior. In Figure 2.15, this actually causes the foot to re-engage the surface although the leg is then loaded in compression rather than tension.

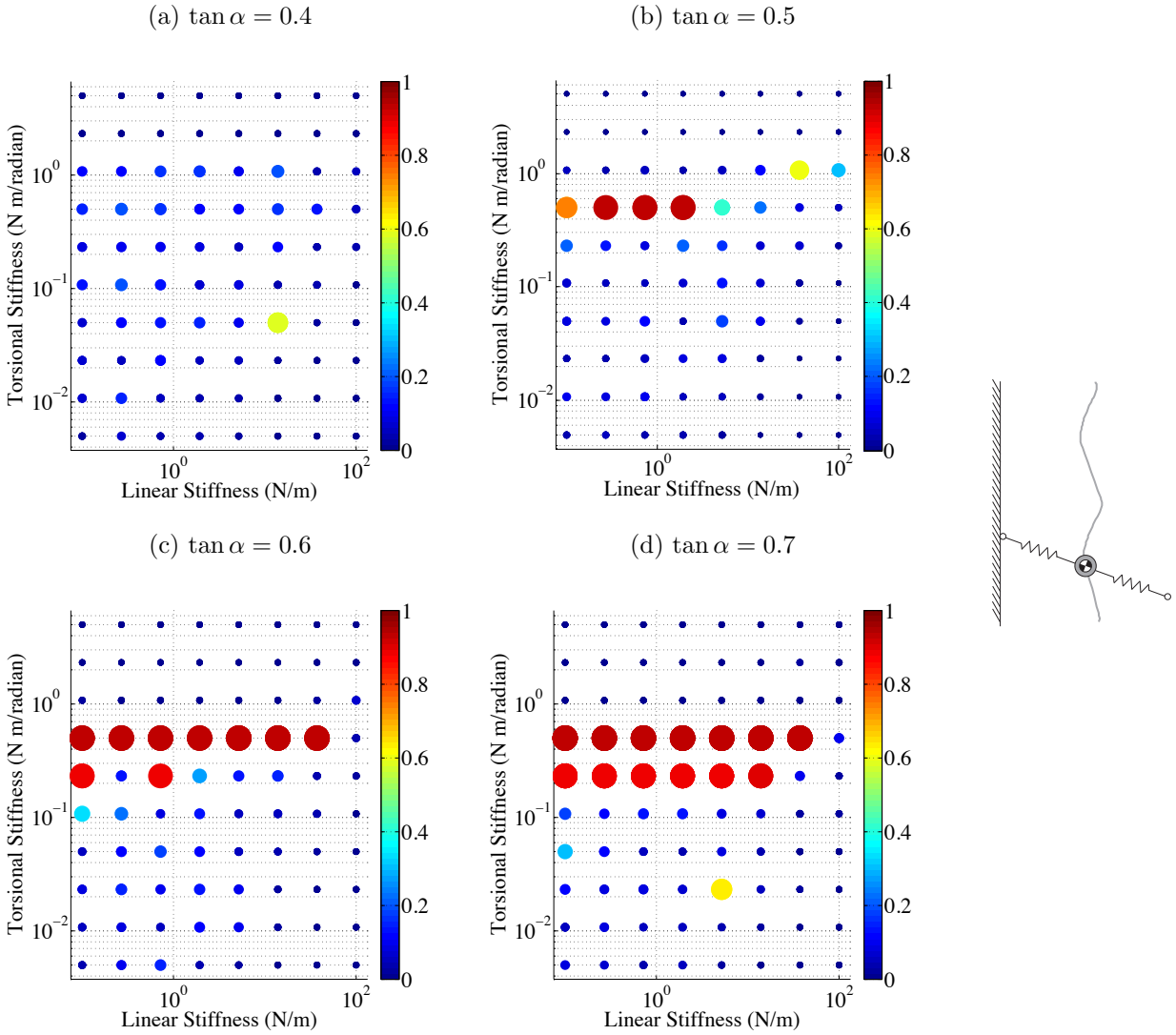

Figure 2.12: A comparison of the performance of the SLAP model on a vertical surface as the shear-to-normal ratio defined by $\tan\alpha$ is increased for $\dot{\theta}$. Velocities are normalized by the product of the angular velocity of the legs and the leg length. Larger, warmer dots indicate a faster normalized average climbing velocity.

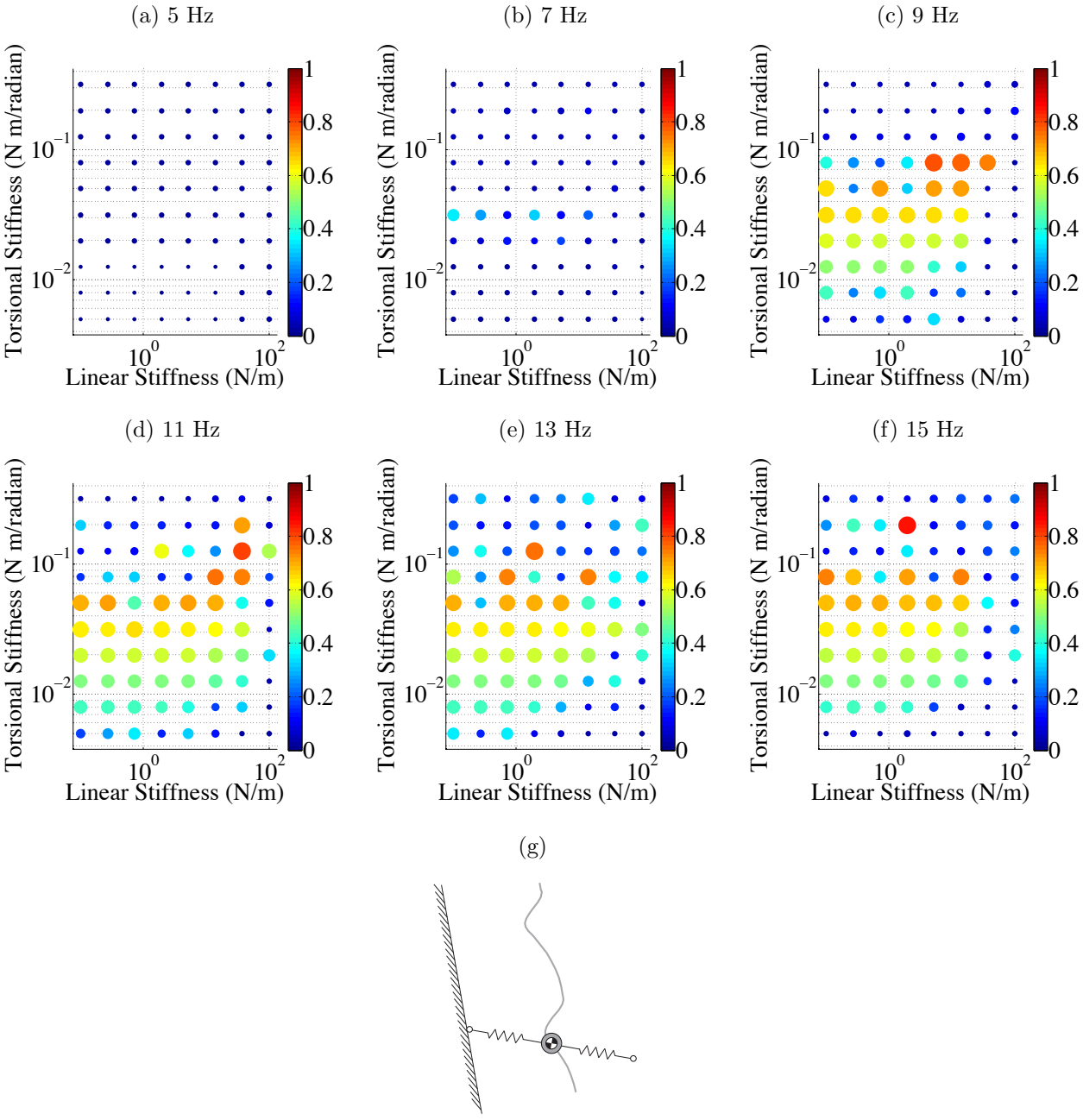

Figure 2.13: Normalized climbing speed of model on 85 degree incline with a gecko-inspired adhesive with properties similar to that used in Chapter 5. Velocities are normalized by the product of the angular velocity of the legs and the leg length. Larger, warmer dots indicate a faster normalized average climbing velocity.

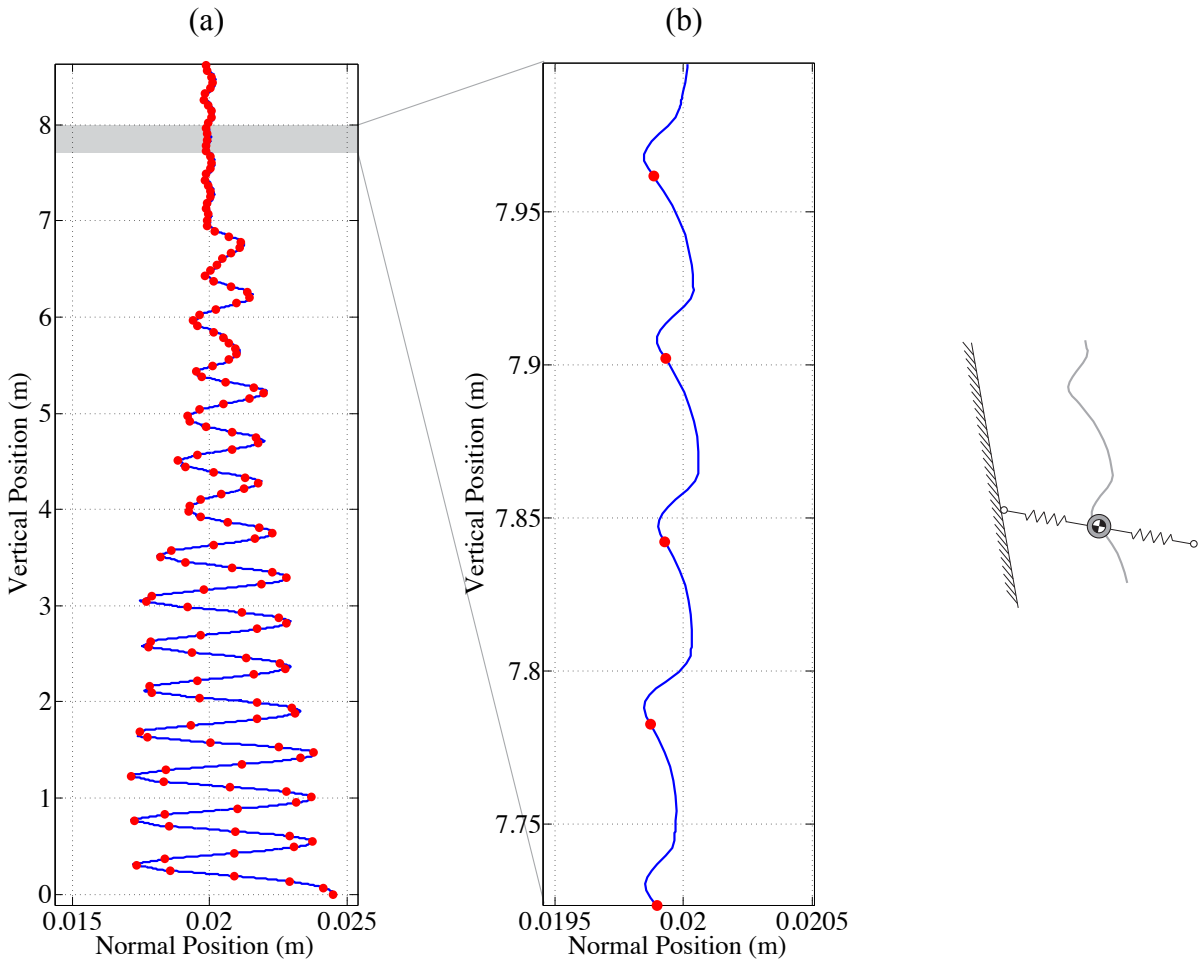

Figure 2.14: The COM translation of the system on a $\gamma = -5°$ surface with the gecko-inspired adhesive foot model. The normal axis is magnified to better show normal motion. (a) Initial conditions produce a significant transient in the COM that stabilizes. (b) Shows a closer view of the COM translations. Red dots show the state of the system at TD events.

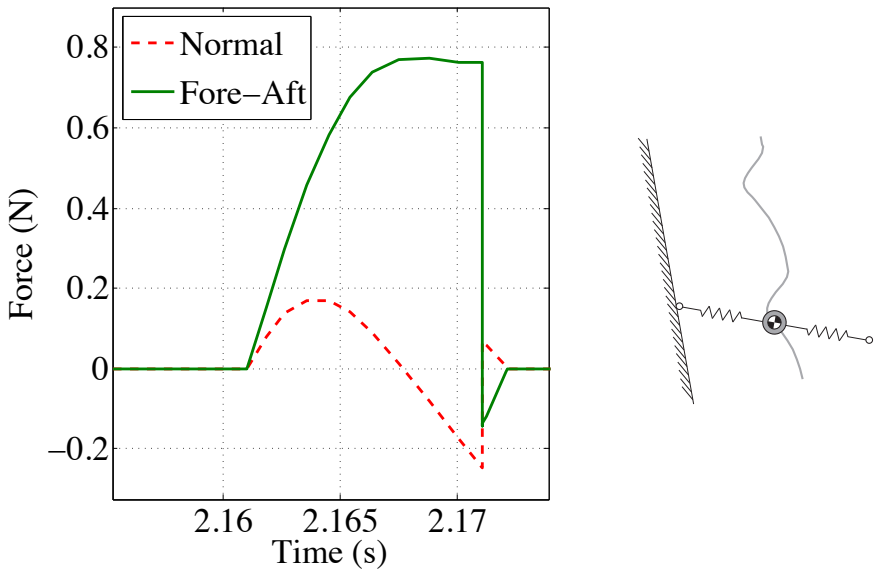

Figure 2.15: The ground reaction forces of the model using the gecko-inspired adhesive as the foot contact climbing an 85-degree surface. Fore-aft forces are green and normal forces are red. Negative normal forces indicate pulling towards the surface. The rapid fall in forces is due to overloading of the adhesive which results in a slip. The forces after the rapid drop in forces are compressive when the foot re-engages with the surface after the slip.

2.7 Phase-Based Release Foot Model

The results in this section feature the SLAP model using the clock-driven release foot model. This foot model makes the assumption that the foot is firmly attached to the surface until the system releases the foot instantaneously. The performance, dynamics, and stability of the system are explored over the range of linear and torsional stiffnesses presented in Section 2.6. The model is also tested on an inverted surface to determine what parameters yield high-speed inverted running and to explore the dynamics and stability that result from this locomotion mode.

2.7.1 Vertical Climbing

Figure 2.16 shows dependence of climbing performance upon the model parameters. Because multiple release angles were tested for each combination of k_ζ, k_τ, and $\dot{\theta}$, each data point represents the best climbing trial across four different release angles: $\theta_{release} = \{\frac{3\pi}{4} - \frac{\pi}{10}, \frac{3\pi}{4}, \frac{3\pi}{4} + \frac{\pi}{10}, \frac{3\pi}{4} + \frac{\pi}{5}\}$. As with the SLAP model with the gecko-inspired adhesive foot properties, high-speed dynamic climbing requires a minimum rotational velocity $\dot{\theta}$. Similarly, the space of leg stiffnesses that yield stable climbing gaits increases as the driving frequency

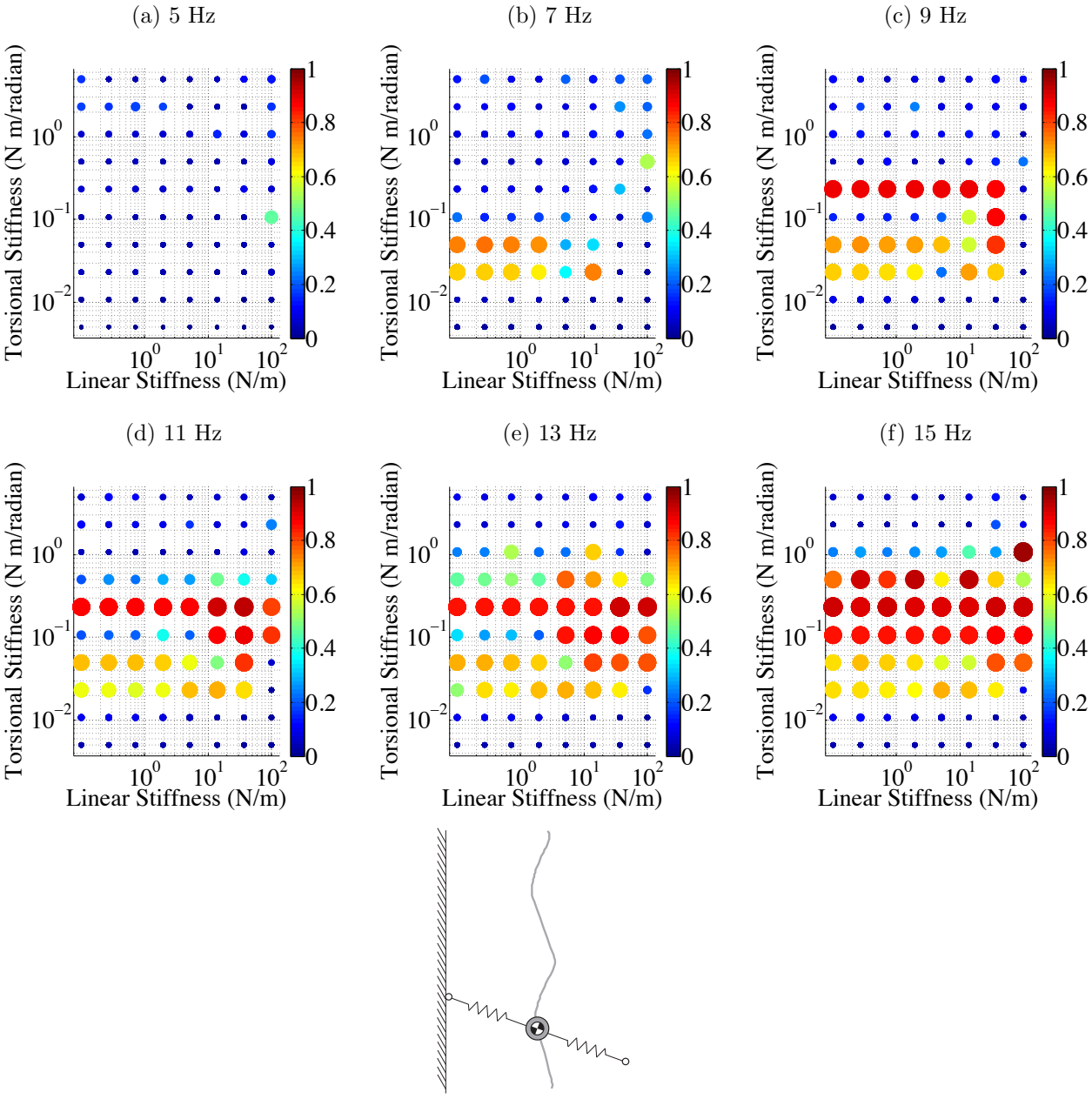

Figure 2.16: Normalized climbing speed on a vertical surface with the controllable phase-release adhesive versus leg frequency. Velocities are normalized by the product of the angular velocity of the legs and the leg length. Larger, warmer dots indicate a faster normalized average climbing velocity. The space of torsional stiffnesses k_τ that yield successful runs covers almost a full order of magnitude at higher frequencies. The sensitivity to linear stiffness is much lower than the sensitivity to the torsional stiffness.

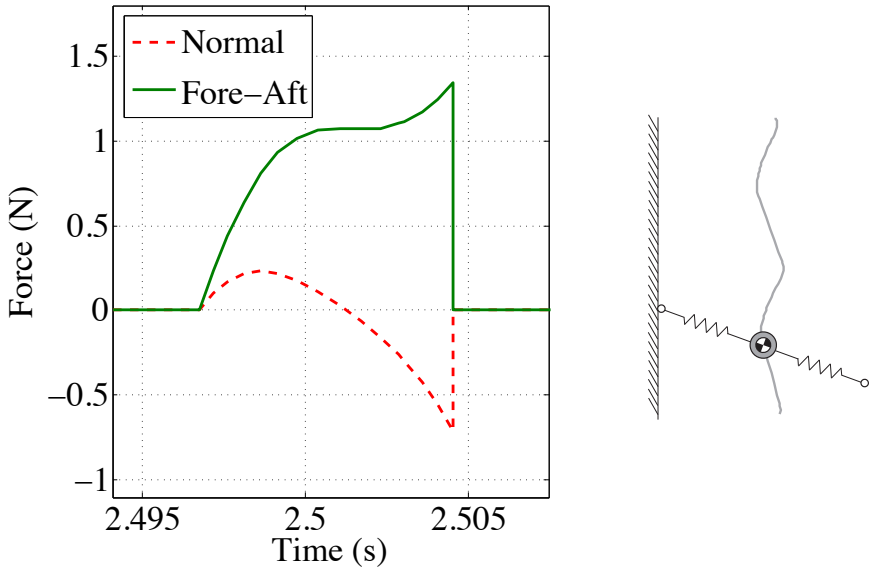

Figure 2.17: Typical ground reaction forces of the model using a controllable adhesive running on a vertical surface. Fore-aft forces are green and normal forces are red. Negative normal forces indicate pulling vertically towards the surface. The initial foot touchdown decelerates the body and accelerates the body away from the surface. Halfway through the stride, the body is accelerated forward and back toward the surface.

increases.

The ground reaction forces created by a single successful high-speed gait are shown in Figure 2.17. The shape of the forces during stance is similar to that seen in Figures 2.10 and 2.15. The fore-aft force is always positive, though it is less flat than those created by the gecko-inspired adhesive foot model. The normal force begins positive (compressive) but then goes negative (tensile) near mid-stance. Viewing the COM translations in Figure 2.18a reveals that the COM is traveling back toward the surface when the foot in stance releases.

Figure 2.19 shows the relationship between the normalized average climbing velocity and k_τ when k_ζ and $\theta_{release}$ are varied with a 15Hz rotational frequency. This data reveals a strong dependence of climbing performance upon k_τ and $\theta_{release}$ and a comparatively weak dependence upon k_ζ. Often climbing performance doesn't change while varying k_ζ over three orders of magnitude for a set k_τ and $\theta_{release}$. A k_τ of 0.232 $\frac{Nm}{radian}$ is able to achieve high speed across nearly all combinations of k_ζ and $\theta_{release}$ considered.

It is possible for the SLAP model to produce stable climbing gaits without normalized climbing velocities near 1. In Figures 2.13 and 2.16, there are parameter sets which create gaits approximately half as fast as the maximum linear leg velocity. Slower stable gaits are observed in parameter sets with lower torsional stiffnesses compared to the stiffnesses which generate faster gaits. In these cases, the torsional spring deflects more to generate the forces

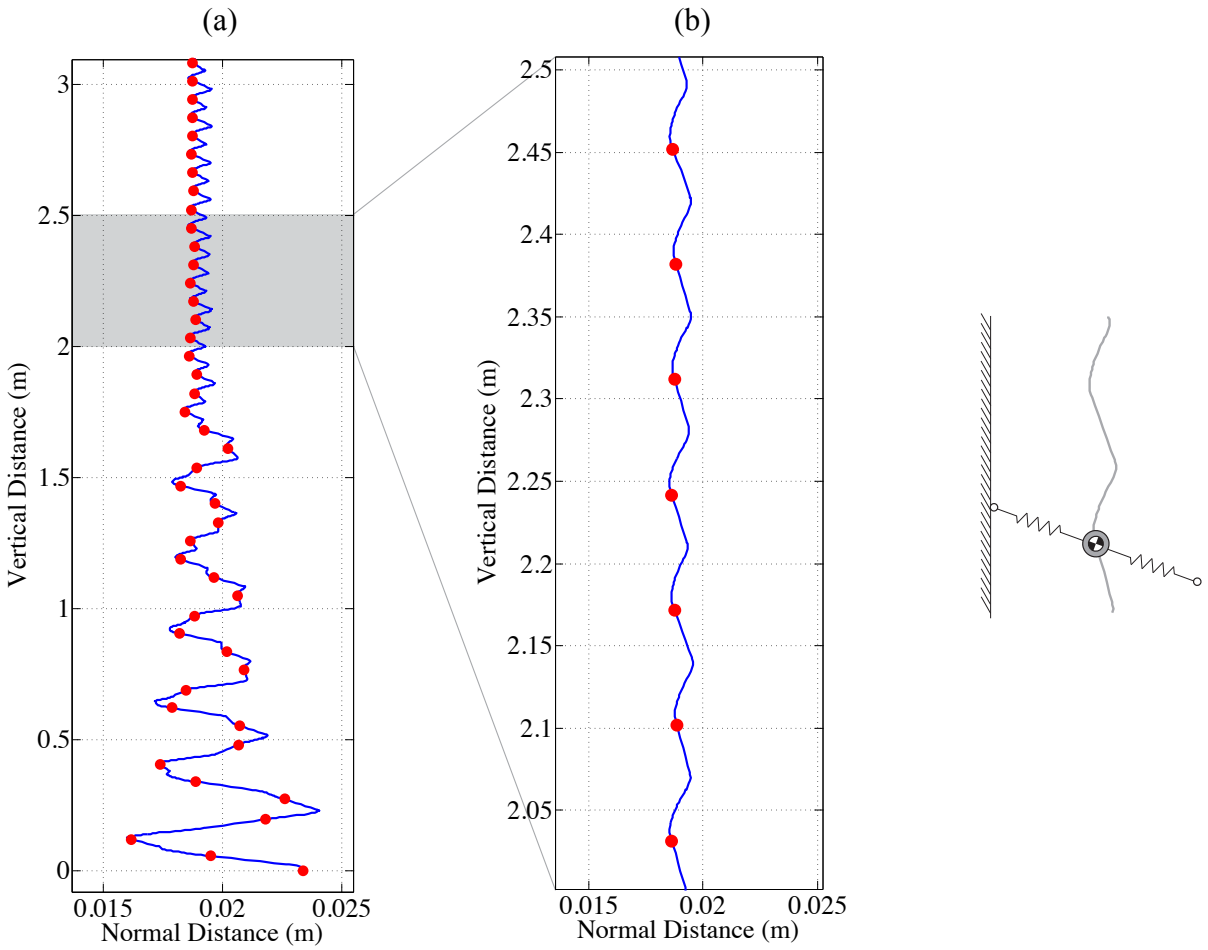

Figure 2.18: The COM translation of the system on a vertical surface with the clock-driven release foot model. The normal axis is magnified to better show normal motion. (a) Initial conditions produce a significant transient in the COM that stabilizes to a periodic gait. (b) Shows a closer view of the COM translations. Red dots show the state of the system at TD events.

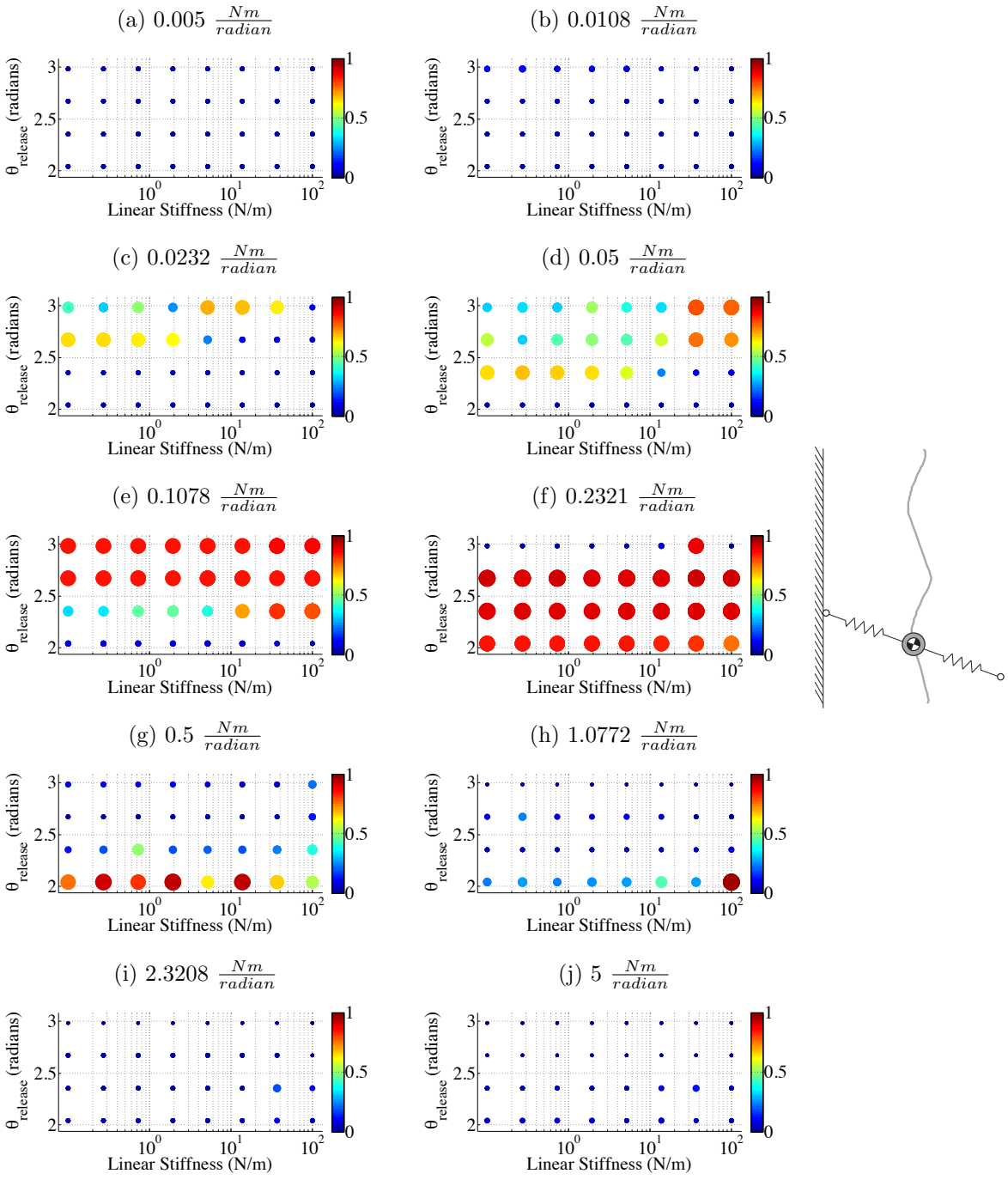

Figure 2.19: Normalized climbing speed of model on a vertical surface with the clock-based controllable adhesive vs. torsional stiffness, linear stiffness, and $\theta_{release}$. Velocities are normalized by the product of the angular velocity of the legs and the leg length. Larger, warmer dots indicate a faster normalized average climbing velocity. The stiffnesses in (e) and (g) have large windows of $\theta_{release}$ which result in effective climbing.

required to maintain steady-state velocity in the presence of gravity. This increased deflection during stance creates a shorter effective stroke, reducing the average velocity. Despite the larger torsional spring deflections, these slower gaits still exhibit ground reaction forces very similar to those observed in Figures 2.10 and 2.17.

As we expect from previous dynamical systems studies and the gecko-inspired foot model results from Section 2.6, the SLAP model with the clock-based release foot model exhibits both quasi-periodic chaotic gaits as well as stable periodic gaits. For those gaits that converge to a fixed point as numerically computed in Section 2.6, analysis of the linearized Poincaré map yields $|\lambda_{max}| = 0.55$ for the typical gait shown in Figure 2.18.

2.7.2 Inverted Running

In this section, the SLAP model with the clock-driven release foot model is examined while running on an inverted surface as seen in Figure 2.20. A similar exploration of the space of model parameters to that seen in Figures 2.13 and 2.16 was used to find stable running gaits of the inverted SLAP. For initial trials, the same set of $\theta_{release}$ values were used ($\theta_{release} = \{\frac{3\pi}{4} - \frac{\pi}{10}, \frac{3\pi}{4}, \frac{3\pi}{4} + \frac{\pi}{10}, \frac{3\pi}{4} + \frac{\pi}{5}\}$). The results of this search can be found in Figure 2.21. In these scenarios, only the fastest systems with stiff linear springs were able to successfully run across the inverted surface.

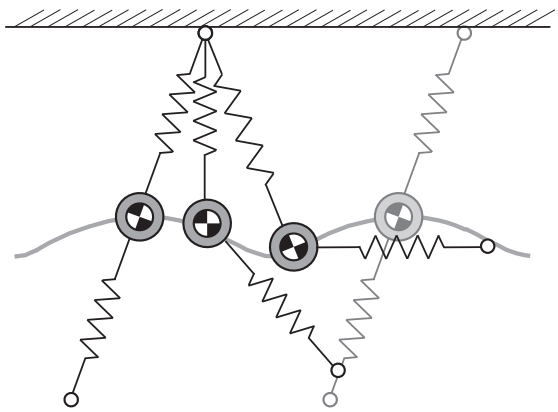

Figure 2.20: Diagram of two-legged dynamic climbing model running on an inverted surface ($\gamma = 90°$).

Examination of the best clock-driven release angles reveals that larger $\theta_{release}$ values result in better performance. Because these gaits are at the edge of the original values tested, a larger set is introduced to see an increased range that results in more stable gaits. Thus, the set of tested $\theta_{release}$ values is expanded to a range from $\frac{3\pi}{4}$ to $\frac{21\pi}{20}$. Allowing for larger, later release angles creates a larger space of linear and torsional stiffnesses that result in

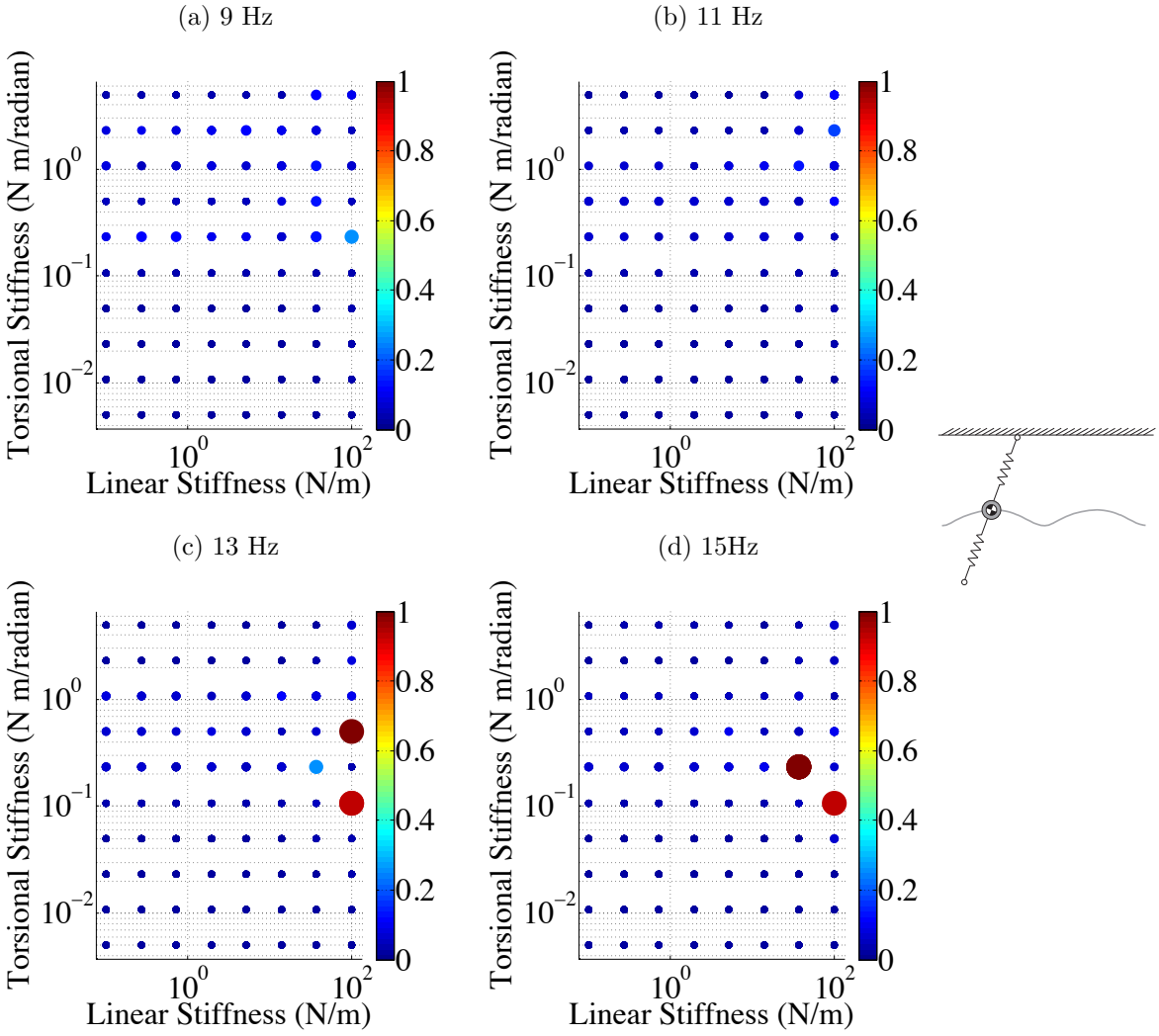

Figure 2.21: Normalized climbing speed of model on an inverted with a controllable adhesive with original parameter set for $\theta_{release}$. Velocities are normalized by the product of the angular velocity of the legs and the leg length. Larger, warmer dots indicate a faster normalized average running velocity.

stable gaits, as shown in Figure 2.22. Since the latter half of stance generates normal forces into the surface, a larger release angle gives the system more time to perform work against gravity and accelerate toward the surface. At 15Hz, the best gaits are those with a torsional stiffness of 0.232 $\frac{Nm}{radian}$ and a $\theta_{release}$ of π, implying the leg position commanded for release is directly backwards. Figure 2.23 shows the dependence of performance upon $\theta_{release}$ and k_τ.

The ground reaction forces generated by the best inverted running simulations reveal interesting and somewhat familiar results. Figure 2.24 shows the ground reaction forces of a typical gait. When the foot touches down, the leg generates a decelerating fore-aft force. Halfway through stance, the fore-aft force becomes positive and accelerates the system forward. This pattern has the same frequency and phasing as the fore-aft forces seen in SLIP dynamics when running on flat surfaces. The normal forces required to stay on the surface depart from SLIP, beginning compressive then going sharply negative to accelerate towards the surface. The system then enters an aerial phase, during which the velocity toward the surface is required to ensure the next foot has a chance to reach the surface. Typical COM motions that result from inverted running are shown in Figure 2.25. As with the other incline foot models tested, the COM can exhibit both chaotic, quasi-periodic and periodic gaits. $|\lambda_{max}| = 0.3168$ is found for a typical stable periodic gait, here $k_\zeta = 1.9307\frac{N}{m}$, $k_\tau = 0.2321\frac{Nm}{radian}$, $\dot{\theta} = 2\pi \cdot 15\frac{radian}{s}$, and $\theta_{release} = \pi$.

2.8 Discussion

With the reduced-order SLAP model, our goal is to create a framework to inspire and guide future dynamic climbing studies as well as a tool which legged robot designers can leverage in the creation of future dynamic robots with adhesive feet. All previous reduced-order incline running or climbing models look only at dynamics in the plane of the climbing surface [16,28,55,70]. This leaves these models unable to inform the requirements of adhesives or judge the response to perturbations in the sagittal dynamics. The SLAP model preserves much of the simplicity of LLS, SLIP, and other reduced-order models while incorporating two adhesive foot models as well as the means of adding energy to the system through a rotational input.

The generalized controllable adhesive model presented in Section 2.7 represents an adhesive capable of generating normal and shear forces whose maximum stress is never exceeded during a stride but can be controllably released at any rotational output set point. Examples of adhesives in this class include switchable electrostatic adhesives or feet with grasping mechanisms leveraging opposing toes with gecko-like or claw-based engagement mechanisms. The shear-induced adhesive in Section 2.6 is used to evaluate the performance of the SLAP system when equipped with an adhesive similar to those currently available and used in physical robotic systems.

Stable gaits are shown to exist for the SLAP model for rapid frequencies but not for slower leg velocities. While it is known that many animals and robots alike can climb

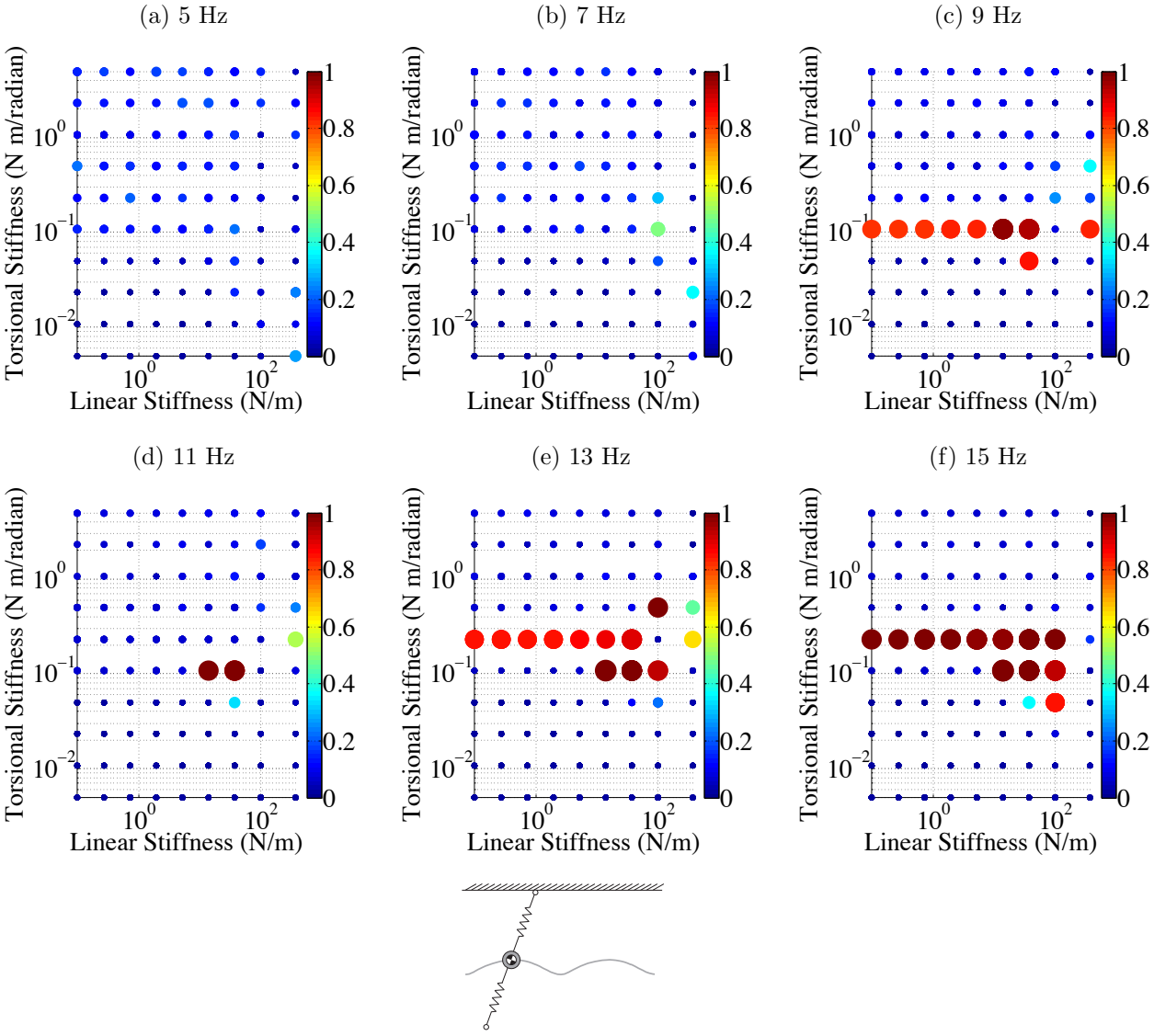

Figure 2.22: Normalized running speed of the SLAP model with the clock-based release foot on an inverted surface with an increased range of possible $\theta_{release}$. Velocities are normalized by the product of the angular velocity of the legs and the leg length. Larger, warmer dots indicate a faster normalized average running velocity. With the extended space of $\theta_{release}$, the space of linear stiffnesses that result in stable running is increased significantly.

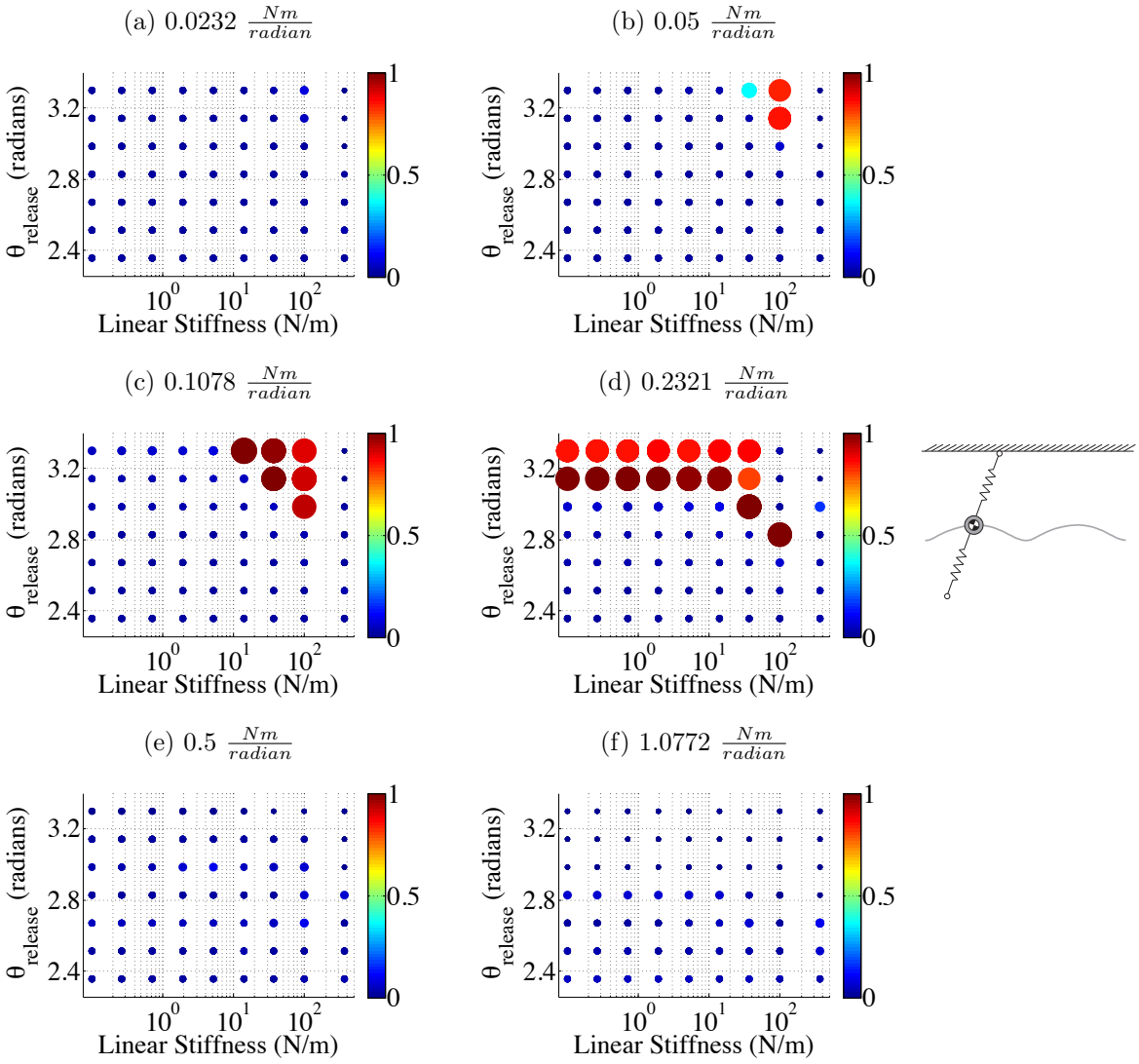

Figure 2.23: Normalized running speed of model on an inverted surface with the clock-based controllable adhesive vs torsional stiffness, linear stiffness, and $\theta_{release}$. Velocities are normalized by the product of the angular velocity of the legs and the leg length. Larger, warmer dots indicate a faster normalized average running velocity.

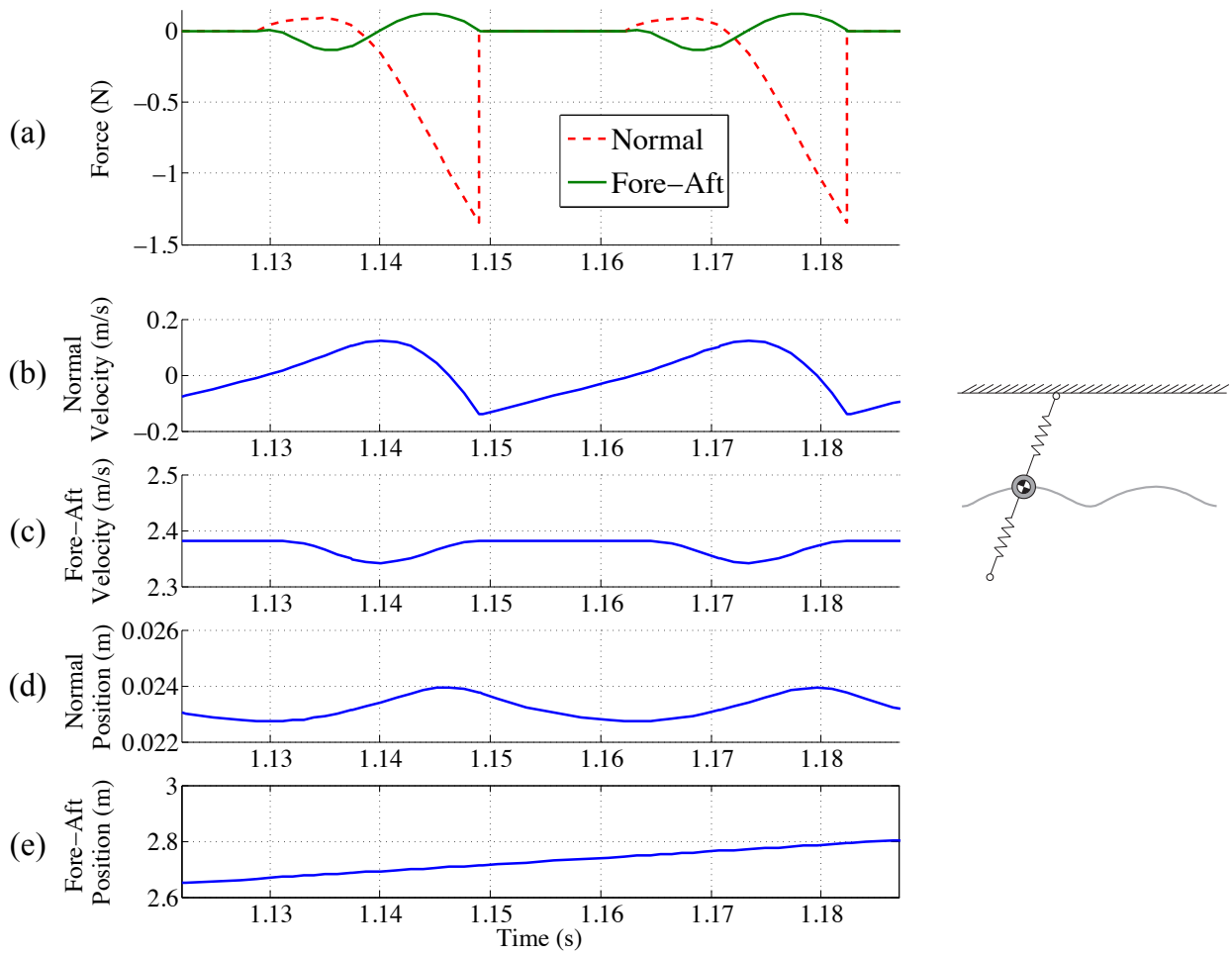

Figure 2.24: Typical ground reaction forces (a), normal and fore-aft velocities (b, c), and normal and fore-aft positions (d, e) of the model using a controllable adhesive running on an inverted surface. (a) Fore-aft forces are green and normal forces are red. Negative normal forces indicate pulling vertically towards the surface. The initial foot touchdown decelerates the body and accelerates the body away from the surface. Halfway through the stride, the body is accelerated forward and back toward the surface.

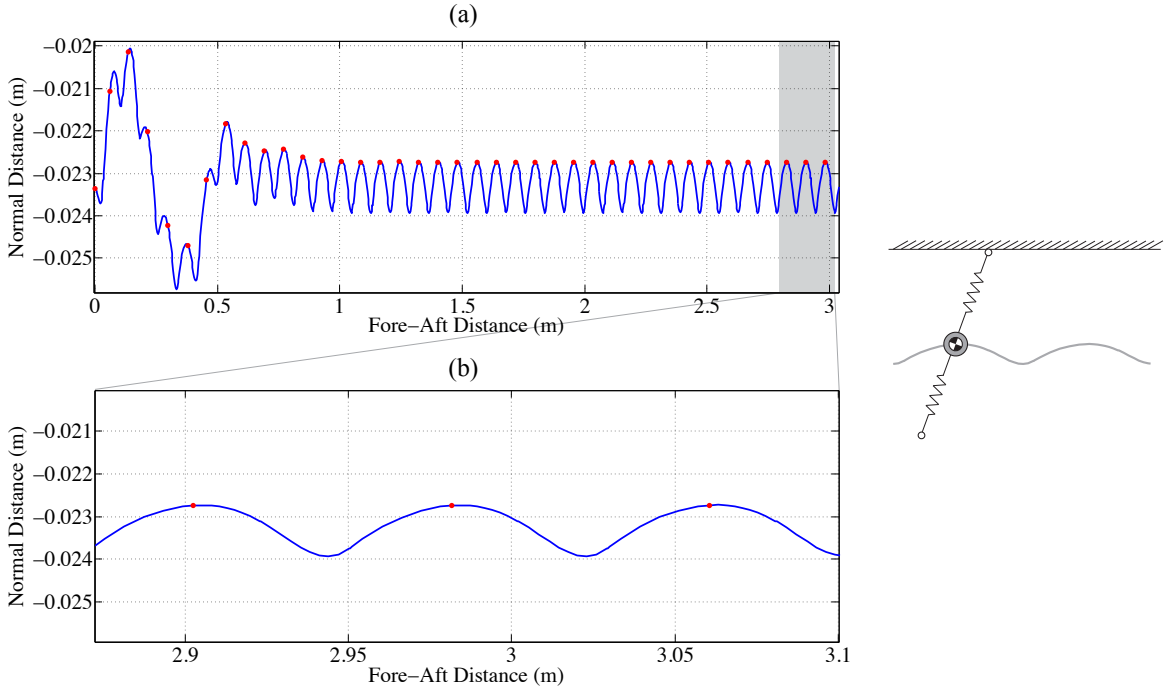

Figure 2.25: The COM translation of the system on an inverted surface ($\gamma = 90^0$) with the clock-driven release foot model. The normal axis is magnified to better show normal motion. (a) Initial conditions produce a significant transient in the COM that stabilizes. (b) Shows a closer view of the COM translations. Red dots show the state of the system at TD events. Note that the y-axis is inverted to more intuitively display the data as a positive normal direction is actually away from the surface, which in this case is directed down the page.

vertical surfaces or walk on ceilings are speeds slower than those predicted by the model, the collision of the COM with the climbing surface that typically results from these gaits cannot be accounted for and thus aren't considered. The behavior of these gaits are also not particularly relevant for the purpose of these studies.

The presence of stable but chaotic gaits makes traditional stability analysis difficult, but even these chaotic gaits exhibit robustness to initial conditions outside of their quasi-periodic steady state gaits. The presence of some stable, period-1 gaits allows for well-established methods using linearized Poincaré maps to determine that vertical climbing gaits using both a gecko-inspired foot model as well as a generalized adhesive model are passively stable on vertical and even inverted surfaces. Unstable gaits result from system parameters that cause an unstable growth of normal kinetic energy at touchdown that is created by the coupling of the rotational output and the system dynamics. Eventually these systems are unable to generate the tensile forces required to keep the system on the surface.

The utility of the model could be improved through the addition of a Buehler clock as

was introduced to SLIP in the CT-SLIP model [73]. This would allow the swing phase of the legs to be reduced, decreasing the time between the stances. Currently, a typical duty factor for the SLAP model on a vertical surface with $\dot{\theta} = 2\pi \cdot 15s^{-1}$ is around 15%. Therefore, to counter the constant force due to gravity, the average fore-aft force required by a single foot is $\frac{1}{.3} = 3.3$ times the body weight. Indeed, this is the case for the ground reaction forces seen in Figures 2.17 and 2.10. By reducing the aerial phase and increasing the duty factor, these large forces can be brought down to levels more like those seen in biological organisms [3,28]. By increasing $\theta_{release}$ for the inverted trials, the duty factor was increased to approximately 30%.

Through both the vertical and inverted climbing simulations, the performance of the SLAP model is robust to large ranges of linear stiffnesses but sensitive to the torsional stiffness. In addition, torsional stiffnesses k_τ with values around 0.1 to $0.2\frac{Nm}{radian}$ are found to consistently give the best climbing performance. The resonant frequency for a mass on the end of a rod with a torsional spring on the other end is

$$f_n = \frac{\omega_n}{2\pi} = \frac{1}{2\pi}\sqrt{\frac{k_\tau}{I}} \tag{2.9}$$

where I is the moment of inertia. For a point mass, the moment of inertia is given by $I = m \cdot l_{leg}^2$. It is interesting to note that for $k_\tau = 0.2321\frac{Nm}{radian}$, the most common k_τ of those tested to produce high-speed gaits for vertical and inverted climbing, the resonant frequency is approximately 22Hz. For $k_\tau = 0.1078\frac{Nm}{radian}$, the resonant frequency is approximately 14.6 Hz. These are at or just above the highest running frequencies tested, which also happened to yield the best climbing dynamics. Future studies of SLAP derivatives could combine the functionality of a Buehler clock with this idea of resonant operation to determine if a stronger link between system resonance, operating frequency, and performance can be established.

Unlike the ground reaction forces observed in the organisms, the ground reaction forces of the SLAP model do not return to zero smoothly before disengagement. Currently, the foot models used for the SLAP model have no mechanism for gradually releasing a foot from a surface, however it is unclear if this would make a difference in the observed dynamics. The gecko-inspired force-based model fails because the adhesive is overloaded by the forces demanded by the leg position and body dynamics. Because the relationship between the maximum normal force is linearly dependent upon the shear force, including a virtual peeling motion of the foot will not create a smooth disengagement. Including some linear leg actuation, as seen in [70], that could prescribe a leg trajectory not constrained to circular orbits may allow the model to gradually reduce the ground reaction forces on an individual foot.

It is hoped that the SLAP model will serve as the foundation for a dynamic *template*, which, according to [25], is the simplest model capable of recreating the ground reaction forces and COM dynamics of a targeted behavior - rapid climbing with sagittal dynamics in this case. Despite its shortcomings, this model still manages to recreate a similar ground reaction force shape and phasing to those observed in organisms. In order for the SLAP model to truly serve as a template and evolve from being merely a descriptive model, the

template should suggest testable control strategies as well as have the ability to be *anchored* in more detailed morphological and physiological models. Already the SLAP model suggests control strategies based upon the leg release angle, and the evolution to include a Buehler clock control would add another control input that is hypothesized to improve performance.

Chapter 3

Mechanical Design of Hexapedal Climber

In this chapter, we present the design of a lightweight, high-power density, low-profile scaled smart composite microstructure (SCM) [38, 85] transmission that serves as the foundation of the Climbing Autonomous Sprawled Hexapod (CLASH) platform also featured in Chapters 4 and 5 as well as Appendix A. The system is driven by a single brushed DC motor, similar to SCM robots DASH and DynaRoACH [8, 37]. The SCM process allows the platform to be small and lightweight to leverage the scaling laws mentioned in Chapter 1 [38]. Because previous SCM robot designs exhibited significant sagittal-plane accelerations which threatened to overload available adhesives, one goal of the design presented here was to reduce out-of-plane accelerations of the COM. The design succeeds in this goal while moving the COM to improve pitching moments and heading stability. The design creates an alternating tripod gait, chosen because of its static stability during stance on horizontal surfaces, added redundancy for generating adhesive forces, and demonstrated performance in an earlier design with similar body size and actuation [8].

Great effort was made to minimize the number of actuators required by the design to produce an effective and efficient gait. This was done for several reasons. First, having a single drive actuator improves power density of the system. For a multilegged system with one motor per leg, each motor does positive work only during stance. Thus, assuming a 50% duty factor, each motor only contributes positive work for approximately 50% of each cycle. Second, by having a single drive actuator, for the same mass one can have a larger, more efficient DC motor. Third, having a single main drive actuator has the potential to simplify control. It generates the primary mode of locomotion while smaller, lightweight actuators can be used to direct the work of the main actuator to produce turns or other behaviors [37].

3.1 Prior Design: DASH

Early work in meso-scale robot design using the SCM process led to the creation of the Dynamic Autonomous Sprawled Hexapod (DASH) [8]. This design was the first SCM-made robot to use a DC motor as the main drive actuator and was able to run at 1.5 meters per second, or 15 body-lengths per second. Its sprawled posture made it stable to roll perturbations and capable of running over rough terrain and in granular media [66]. The morphology of the system combined with the advantages derived from the manufacturing process enable it to survive impacts at its own terminal velocity.

3.1.1 COM Motion

Due to its great success on horizontal locomotion, DASH was initially explored as a platform for vertical climbing trials. However, the operation of the DASH transmission created large accelerations on the COM in the sagittal plane that made adhering to the wall more difficult [6, 62].

To create the alternating tripod gait used in DASH, the system is designed such that the circular motions of the output stage of the DC motor moves linkages in a circular motion in the sagittal plane. It is this circular motion of the linkages which drive the hips and legs. See [8] for specific implementation details. The motion of the linkages during operation are apparent when viewing DASH from the side, as in Figure 3.1. To move in this circular motion, forces in the sagittal plane must be applied to the linkages. Because the drive linkages represent approximately half of the total system mass, the forces required are significant when operating at high angular velocities. To remain on a vertical surface in the presence of

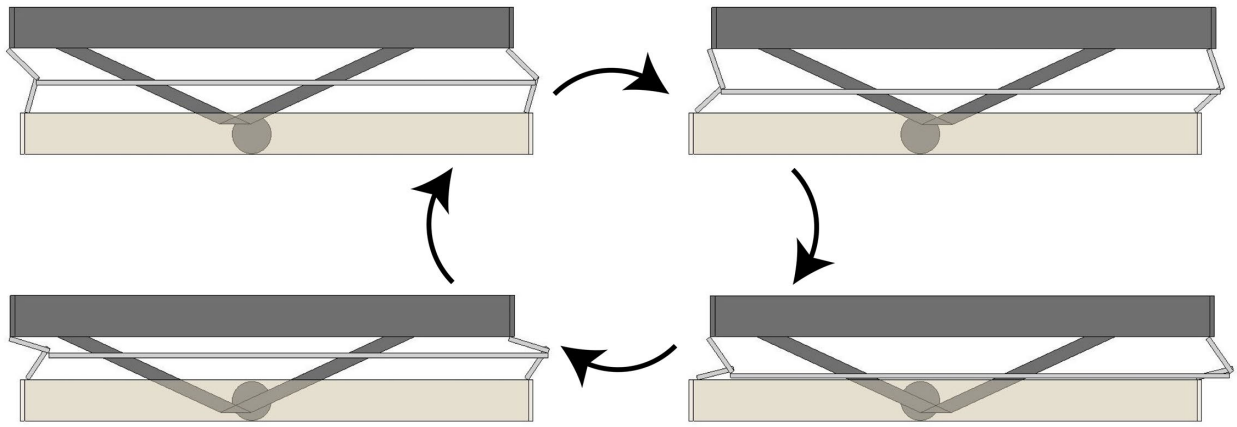

Figure 3.1: Model of DASH body transmission during operation at four different points in a stride. The top horizontal linkage moves vertically during operation, creating normal accelerations of the center of mass. Arrows show the progression of the system during operation.

such normal accelerations would require significant additional adhesive forces beyond those required to overcome ground reaction forces and pitching moments. And because the masses of these robots are small at around 15-25 grams, the drive linkages will typically represent a large fraction of the total mass and create non-negligible COM oscillations during operation. Thus, the accelerations created by the mere operation of an SCM transmission must be designed in these systems to minimize the negative impact on body dynamics and adhesive loading.

3.2 CLASH Design

3.2.1 Design Considerations

CLASH was designed to address the shortcomings DASH faced when climbing. As DASH was not originally envisioned for climbing applications, concerns such as placement of the COM to control pitching moment and stability while climbing were not considered. DASH had a COM located forward and high vertically as this was found experimentally to be better suited for rapid horizontal locomotion, but the resulting dynamics were unsuitable for climbing.

The COM placement on a climbing robot is critical to improve yaw stability and reduce the adhesive load required. Placing the COM closer to the climbing surface linearly reduces the pitching moment on the body and thus reduces the tensile load on the feet. Moving the COM towards the rear of the robot has been previously shown to create yaw stability in a climbing system; [16, 17, 28] demonstrated that by having the COM below the effective foot purchase, it is possible to gain passive heading stability using a simple open-loop controller.

As discussed in Section 3.1, while SCM robots are lightweight and power dense, the transmissions often have COM accelerations that result from drive linkages with non-negligible mass. While actuators other than DC motors may be able to reduce the COM accelerations inherent to a transmission, DC motors have been shown to be an excellent choice for systems at this scale [80]. Thus, for reasons discussed in Section 3.1, the circular output of the motor and circular motion of the drive linkages should be oriented in a manner that reduces normal accelerations. For this reason, the design of CLASH is constructed such that the drive linkage is driven parallel to the climbing surface.

3.2.2 Mechanical Design

The SCM design which incorporates the above design considerations is shown in Figure 3.2. The system is 2 cm tall, 5 cm wide, 10 cm long, and weighs 10.8 grams with the motor installed. The addition of a 60 mAh lithium polymer battery and electronics adds 2.9 grams, and an optional tail adds 1.3 grams. The CLASH platform uses a single drive actuator to achieve the high-power density required for climbing and maintains the alternating tripod gait of its predecessor. The sprawled posture it generates allows the system to maintain a

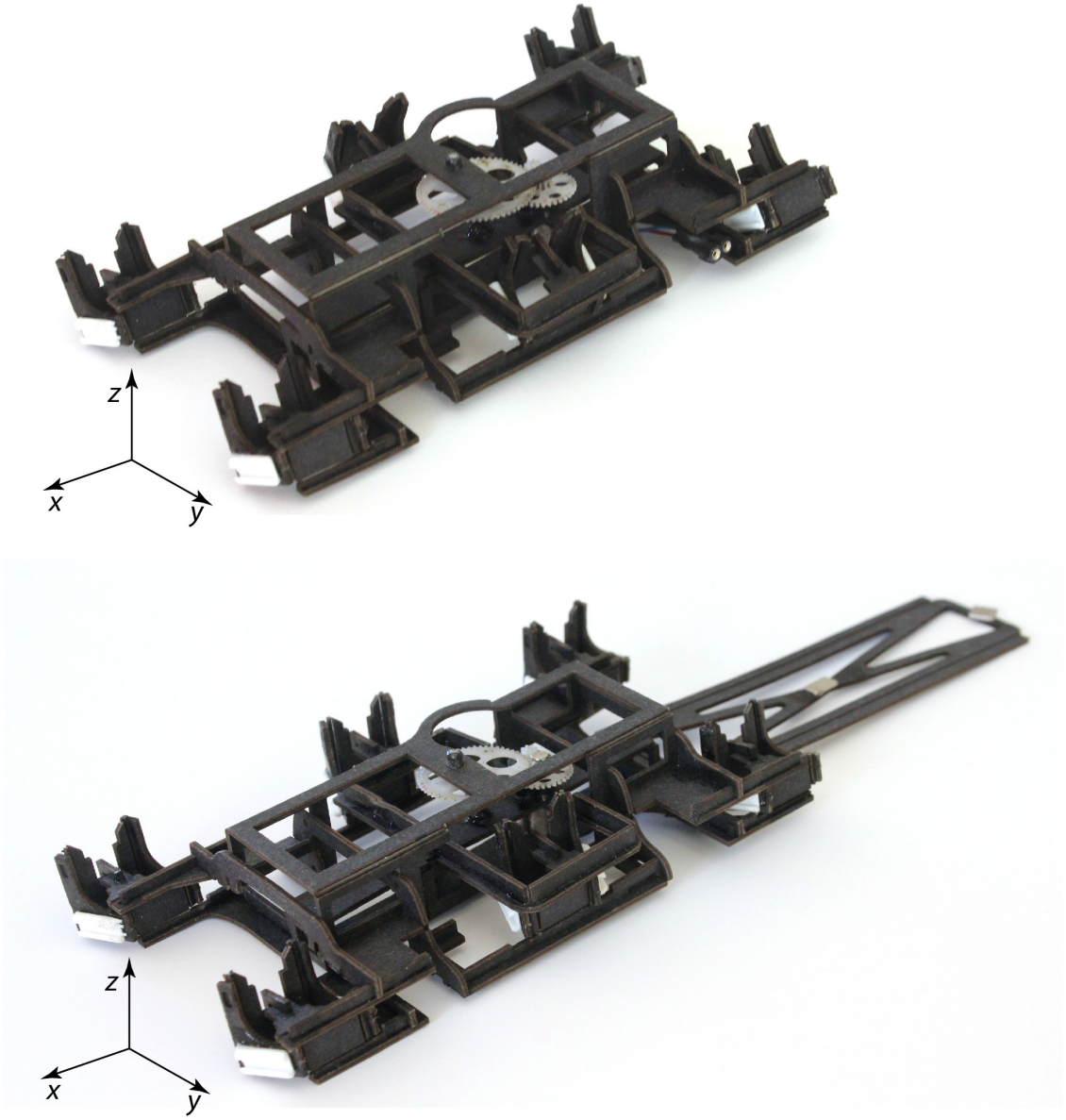

Figure 3.2: CLASH transmission with no legs attached. White leg press-fit connectors allow the legs to be quickly and easily replaced. A tail can be included without modification to the transmission.

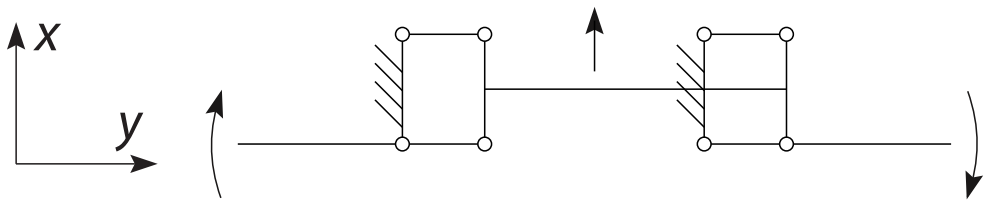

Figure 3.3: Motion of the legs in the x-y plane is achieved by moving the drive linkage in the middle in the x-direction. The grounded linkages are coupled rigidly to the motor case. Each pair of opposing hips is driven in a similar manner, though the middle legs are mirrored from the front and rear legs.

low profile and pitching moment during climbing. Sprawled posture has also been shown to yield passive stability even when using open-loop commands [8, 16, 28, 70].

To minimize accelerations of the COM out of the plane of the surface, CLASH uses a DC motor mounted orthogonally to the climbing surface, with the bottom of the motor flush with the belly of CLASH and the top output gear assembly located dorsally. Referring to the coordinates defined in Figure 3.2, the final stage of the output gears moves in the x-y plane, i.e. parallel to the foot-contact surface, driving the top drive linkage in both x- and y-directions.

The hip mechanism, abstracted in Figures 3.3 and 3.4, was designed to be driven by displacements of a drive linkage in the x- and y-directions as in Figure 3.5. In these figures, the grounded linkages in Figures 3.3 and 3.4 are rigidly coupled to the white-highlighted linkage in Figure 3.5 in which the motor casing is mounted. The bold linkages in Figures 3.4a and 3.4b are driven by the output of the motor, which is connected to the red linkage in Figure 3.5.

When the motor drives the linkage along the y-axis, the motion drives opposing pairs of hips as shown in Figure 3.4. For the front and rear hips, the mechanism is driven as in Figure 3.4a with the grounded linkage flush with the belly. For the middle hips (Figure 3.4b), the drive and grounded linkages exchange vertical positioning. This causes the middle legs to move in the opposite direction from the front and rear legs as is required for an alternating tripod gait. To achieve motion of the legs in the x-direction, the x-directed motion of the motor output drives the front and rear pairs of hips as shown in Figure 3.3. The middle legs have a similar mechanism but simply mirrored across the sagittal plane. In this way, the circular output of the single drive motor drives all six legs in an alternating tripod gait. The hips have a fore-aft angular sweep of $+/-23^\circ$ centered orthogonal to the sagittal plane. The hips have a normal sweep of $+/-25^\circ$ centered on the horizontal plane. Viewed from above as in Figure 3.5, the drive linkage, as well as the COM, moves primarily in the x-y plane.

(a)

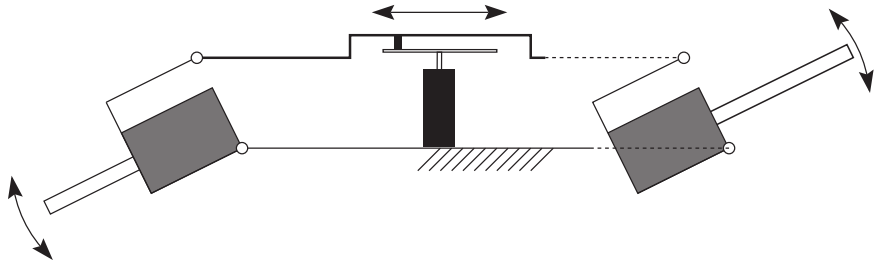

(b)

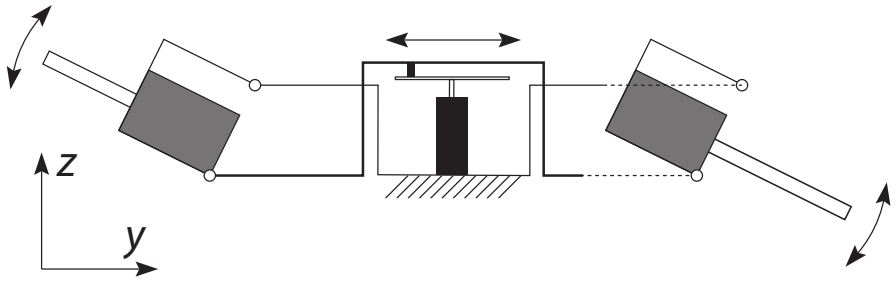

(c)

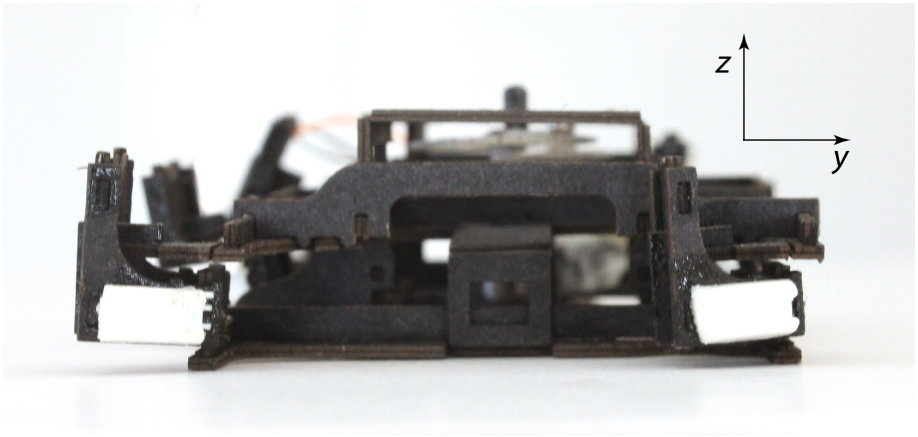

Figure 3.4: Kinematic drawings show how the legs are raised and lowered by moving the top drive linkage (bold) along the y-axis. The motor is mounted to the grounded linkage while the output of the final gear stage drives the top linkage. (a) shows how front and rear legs are driven, and (b) shows how the mid-legs are driven. The grey rectangle is the side view of the four-bar mechanism in Figure 3.3. Linkages are dashed to not obscure other linkages. They do not collide when realized in three dimensions. (c) is a view of CLASH from the same perspective as (b).

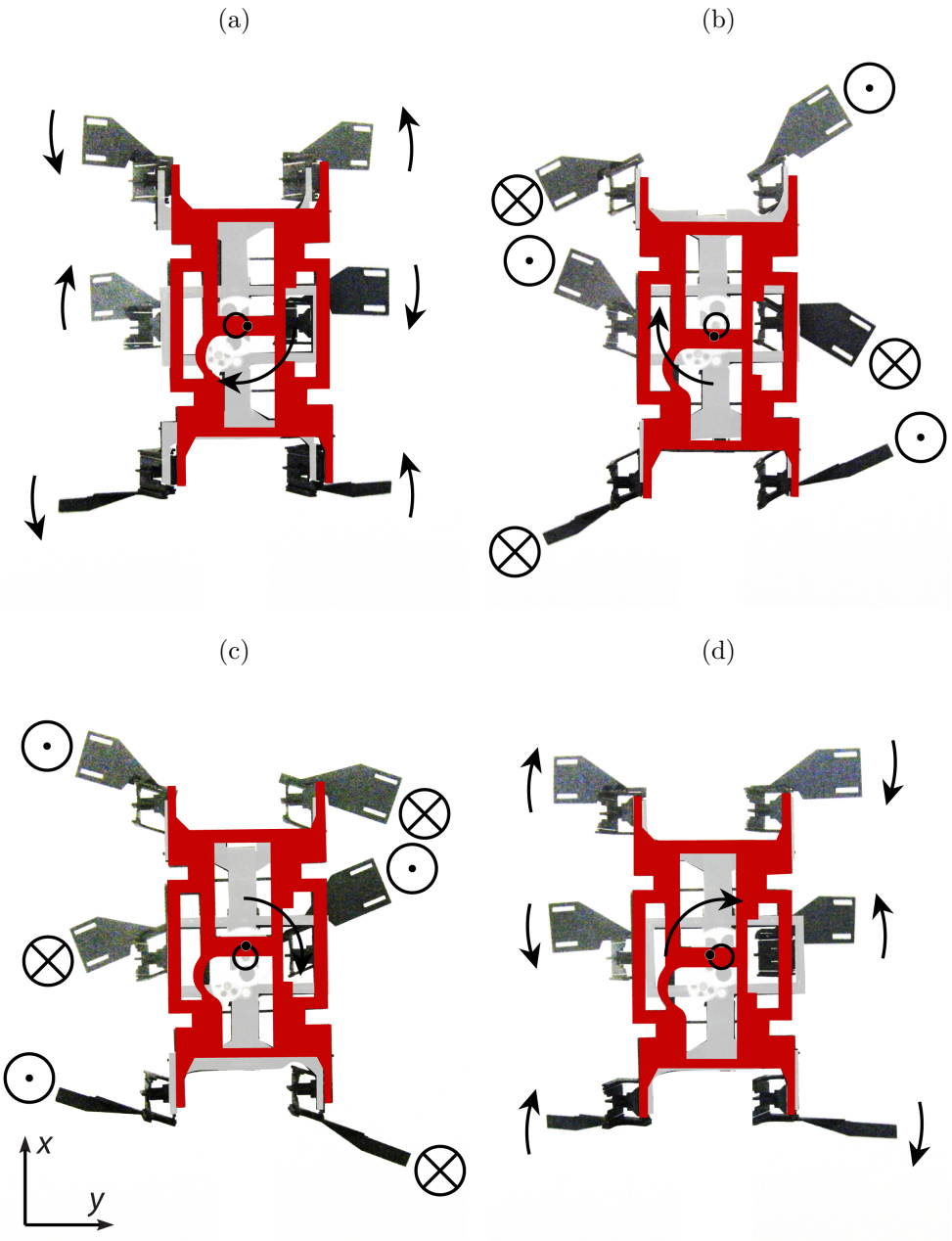

Figure 3.5: CLASH body motion during operation, viewed from above. Legs are attached to the transmission to highlight resulting leg motions. The motor is mounted to a linkage that runs down the middle of the robot, highlighted in light grey. The output of the motor drives the linkage highlighted in red, rotating in a circular output dictated by the motor (indicated with arrows). Resulting leg motions are also shown with arrows. Body motion is confined to the x-y plane. (a) to (d) show linkages at 90° increments of the transmission.

The total system height of CLASH is 2 cm tall, reduced from 5 cm in DASH. The motor is mounted in the center of the robot, lowered down the z-axis to be flush with the bottom of the robot. The battery is placed low along the center of the body, encased by the structure to protect it (Figure 3.6). Alternatively, the battery can be placed on a tail that extends below the body, as in Figure 3.7. The placement of these elements in the robot brings the COM to approximately 6 mm above the bottom of the robot, reduced from an average of 30 mm above the bottom of DASH. The design also consolidates the mass of the system to a single element of the drive transmission. This reduces the x- and y-displacement of the COM motion during locomotion and thus further lowers the accelerations caused by the operation of the differential drive mechanism.

(a)

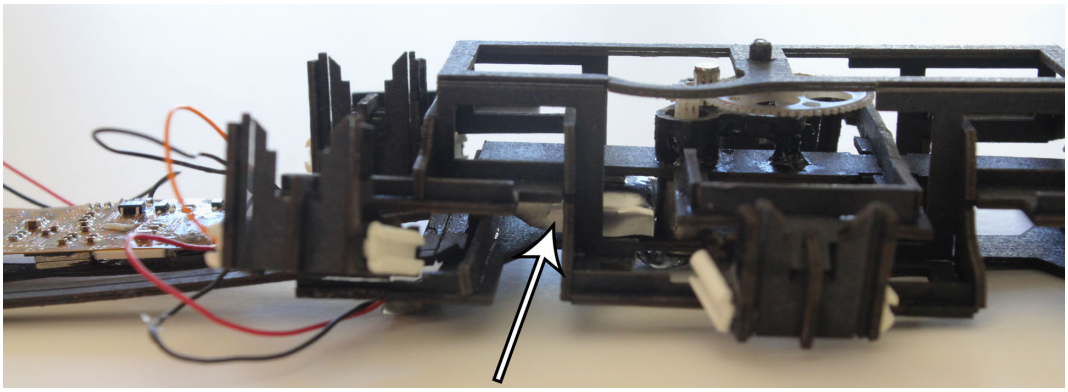

(b)

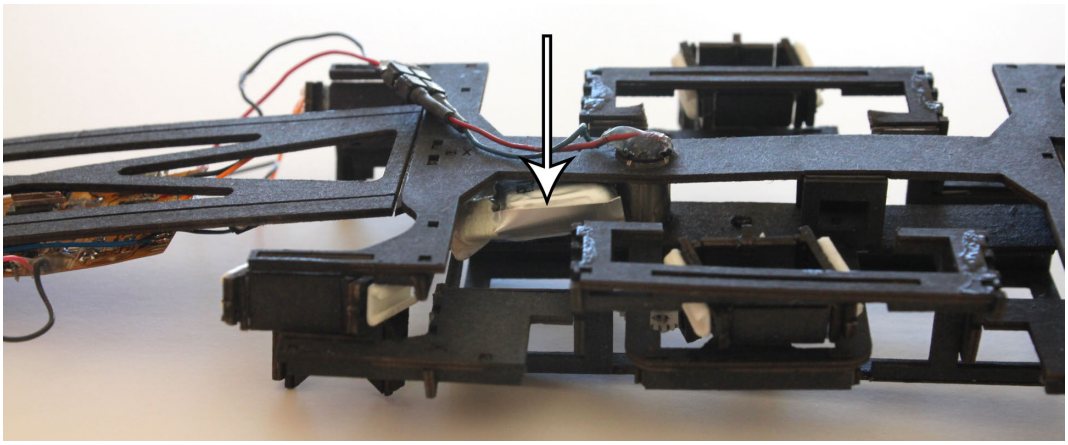

Figure 3.6: Battery placement in CLASH. There is space along the spine of CLASH to house a 60mAh lithium polymer battery to power the system. The battery placement is low and toward the rear of the system to promote a lower pitching moment and passive heading stability. (a) looks at the battery from the side of the system. (b) looks at the battery from the bottom of the robot. Arrows highlight the battery in the structure.

(a)

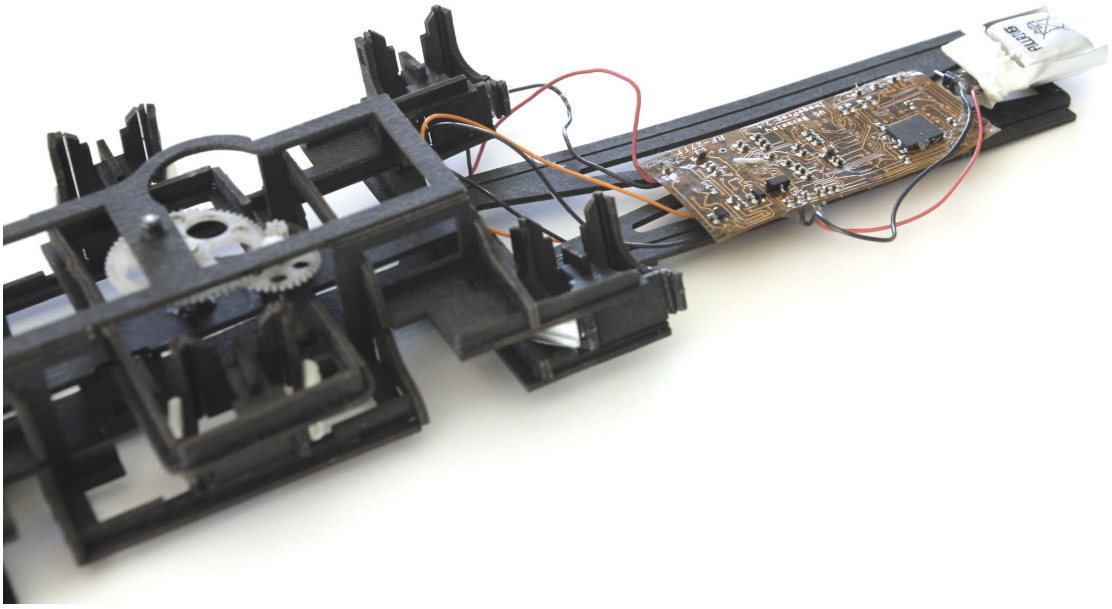

Figure 3.7: When a tail is used with the system, the electronics and battery can be mounted on the tail, further reducing the pitching moment and moving the COM toward the rear of the system.

To demonstrate the improvement in the COM dynamics produced by the linkage motions during operation, both DASH and CLASH were mounted to a 6-axis force-torque sensor (ATI Nano 43 F/T sensor) and operated at a motor frequency of 17 Hz. The experimental setup is shown in Figure 3.8a. The average magnitude of the normal force generated by CLASH is 85 mN, or roughly half of the body weight; the average normal force magnitude for DASH is 283 mN. The peak-to-peak normal forces are also 2.6 times larger in DASH than in CLASH. By reducing the normal accelerations of the COM caused by the drive linkages in the transmission, the CLASH platform increases the likelihood that a chosen adhesive will be able to sustain the normal forces required to remain attached to a surface.

3.3 Conclusions

In this chapter, we present an SCM transmission that serves as the foundation for the work presented in Chapters 4 and 5 and Appendix A. The body and transmission successfully reduced the mean magnitude of the COM accelerations out of the plane of the climbing surface by 70% from the DASH design and static pitching moment is reduced by 80%. It maintains a low mass, moves the average COM position to only 6mm above the surface, and reduces the profile of the robot. The reduced profile, in addition to lowering the gravitational

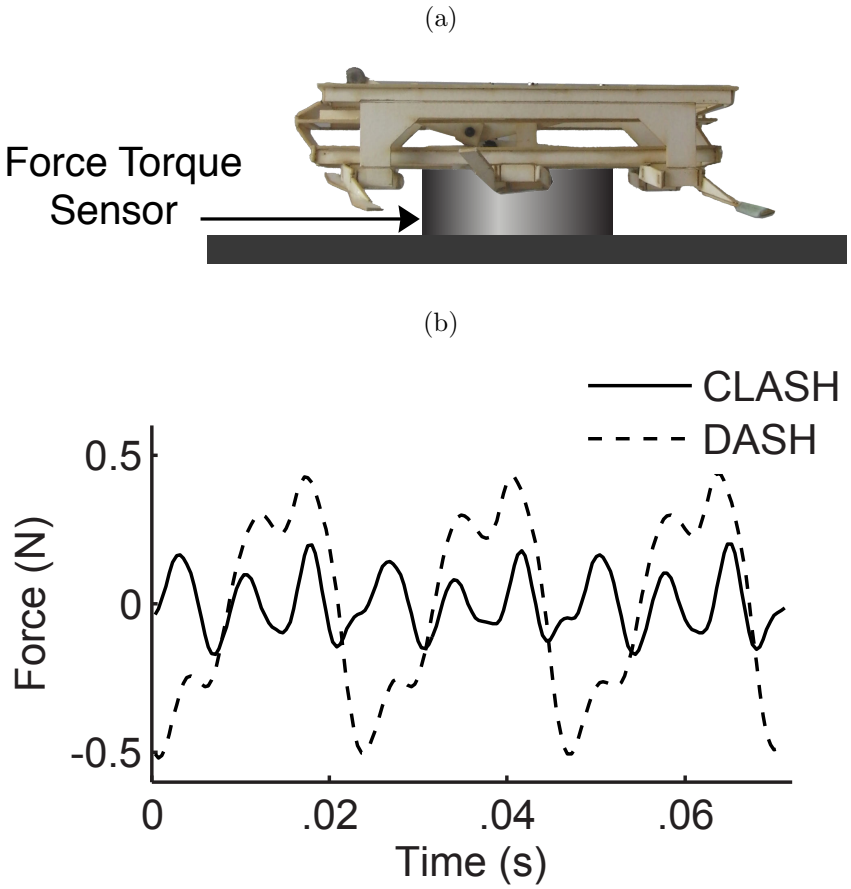

Figure 3.8: Measuring normal forces generated by body dynamics without ground contact by mounting to force torque sensor (a). Sensor is tared to remove body weight. (b) Comparison of forces of CLASH (solid line) to DASH (dashed line).

pitching moments, may also improve mobility by allowing it to navigate smaller openings.

By incorporating a press-fit connector into the hips (Figures 3.2 and 3.4c), this same transmission can easily be tested with different legs and attachment methods without modification of the body and transmission presented in this chapter. The kinematics of the hip mechanisms presented here prescribe the angular rotations of any attached leg. As such, any leg and foot design that is used must be capable of performing well in an alternating tripod gait defined by the rotations prescribed by the CLASH mechanism.

Chapter 4

Cloth Climbing

In this chapter, we present the design of passive claw mechanisms which enable CLASH to become the first robot to climb loose vertical cloth. Previous robot designs, including those presented in Chapter 1, have all relied upon rigid or rigidly backed surfaces to be able to climb. The system presented here has the advantage of low mass and a low profile which limits the cloth deflection created by the reaction forces of the system, allowing it to climb cloth without sensors to determine the surface orientation. A passive foot mechanism utilizing microspines sustains tensile loads during stance yet provides low resistance during retraction to facilitate smooth and efficient climbing. The single DC motor of CLASH provides a feedforward clock-driven gait which enables CLASH to climb cloth vertically at 15 cm/s (1.5 body-lengths per second). CLASH equipped with passive microspine feet can be seen in Figure 4.1.

4.1 Foot Design

Great effort was taken to create a foot design for climbing cloth surfaces which can function without additional actuators. Passive mechanisms minimize total system mass and maintain high power density in the system by minimizing the number of actuators and necessary control electronics. Passive mechanisms also have the ability to respond faster to external stimuli as they do not have feedback control delays and actuator response times; instead, they depend on the mechanics and dynamics of the structure. However, without actuation, a mechanism must not only engage and disengage passively, but it must also tolerate a wide range of approach angles, surface curvature, and retraction angles as there is no control to compensate for such realities.

Because the unloaded leg motions of CLASH are entirely determined by the kinematic structure, the loading and unloading directions relative to the surface during climbing can be loosely bounded. Using the SLAP model with the clock-driven release foot, we consider the commanded foot velocities relative to the inertial reference frame of the climbing surface to estimate what those loading and unloading directions are during steady state. Figure

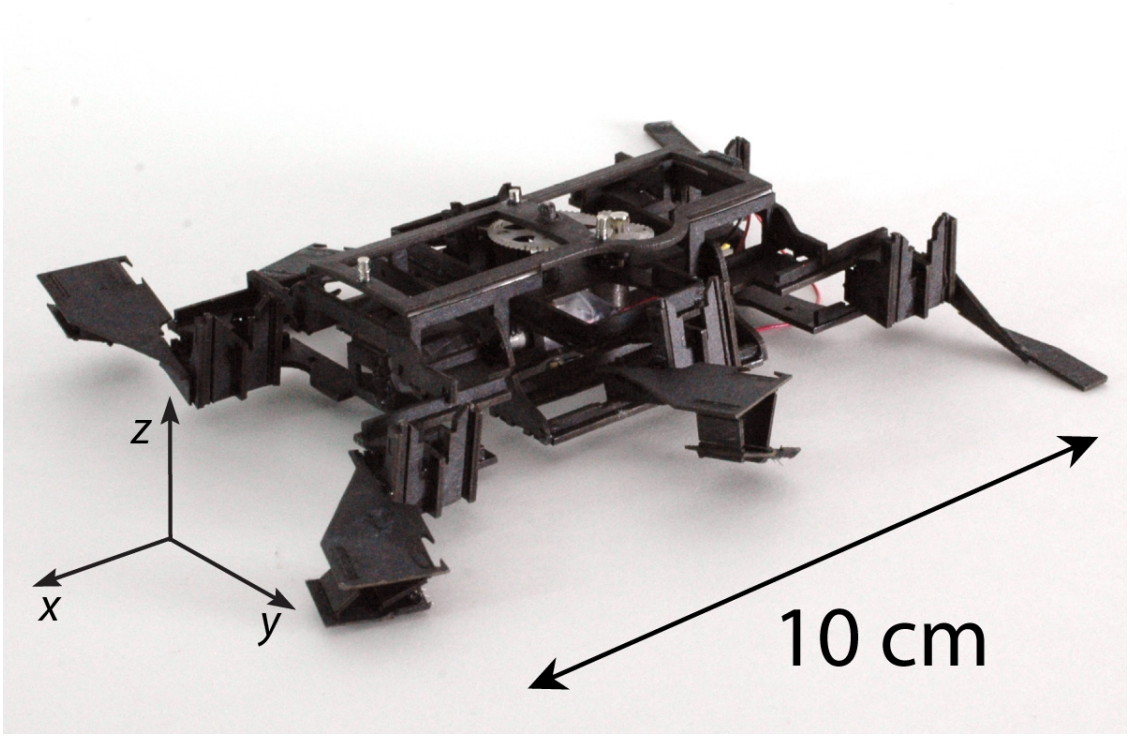

Figure 4.1: CLASH equipped with microspine feet capable of climbing loose and rigidly-backed cloth surfaces.

4.2 shows the commanded foot velocity relative to the climbing surface for a representative climbing simulation. At TD (I), the foot is moving into the surface and forward vertically relative to the surface. The commanded foot position then begins to move down relative to the surface and goes from moving into the surface (II) to pulling away from the surface (III). For parameter sets that result in high-speed climbing such as the one shown in Figure 4.2, the normal-to-fore-aft velocities of the commanded foot position at LO were near 2:1. Referring to Figure 4.2, this corresponds with $\phi = 120°$. Thus, the target design for a passively disengaging foot is one which can sustain tensile normal loads for ranges of loading directions given from I-IV in Figure 4.2 but removes easily when loaded near V.

The foot mechanism used by CLASH (Figure 4.3) consists of a four-bar mechanism with the top linkage grounded on the leg and the bottom linkage extending forward with embedded spines. The mechanism is designed to move the instantaneous center-of-rotation of the spines beneath the plane of the climbing surface. Having the center of rotation beneath the climbing surface causes the spines to rotate in the opposite direction, as shown in Figure 4.3c. In a passive foot, having the center of rotation above the surface would cause the spines to roll away from the surface during stance, increasing the likelihood that they will lose engagement with the surface as illustrated in Figure 4.4. When CLASH's spines have penetrated the cloth, the foot rotation causes the spines to hook the fabric and pull the robot towards

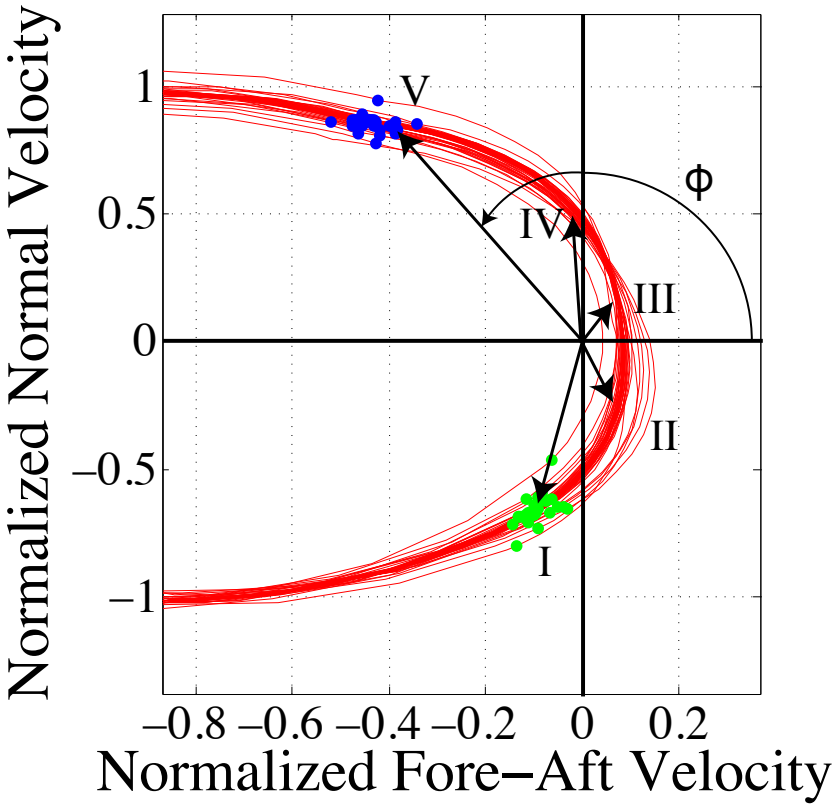

Figure 4.2: Velocity of foot set point relative to the inertial frame of the SLAP model with a clock-driven release foot when climbing a vertical surface. Blue dots (V) indicate the relative foot velocity at TD, and green dots (I) indicate touchdown. (I) The foot is moving into and up the surface. (II) The foot velocity is still into the surface, but now moving down relative to the surface. (III) The relative velocity is down and away from the surface, accelerating the system into the surface. (IV) and (V) The system continues to be pulled into the surface until the release setpoint is reached. The ratio of the normal-to-fore-aft velocities that are associated with lift-off can be determined by ϕ. Velocities are normalized by the maximum foot velocity magnitude $\dot{\theta} \cdot \zeta_0$.

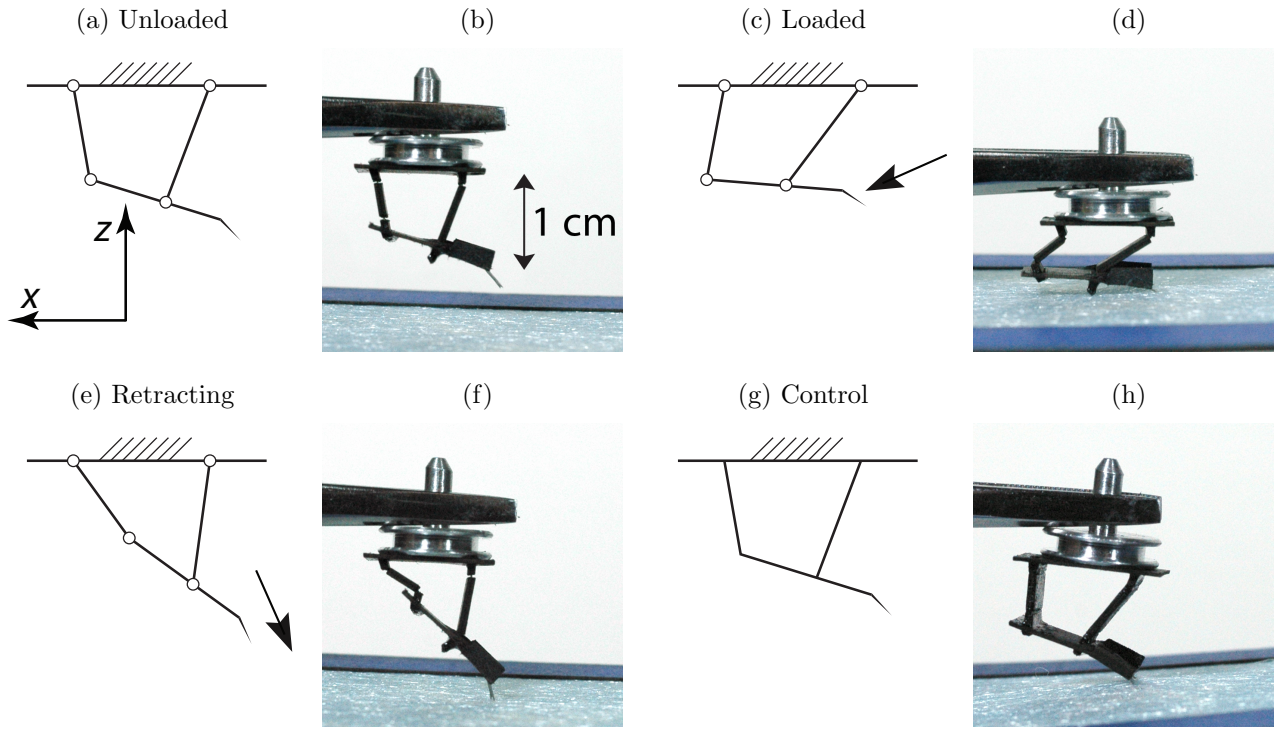

Figure 4.3: Kinematic drawings with corresponding photos of the four-bar foot mechanism on a metal mount. The grounded linkage is where the mechanism attaches to the leg. (a, b) When not loaded, the spines angle slightly downward to facilitate penetration at impact. The coordinates in (a) correspond with those in Figure 4.1. (c, d) When loaded during stance after engagement, the foot deflects slightly under the load and rotates the spines up, hooking the cloth to generate tensile normal forces. (e, f) When the foot is retracted, the spines easily collapse and rotate downward to be easily withdrawn from the cloth. (g, h) A four-bar mechanism with locked joints serves as the control to compare during force testing. Note how the cloth is being pulled up as the foot is retracted.

the cloth surface, increasing normal force during the stroke. The passive Shape-Deposition-Manufactured SpinybotII foot nearly eliminates the unwanted passive rotation of the spines, and both the SpinybotII and RiSE groups mention that the opposite spine rotation, achieved here in the CLASH foot, would be beneficial in passive engagement for climbing [43, 64].

During foot touchdown and stance, the feet are expected to be pressing down and against the climbing surface, with some preload required to embed the spines and tensile forces to keep the robot from pitching backward during stance (Figure 4.3c). In these situations, the foot mechanism will deflect as seen in Figure 4.3d. At the end of stance, CLASH will raise its foot from the surface, and the ground reaction forces will be primarily in the normal direction as the cloth impedes the retraction of the spines (Figure 4.3e). The four-bar mechanism was designed to reduce resistance when retracted nearly orthogonally to the surface; when the

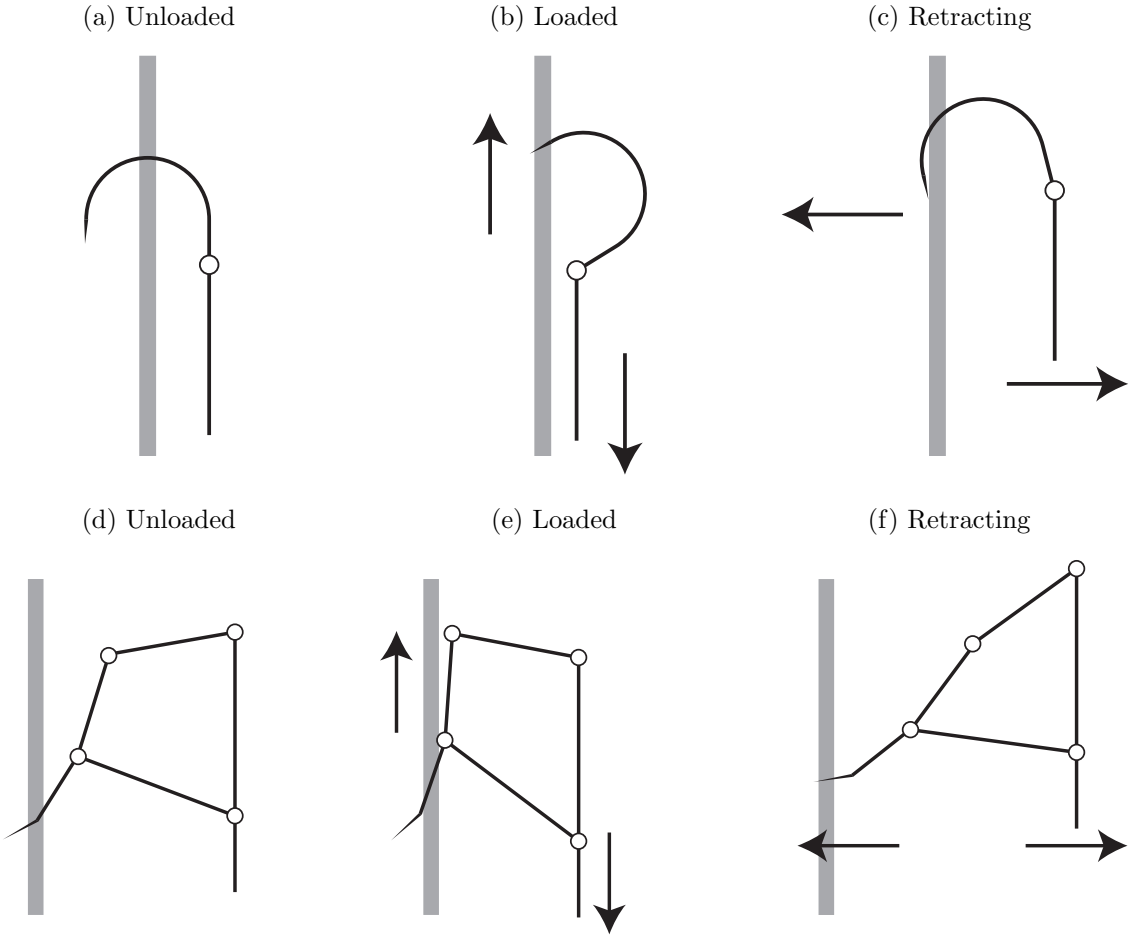

Figure 4.4: Kinematic drawings comparing a how the CLASH claw foot mechanism compares with a simple passive hinge above the climbing surface. (a) and (d) show the unloaded configurations of the simple hinge and the CLASH design, respectively. (b, e) When loaded during stance after engagement, the CLASH foot rotates toward the cloth, hooking the cloth and pulling the robot toward it. This rotation also allows for tensile normal forces to be sustained without failure. The passive foot rotates away from the surface such that tensile ground reaction forces will result in failure. (c, f) When being unloaded, the CLASH foot enables the spine to orient orthogonally to the surface for easy retraction. The simple foot design does not facilitate easy retraction.

load is oriented in this direction, the foot mechanism moves through a geometric singularity and collapses to a configuration in which the spines are more orthogonally oriented where they offer little pull-out resistance (Figure 4.3f). Although the mechanism may deflect through a singularity, the stored elastic energy in the deflected flexures restores it to the unloaded configuration when the load is removed. The direction of the loading vector determines

whether the foot will deflect to the configuration shown in Figure 4.3c or in Figure 4.3e.

4.2 Foot Performance

To test foot-ground reaction forces, load-drag-pull step tests were performed on a custom built force displacement apparatus (Figure 4.5a) which consists of two main components. The first is an acrylic chuck used to hold the foot that is attached the force torque sensor, a goniometer (Newport GON-U-60) and two linear slides (Newport 423 slide). The second component is a custom built aluminum frame used to hold the substrate. This frame is mounted on two perpendicular stepper-motor-controlled linear stages (Zaber T-LSR 150B) and a second goniometer. The entire apparatus is mounted on an air table (Newport VH series) to dampen vibrations. This force displacement apparatus enables testing to be performed in a repeatable manner and various foot designs to be directly compared with each other.

Load-drag-pull steps (Figure 4.5b) were performed on the force displacement apparatus under displacement control for two foot designs; the first, a flexure-jointed four-bar as found on the CLASH robot, and the second, a control foot with fixed four-bar joints. Each foot was tested on a cloth substrate at a variety of pull-off angles, θ, that simulates the robot running at a variety of speeds.

(a)

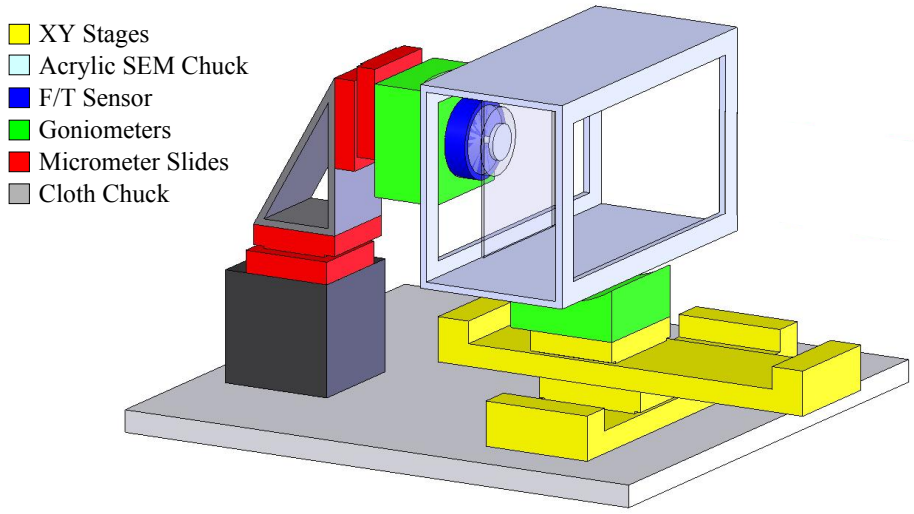

(b)

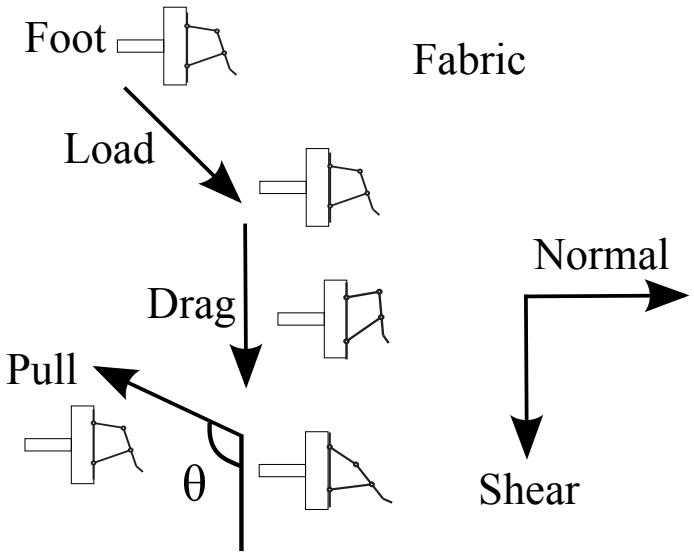

Figure 4.5: (a) The force-displacement apparatus used to test the different foot designs. Feet were mounted on a force sensor and simulated steps were performed on a cloth substrate under displacement control. (b) The simulated step taken by the foot showing the varying pull-off angles that correspond to different running speeds.

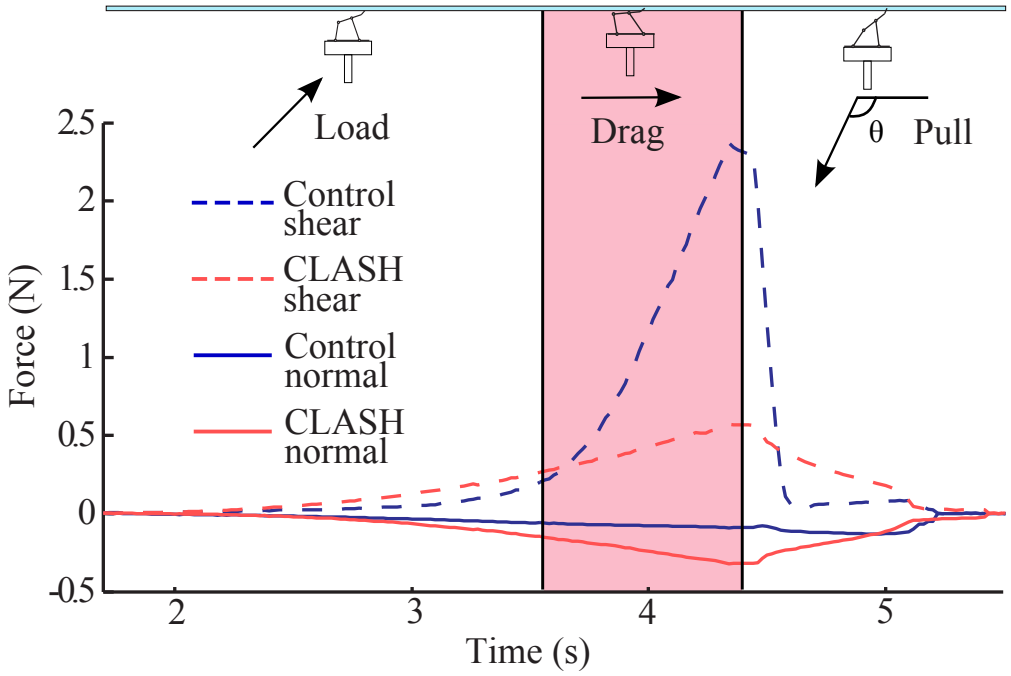

Figure 4.6: An example plot of shear and normal forces during a simulated step for the CLASH and control foot. Note the larger normal engagement force and faster disengagement of the CLASH foot.

An example load-drag-pull cycle for the CLASH foot and the control foot (Figure 4.6) shows that during the load phase, the claws start to engage the cloth, and the shear and tensile normal forces increase. For the CLASH foot, the four-bar mechanism hooks and pulls against the fabric causing a larger tensile normal force than the control foot. During the drag phase, the foot engages further with the cloth. Since the control foot is very stiff, it experiences a much higher shear force as the claws fully engage and the fabric pushes against the foot structure. During the pull phase, the CLASH foot disengages rapidly due to the four-bar mechanism, as is seen by a decrease in the normal force. However, as the control foot disengages, the normal force increases as the entire foot structure cannot bend to release as the CLASH foot can. Once the claws finally release, the foot rapidly releases the surface and the forces return to zero.

To compare the design of Figure 4.3 with the target retraction angle of $\phi = 120°$ determined by the analysis of the SLAP model presented in Section 4.1, normal pull-off forces were compared to the control foot at pull-off angles of 170°, 150°, 130° and 110° (Figure 4.7). At high angles ($\phi = 170°$), the control and CLASH foot both decrease rapidly, showing that the feet can easily disengage from the surface because the retraction angle corresponds approximately with the angle of the spines relative to the surface. However, for $\phi = 150°$ and $\phi = 130°$, the control foot cannot easily disengage from the surface like the CLASH foot can. This is seen as a large increase in the normal force during retraction of the control

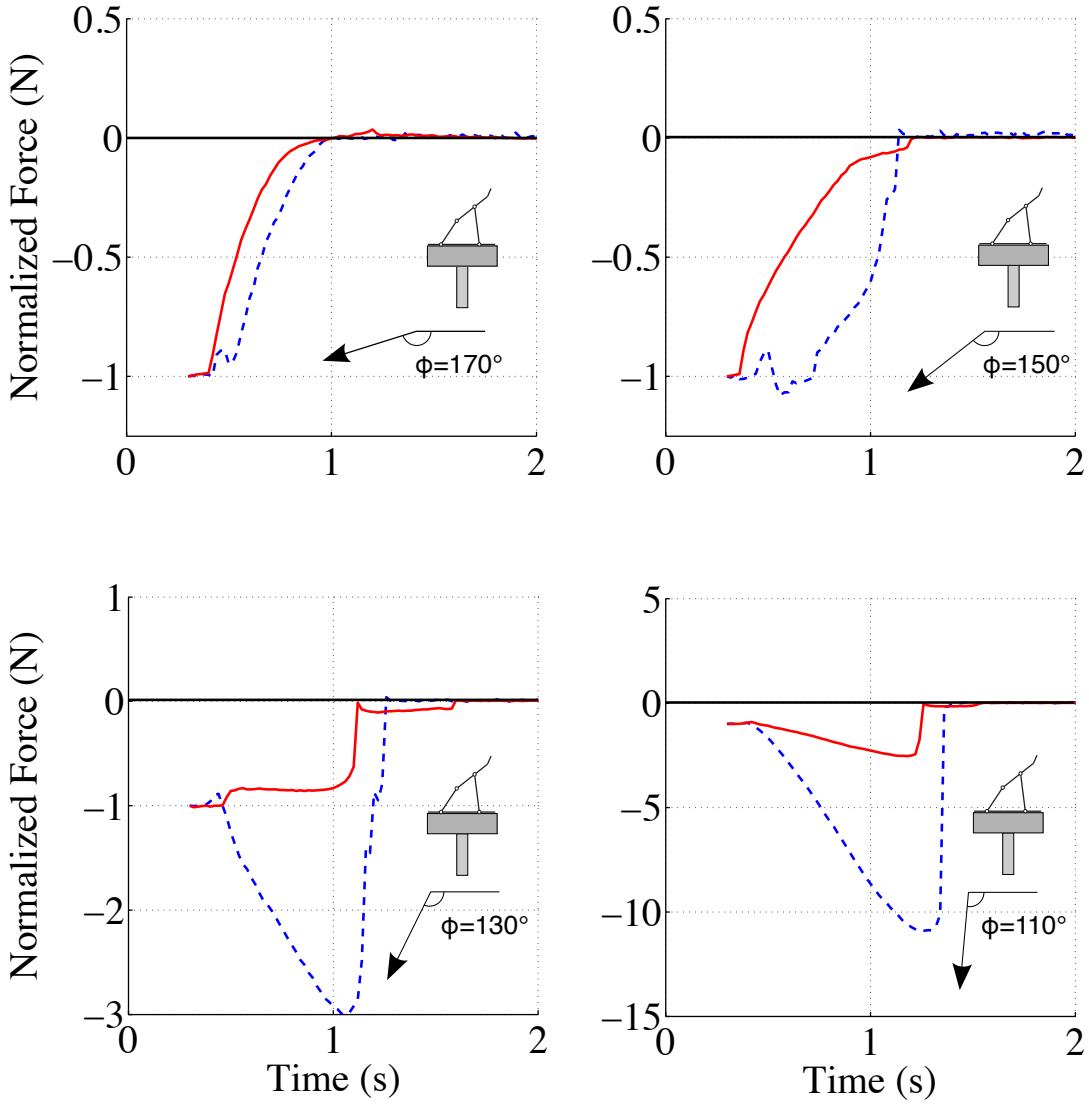

Figure 4.7: Normalized forces during the pull-off phase for the CLASH and control foot for a variety of pull-off angles. As the pull-off angle decreases, the control foot requires a large increase in the normal force to disengage, whereas the CLASH foot disengages with a much lower force, a trait necessary for effective climbing.

foot. Without the four-bar flexure in the CLASH foot, large normal forces are required to disengage the foot at low speeds, which makes climbing very difficult. When $\phi = 110°$, the CLASH foot still retracts more easily than the control foot, but it resists disengagement in

Table 4.1: Comparison of Comparable Climbing Robots Using Mechanical Engagement

	CLASH	SpinybotII [2]	Mini-Whegs [18]	RiSE v3 [34]	DynoClimber [16]	ROCR [65]
Size (cm)	10×10×2	58×27	8.9×5.4×3	70×51.5	40×11.6×7	46×31.1
Mass (g)	15	400	87	5400	2600	550
Mode of engagement	Spines	Spines	Velcro	Claw	Claw	Claw
Tested Media	loose cloth	brick, stucco	rigidly-backed fabric	wooden pole	carpeted wall	carpeted wall
Vertical Speed (body-lengths s^{-1})	1.5	0.04	0.28	0.3	1.5	0.34
Number of Actuators[1]	1	7	1	9	2	1

[1]None of the robots presented above have demonstrated turning. CLASH would likely require an additional actuator to be able to turn.

order to continue to generate tensile forces to keep it on the surface until the retracting angle increases further.

4.3 Climbing Performance

CLASH was tested on a piece of cloth draped over the edge of a table, thus constraining it only along the top edge. Figure 4.8 shows frames from these trials where CLASH climbs up this loosely hanging cloth. In these trials, CLASH is not equipped with either rear legs or a tail. On this vertical cloth, CLASH achieves a forward velocity of approximately 19 cm/s, though its vertical velocity up the cloth is approximately 15 cm/s. These correspond to 1.9 and 1.5 body-lengths per second, respectively.

CLASH was also tested on fabric draped over a cushioned surface with an incline varying from 85° and 90° above horizontal. In these trials, CLASH was equipped with stiff leg design from DASH on the rear hips, neither with any engagement mechanism. The front four legs were equipped with the four-bar foot mechanisms. CLASH was also given a passive, rigid tail to which the electronics were mounted. In these trials, CLASH was able to achieve vertical velocities of approximately 24 cm/s.

4.4 Discussion of Results and Conclusions

CLASH achieves a vertical climbing rate of 15 cm/s on loose cloth and 24 cm/s on near-vertical draped fabric, velocities that are comparable to the current fastest legged climbing robots when normalized by body length [54]. To the authors' knowledge, this is the first robot capable of climbing loose cloth, and its speed is comparable to DynoClimber which had set the current benchmark for vertical climbing when normalized by body length [54]. CLASH only requires the four-bar foot mechanisms on the front and middle legs to achieve climbing, and thus the rear hips can be equipped with stiff, oar-like legs originally used in the DASH design [8].

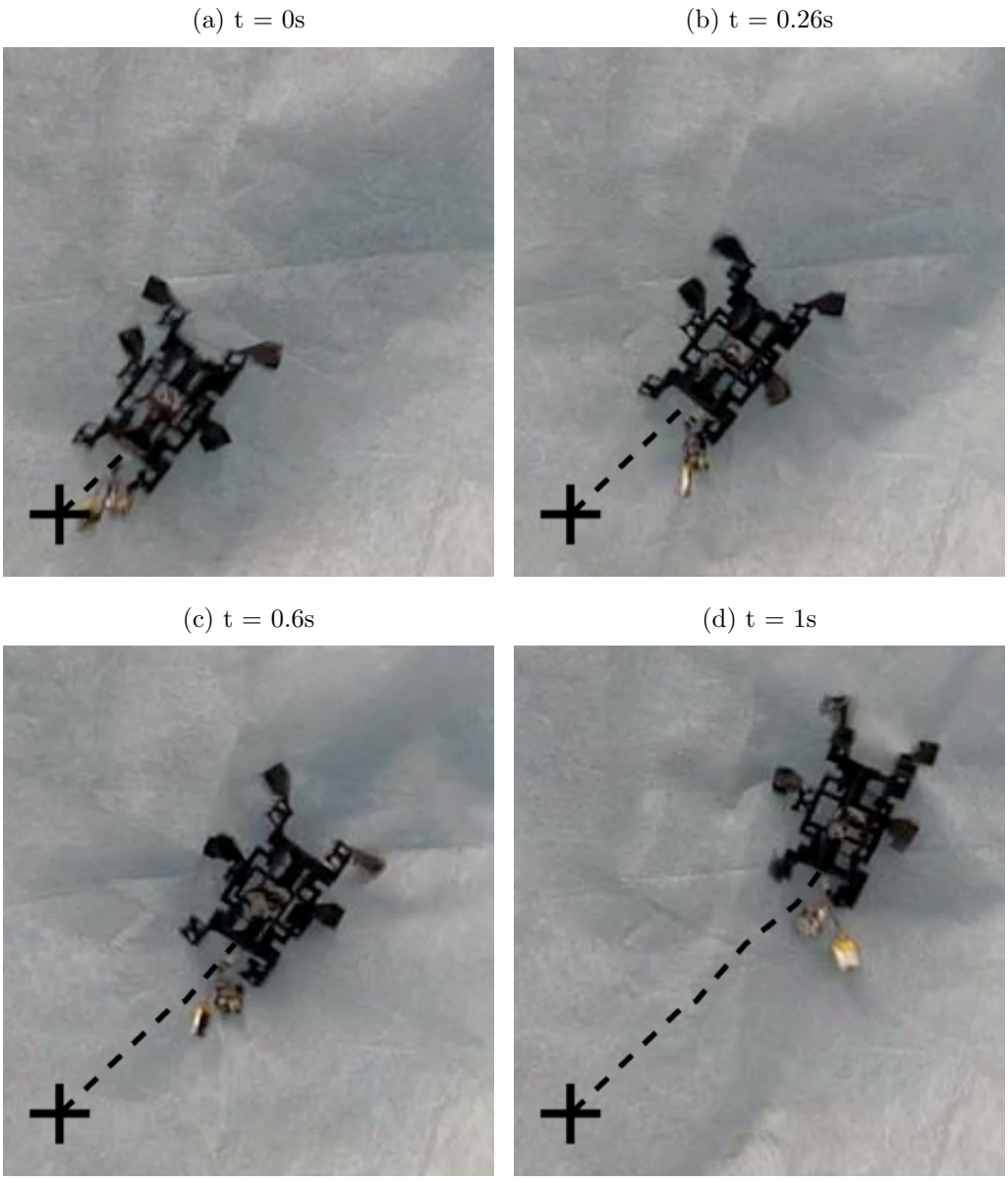

Figure 4.8: A sequence of frames from a video of CLASH climbing a loose vertical cloth demonstrating vertical climbing at 15 cm/s.

Figure 4.7 shows that the passive foot design of CLASH provides both enhanced tensile forces during stance and lower pull-off forces relative to the maximum tensile force during stance over the control foot. The foot increases the range of possible pull-off angles of the foot from the surface when compared to the rigid control foot. The retraction angle of the foot from the cloth surface not only depends on the leg trajectory and cloth curvature, but it also depends on the forward velocity of the robot. The motion of the foot relative to the

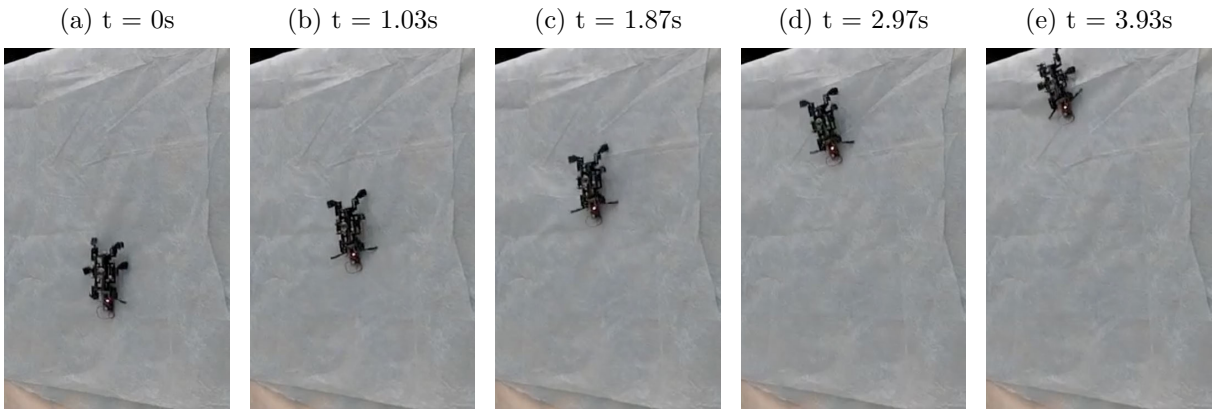

Figure 4.9: A sequence of frames from a video showing CLASH climbing rigidly-backed cloth climbing at approximately 9.5 cm/s.

ground is the difference between the foot motion relative to the body and motion of the body relative to the ground. Therefore, if the robot is climbing more slowly, the pull-off angle will be closer to vertical. However, when moving quasi-statically, the system has periods when both tripods are in stance and thus decreases the likelihood of failure by falling off of the surface.

Numerical simulations of the SLAP model with stiffness parameters similar to those measured in CLASH suggest that high-speed runs with a clock-based controller result in foot retraction angles of approximately $\phi = 120°$. This gives the system sufficient time to generate tensile forces to bring the system back toward the surface for the next engagement. The four-bar foot presented in this chapter enables easy retraction at relative angles $\phi \geq 130°$, a value close to that recommended by the SLAP model.

A control foot is tested and yields low pull-off forces when the pull-off angle ϕ is aligned with the spines and thus nearly parallel to the surface $\phi = 170°$. However, it generates large pull-off forces once ϕ decreases. The four-bar foot mechanism presented in this chapter allows low pull-off forces for the desired angles $\phi \geq 130°$. For angles $\phi \leq 110°$, the foot mechanism requires much more tensile normal force to move through the geometric singularity for easy retraction, enabling the foot to sustain large tensile normal at these angles. Being too easily removed could also make climbing difficult as it may not permit the robot to generate the required normal forces to overcome the gravitational pitching moment. However, as the foot mechanism is withdrawn at angles $\phi \leq 110°$, as would be the case when falling down the surface, the mechanism resists retraction and generates significant tensile normal forces. The foot design in CLASH does not use multiple actuators to disengage, such as seen in SpinybotII or RiSE, and does not require rigid, flat surfaces as with DynoClimber, MiniWhegs, or WaalBot II.

CLASH with claws does not climb as well as predicted by the SLAP model for several reasons. First, despite demonstrating easy retraction for most strides, there are occasions

when either the spine doesn't retract or another feature on CLASH becomes ensnared in the climbing surface. Redesigning CLASH to remove sources of these unintended grasps of the surface would improve performance. Also, when the tension in the fabric is low due to lightweight cloth and short cloth lengths, the force required to extract the spines from the cloth can be sufficient to pull the cloth up with the foot rather than extract. In this case, forward progress is impeded because not every stride results in a touchdown further up the climbing surface.

Because CLASH can use rigid rear limbs, future work will try to use these rear legs to maintain horizontal running performance. Initial observations do not suggest dramatic improvements in climbing performance with the inclusion of a tail. The design allows room for tails, and the electronics may be moved to the tail to allow for lower and more posterior center of mass. Future work should explore the use of tails to determine their utility in stability and turning, as suggested by biological studies [42].

The coauthors of this work created the apparatus required to perform simulated steps and record force data during those steps using the claw foot mechanisms. The coauthors also generated some the figures of this experimental setup as well of the data collected for the foot performance.

Chapter 5

Running Up Hard Vertical Surfaces

This chapter presents work enabling CLASH to climb hard, smooth, near-vertical surfaces using externally developed gecko-inspired adhesives. While climbing cloth as in Chapter 4 presents challenges associated with an unstructured surface, the penetration-based engagement mode is straightforward and the surface compliance reduces normal ground reaction forces at foot impact. We present the design of a remote-center-of-motion ankle (RCM) which allows the foot to passively conform to a surface in the roll degree-of-freedom with low work performed on the foot. Although this structure provides roll conformation, it is rigid to loads in the fore-aft direction. This creates an effective coupling between the adhesive and the COM. A compliant support with an elastic tendon introduces a degree-of-freedom that enables pitch conformation to the surface. Controlled loading experiments demonstrate that the ankle is capable undergoing large deformations to achieve conformation with the climbing surface without significantly effecting the maximum available adhesion possible from the adhesive. Climbing experiments were conducted which demonstrate climbing with significant sagittal-plane dynamics on near-vertical surfaces. A simple foot-impact model was created to understand the robot's inability to climb vertical surfaces. CLASH equipped with the RCM ankle and gecko-inspired adhesive is shown in Figure 5.1. With the RCM ankle, gecko-inspired adhesives, tail, electronics and a 60 mAh lithium polymer battery, CLASH has a mass of 19 grams.

5.1 Leg and Ankle Design

The kinematics of the hips in CLASH dictate that the legs move through an elliptical path during locomotion with significant yaw and roll deflections on the legs as described in Chapter 3. If an adhesive foot were rigidly mounted to the end of a simple leg as in Figure 5.2a, the yaw displacement would result in the adhesive twisting and shearing at the ground contact and likely result in failure of the adhesive. To remove this yaw deflection of the foot, a simple parallel four-bar leg structure is introduced. The leg structure, as seen in Figure 5.2b, enforces the constraint that the foot remain parallel with the orientation of the robot.

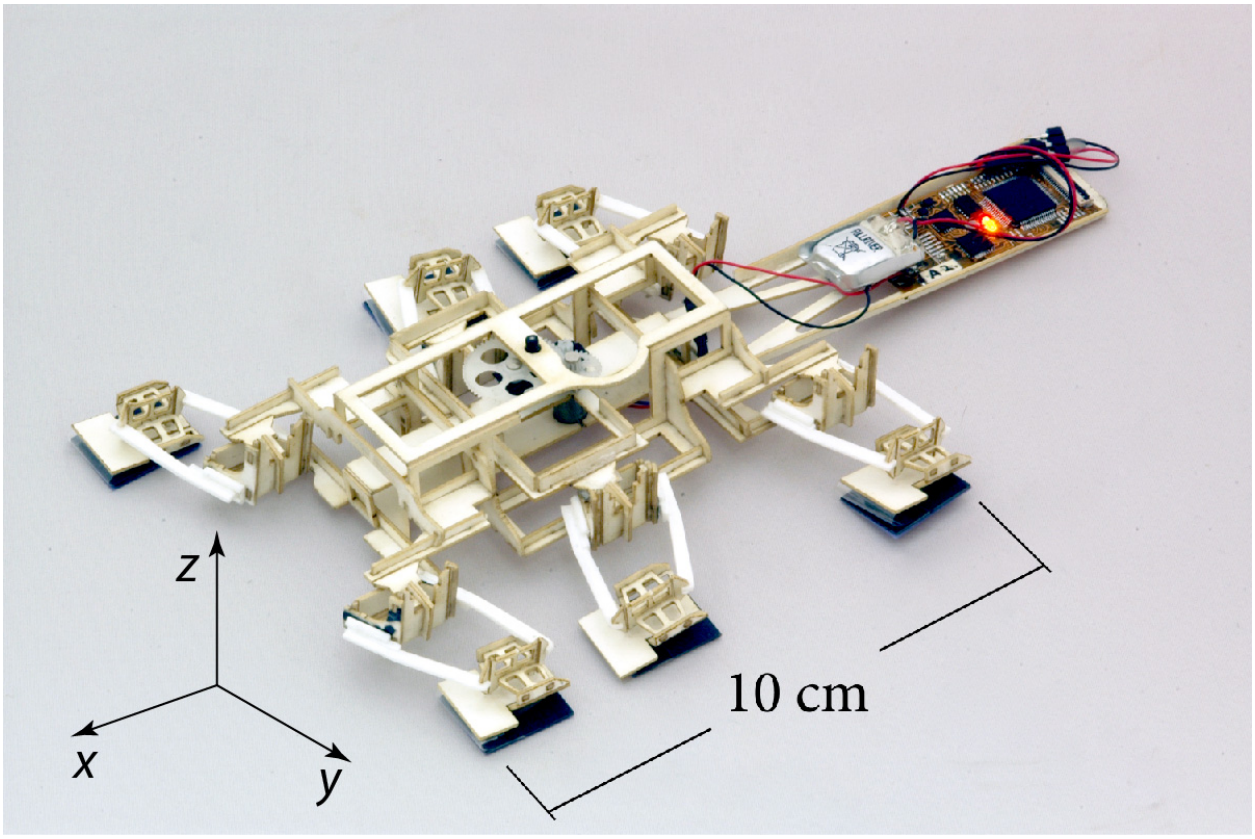

Figure 5.1: CLASH equipped remote-center-of-motion ankle that enables dynamic climbing of near-vertical smooth surfaces.

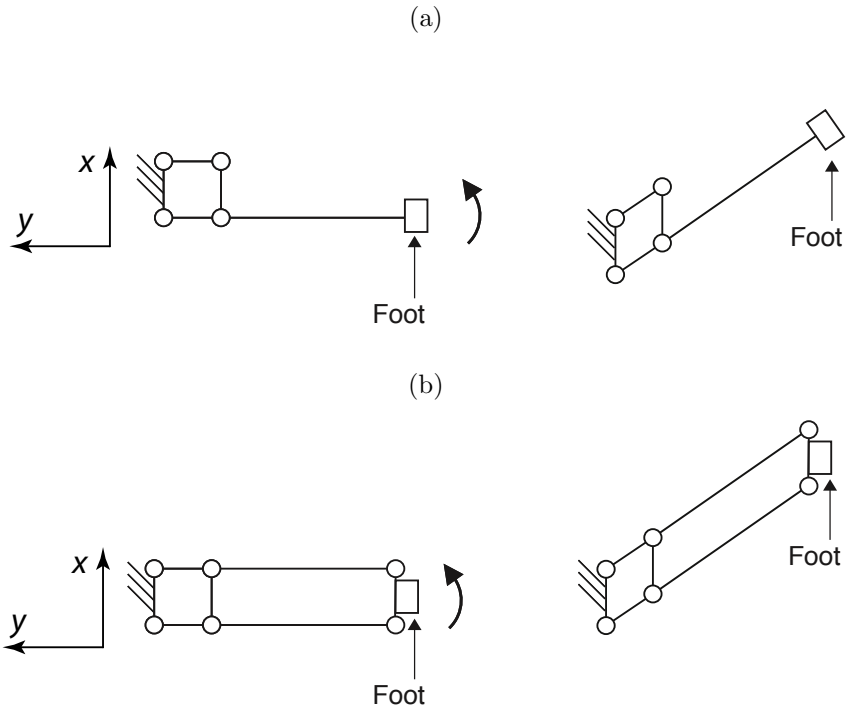

Figure 5.2: The claw-equipped CLASH used a traditional oar-like leg that goes through significant yaw deflections during stance (a). A four-bar leg linkage is used to keep the foot oriented parallel to the body and reduce twisting of the adhesive on the surface (b).

During climbing, the foot will approach the surface with a range of roll and pitch angles due to leg rotations dictated by the CLASH transmission as well as variable surface angles and body orientations during climbing. Figure 5.3 shows an ankle that allows the foot to roll relative to the leg, allowing the foot to adapt to a range of roll angles during touchdown and stance. The design is based upon an isosceles trapezoid four-bar mechanism that creates an instantaneous remote center-of-motion at point O in Figure 5.3a [87]. The RCM of the ankle is designed to be near the surface of the adhesive (Figure 5.3b). This allows the adhesive to not translate laterally as it is rotates into alignment with the surface. If the center-of-motion were above the surface, the adhesive would slide laterally along surface for the foot to rotate into alignment. Alignment without translation is crucial to achieving passive alignment. Without an actuated ankle, the work required to do this translation would prevent alignment and engagement of the adhesive.

Another critical reason for the ankle RCM to be at the surface is to prevent peeling moments from disengaging the foot during the stroke. Having the ankle rotation axis coplanar with the surface prevents a peeling moment from arising, and therefore full contact is always retained between the foot and the surface [33, 83].

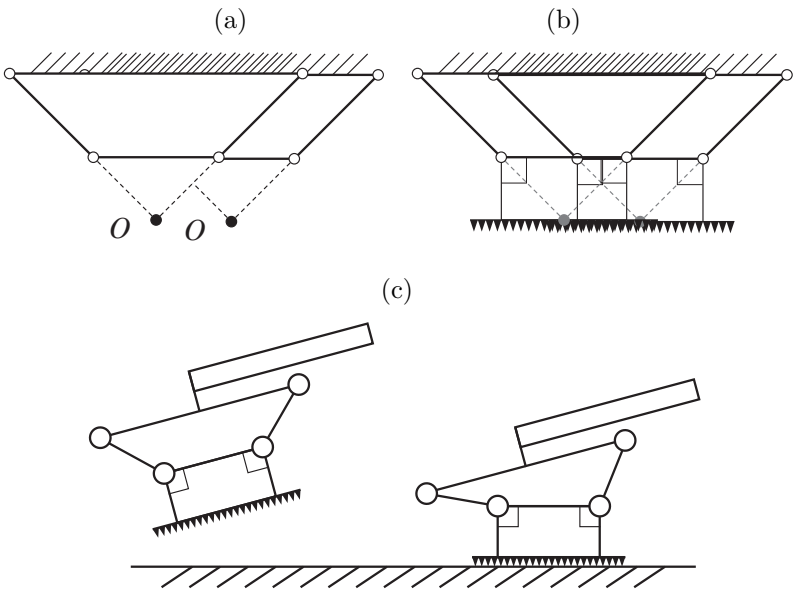

Figure 5.3: (a) The ankle is an isosceles-trapezoid four-bar that creates a remote center-of-motion at O. (b) The remote center-of-motion is designed to be at the bottom of the adhesive. (c) This mechanism allows the foot make coplanar contact with the surface and reduces roll peeling moments.

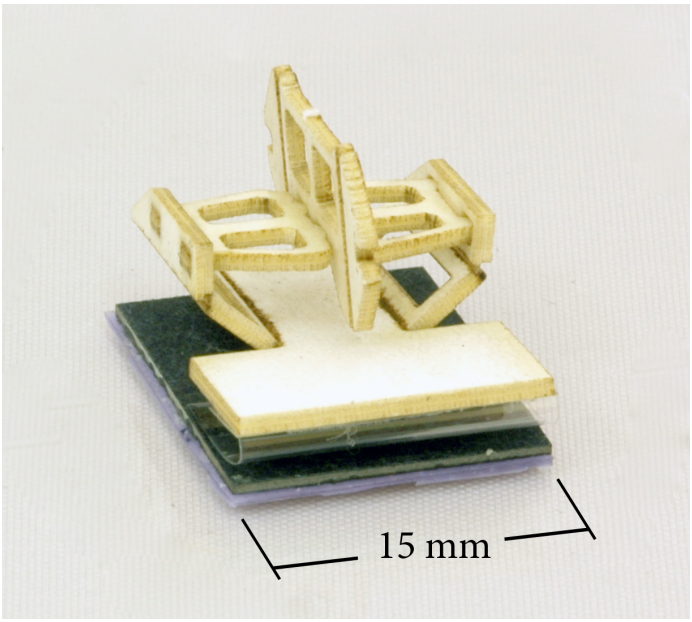

Figure 5.4: The gecko-inspired adhesive foot and RCM ankle joint.

5.2 Adhesive Foot Design

5.2.1 Gecko-Inspired Adhesive

Gecko-inspired adhesives have been proposed for use in all-terrain robots due to their ability to adhere to a variety of surfaces in a controllable manner conducive to climbing [50, 53, 61]. Specifically, gecko-inspired adhesives allow for modulation of normal adhesive force through the application of a shear force, which facilitates easy detachment of the feet at the end of the stroke [29]. Such a gecko-inspired adhesive was leveraged in this work.

The adhesive created in the Biomimetic Millisystems Laboratory and used in CLASH is explained with permission from Gillies [7] to understand the performance and constraints of the adhesive. The adhesive consists of an 18x15 mm pad of microfabricated PDMS ridges, using techniques similar to those developed by Sitti [78] and Hawkes *et al* [33]. The ridges, seen in Figure 5.5, measure 80 μm wide by 330 μm high, and are spaced 300 μm apart.

The adhesive performance of the microridge adhesive was determined using a custom force displacement apparatus in a manner previously discussed in Chapter 4. Rigidly mounted adhesive samples with two different patch sizes (10×10 mm and 15×18 mm) were tested with a simulated load-drag-pull step under displacement control at speeds ranging from 1 mm/s to 20 mm/s. Figure 5.6a shows force versus time for an example trial of one foot. Engagement starts with a pre-load of the patch, followed by dragging the patch into a sheared state. Once the patch is sheared, the foot is pulled to a normal tensile force that will keep

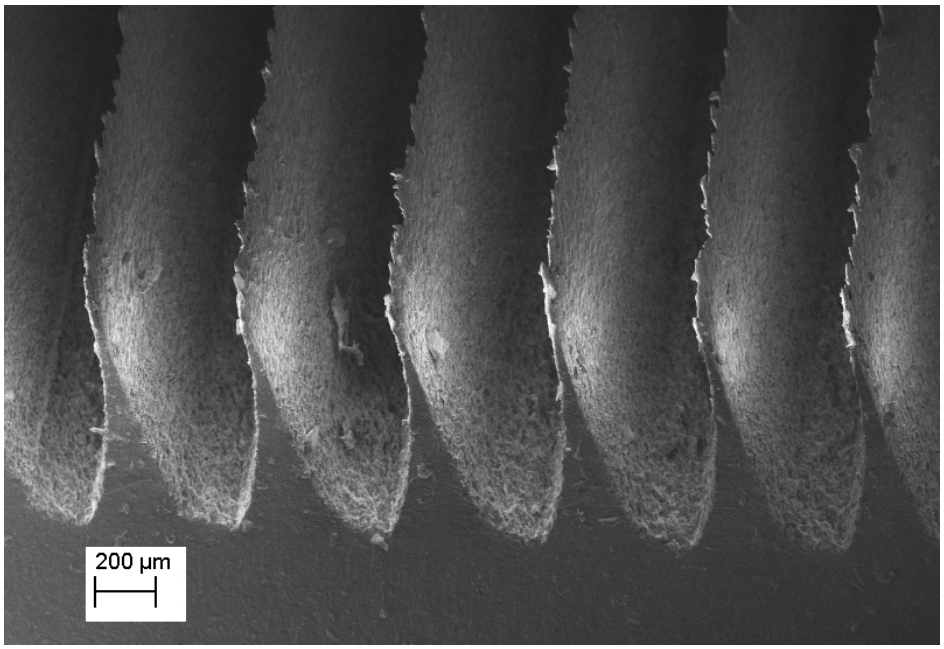

Figure 5.5: An image of the gecko-inspired adhesive taken from a scanning electron microscope.

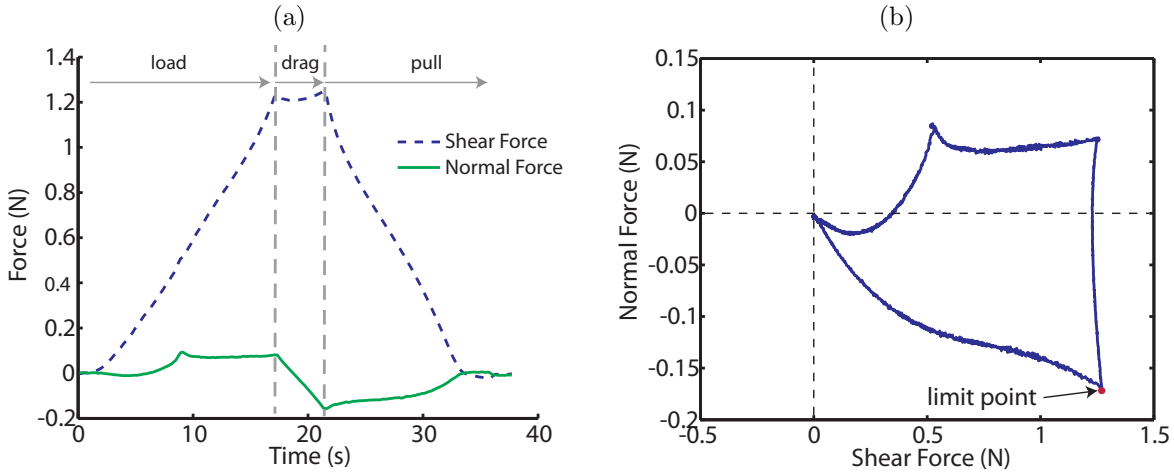

Figure 5.6: (a) Force versus time of the gecko-inspired adhesive foot undergoing a load-drag-pull simulated step at 1 mm/s. (b) The same load-drag-pull step in force space showing the limit point of the gecko-inspired adhesive foot.

the robot adhered to the surface during the stroke. Once the stroke is completed, the shear force is released and the normal force returns to zero, facilitating easy removal of the patch and the end of the stroke. Figure 5.6b shows the example trial in force space. Noteworthy is the lowest normal force maintained while under shear. Drawing a line from the origin to this point gives the lower limit surface of the adhesive, which acts as a useful tool to determine if the adhesive will be able to hold the robot to the surface. In practice, the adhesive should be able to maintain contact with the surface as long as loads placed on the foot are within this limit surface.

Figure 5.7 plots the limit surface for the flat-mounted adhesive. The best flat samples maintain 0.4 N of tension under 1 N of shear, giving a $\tan\alpha = 0.4$ as defined in Figure 2.4. The adhesive is able to maintain loads far in excess of the robot weight; up to 1 N of shear force compared to 0.19N robot weight, giving a safety factor of 5 for a single foot in contact. This safety factor is critical for rapid climbing, because the adhesive pads must also withstand the dynamic forces of the robot. Engagement and adhesion were noted to be independent of step velocity which is another necessary attribute for rapid vertical climbing.

5.2.2 Effective Loading

Given the performance of the adhesive detailed above, the engineering challenge becomes utilizing the adhesive to its fullest extent to maximize possible climbing performance. The adhesive is rigidly mounted on an SCM-compatible cardboard backing and attached to the ankle by a thin latex strip and a thin polymer loop, as seen in Figures 5.4 and 5.8. A rigid backing is chosen because it transfers the load evenly across the adhesive. The latex strip and thin polymer loop are designed so that during loading, the polymer loop complies in the

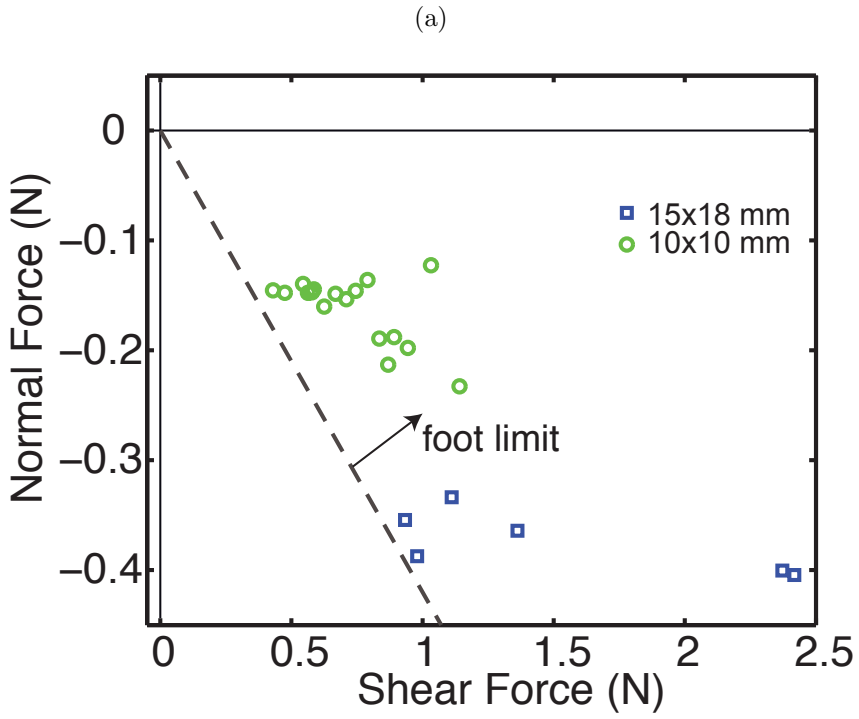

Figure 5.7: A plot of the limit surface of 10x10mm samples (green circle) and 15x18mm adhesive samples (blue square).

normal and pitch direction in a manner that promotes engagement of the adhesive pad. This normal and pitch compliance work in conjunction with the previously mentioned four-bar ankle to allow the foot to make coplanar contact with the surface, while preventing peeling moments from disengaging the foot during the stroke. Coplanar contact is important to engage all of the terminal features of the adhesive.

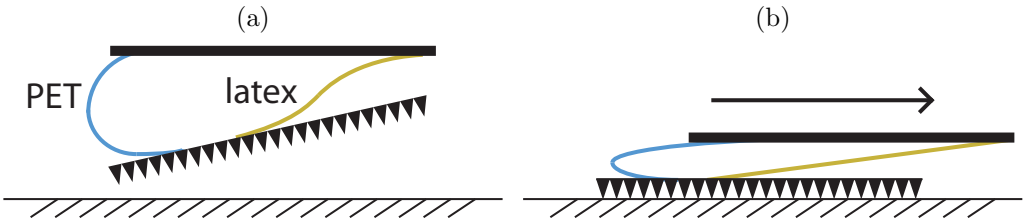

Figure 5.8: Side view of the CLASH foot. (a) The polyethylene terephthalate polymer loop offers a compliant constraint that keeps the rigidly-backed adhesive attached to the RCM ankle but complies in the normal and pitch directions. (b) When loaded, this polymer loop shears with high compliance, allowing the latex tendon to bear most of the load during stance.

Once engaged, the adhesive pad is loaded through the latex strip, which is mounted low and near the center of the adhesive pad, and acts as a tendon in a similar manner to the foot designed by Hawkes *et al* [32]. Attaching the tendon low results in a low pitching moment, and mounting it near the center ensures symmetric loading on the patch to prevent other peeling moments. Under loading, the thin polymer strip unfolds to ensure it does not apply a peel moment to the foot and the latex strip stretches. This stretching is important because due to the dynamics of the running robot, the legs undergo kinematic oscillations and impulses. Without the compliance of the tendon, these rapid kinematic motions would quickly overload the adhesive capabilities of the foot, and the robot would fall. This stretching also allows the robot to catch a slip or arrest a fall by accelerating the system from free-fall over a larger time and distance, once again ensuring that the adhesive pad is not overloaded.

5.3 Results

5.3.1 Foot Performance

The goal of the RCM foot presented in Sections 5.1 and 5.2 was to create a complementary set of mechanisms that enable a foot to rapidly align with a surface and effectively utilize the gecko-inspired adhesive outlined in Section 5.2.1. Figure 5.7 demonstrated the maximum

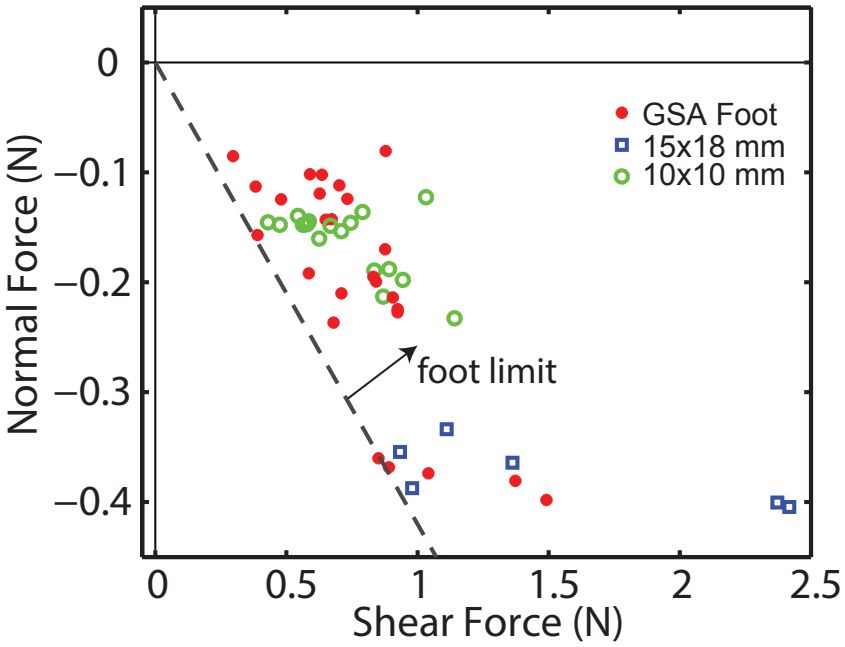

Figure 5.9: A plot of the limit surface of 10x10mm samples (green hollow circle), 15x18mm adhesive samples (blue square) and gecko-inspired adhesive feet (red filled circle).

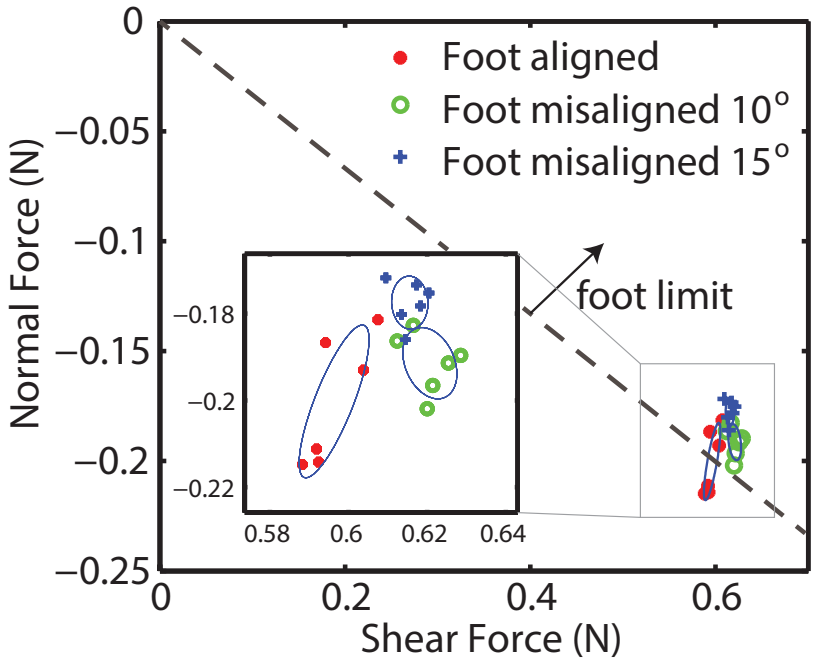

Figure 5.10: (a) A plot of the performance limit of a foot aligned to the test surface and misaligned by 10 and 15 degrees. (b) A plot of the performance limit of 10x10 mm samples (green circle), 15x18 mm adhesive samples (blue plus) and gecko-inspired adhesive feet (red star).

performance observed in the gecko-inspired adhesives when all surfaces are manually aligned. When adding the RCM ankle and the tendon loading mechanisms, the total foot adhesion possible is shown in Figure 5.9. Here, the best foot maintains 0.37 N tensile with a 0.9 N shear load, which corresponds with $\tan\alpha = 0.41$. This indicates that the ankle is successfully able to limit the peeling moments on the adhesive that might otherwise cause the foot to disengage at lower normal forces.

5.3.2 Climbing Performance

Figure 5.10 shows the performance of the ankle when intentionally misaligned with the surface prior to a load-drag-pull test. The foot is able to maintain loads even when engaged under a severe roll misalignment of 10 and 15 degrees. Under these misalignments, the generated normal adhesion drops less than 10% from the aligned feet. This is also important because due to the rapid motion of the legs and variation in the gait, the feet must be able to maintain an adhesive force even under severe misalignment.

For the climbing trials with the gecko-inspired adhesive feet, a large plate of smooth acrylic is used as the climbing surface. Starting at an incline of 30 degrees above horizontal and incrementing the angle by 10 degrees, CLASH is operated at a range of frequencies to

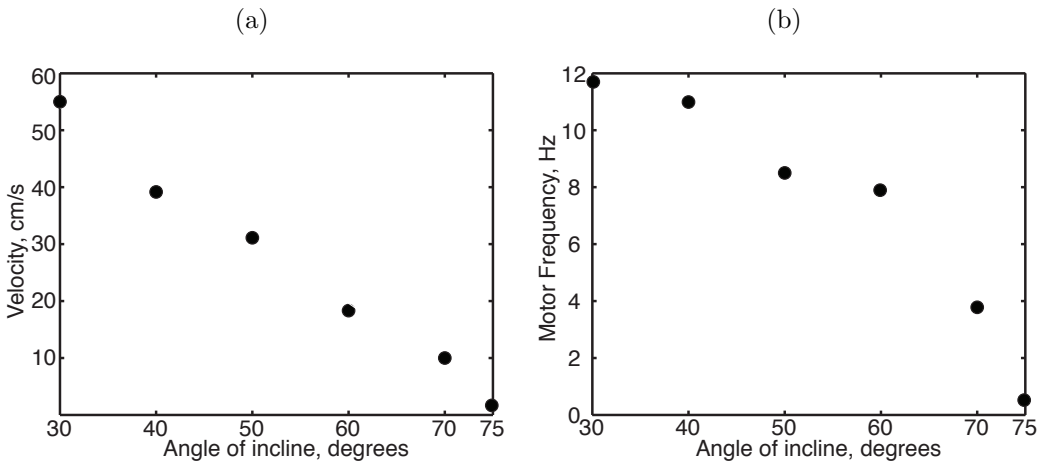

Figure 5.11: (a) The maximum climbing velocity achieved at a given angle of the smooth acrylic above horizontal. (b) The stride frequency of the robot when it was climbing with the maximum achieved velocity.

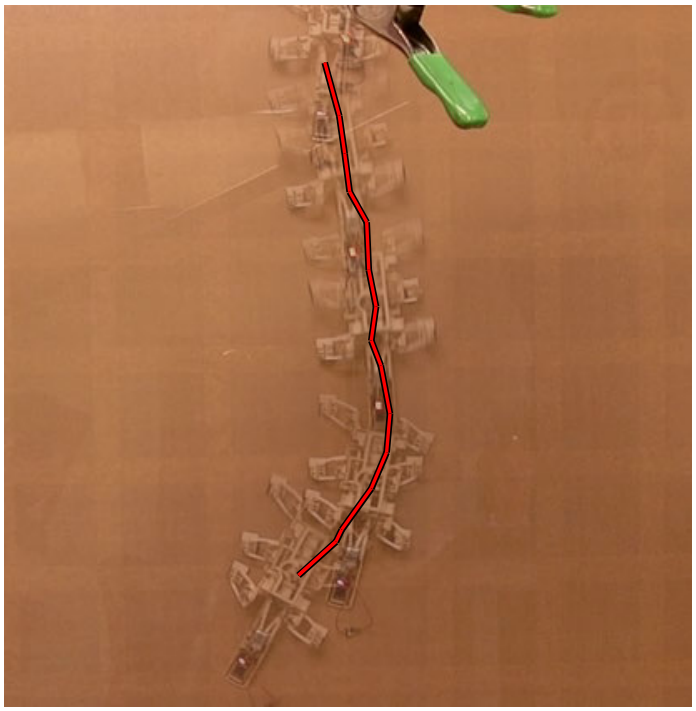

Figure 5.12: Superimposed frames of CLASH climbing a 70 degree incline slope at 10 cm/s. The robot had an initial yaw offset but passively corrected its heading during the climb.

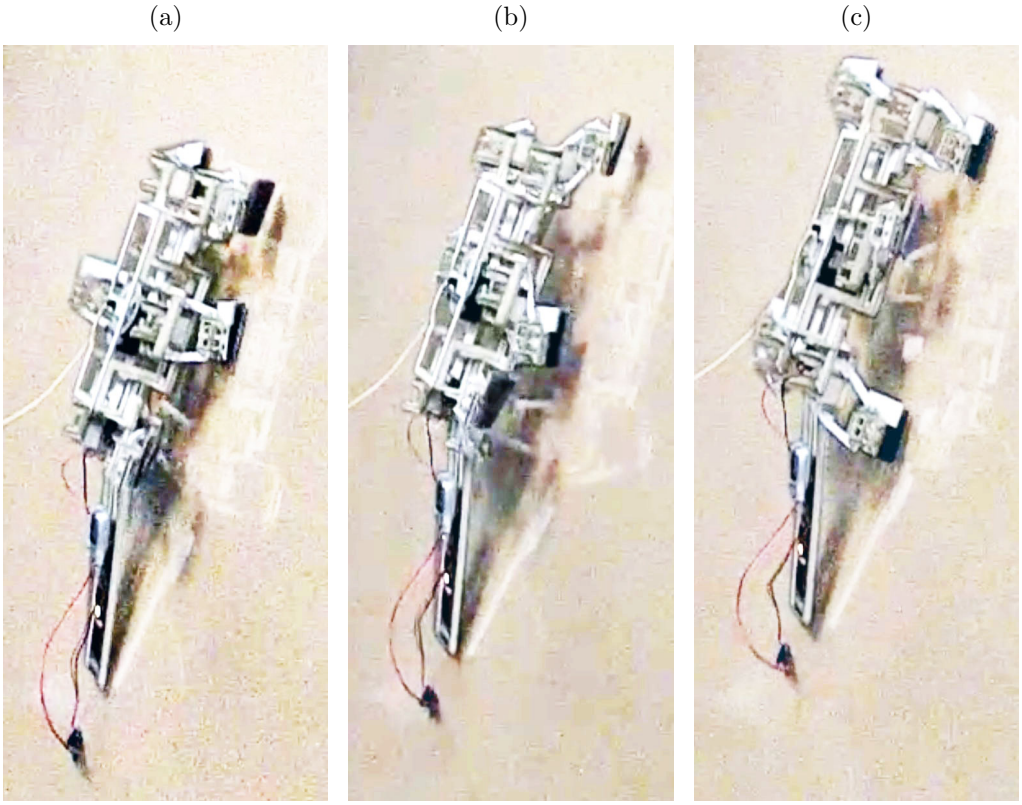

Figure 5.13: Contrast-enhanced frames from high-speed video of CLASH climbing a 70 degree incline at 10 cm second^{-1} showing (a) one leg tripod touching the ground, (b) an aerial phase, and (c) the second leg tripod touching down.

determine a maximum climbing velocity. The maximum climbing velocity and the stride frequency associated with that velocity are shown in Figure 5.11. CLASH achieves speeds above 10 cm second^{-1} up to an incline of 70 degrees (Figure 5.12). Failure to climb an 80-degree incline prompted trials at 75-degree incline to better determine the current limitation of the system. At 75 degrees, CLASH climbs at approximately 1 cm second^{-1}.

Figure 5.11a shows that the maximum velocity decreases approximately linearly as the incline increases. However, the frequencies associated with these velocities have a nonlinear inverse relationship with the incline angle.

While climbing up near-vertical inclines, CLASH exhibits a gait with small aerial phases. Figure 5.13 shows an aerial phase during 10 cm second^{-1} climb up a 70-degree incline from a high-speed video. To the author's knowledge, this is the steepest climbing to exhibit aerial phases or significant sagittal-plane dynamics. Even at these fast operating frequencies and aerial phases, the feet provide rapid reengagement with sufficient adhesion and shear force to continue climbing.

5.4 Discussion of Results

The SLAP model of Chapter 2 demonstrated that only a small space of parameters for a system with body mass, leg length, and adhesive properties similar to those of the robot in this chapter can result in high-speed, stable climbing. The torsional and linear stiffness of the system presented here are near but outside of that successful space. Indeed, to improve climbing speed over a significant space of parameters in the SLAP model with the adhesive properties demonstrated in Section 5.2.1, the engagement problem had to be relaxed by decreasing the angle of the surface below vertical.

The SLAP model predicts faster climbing than observed in CLASH despite the latter climbing on inclines. Designed to be the simplest model that captures the body dynamics and ground reaction forces seen in geckos when climbing dynamically, SLAP neglects some of the non-idealities present in the physical CLASH system. As mentioned in Chapter 3, the COM dynamics that result from the operation of the CLASH transmission have been significantly mitigated but have not been removed entirely. The measured out-of-plane accelerations of the COM increase the normal load required by the feet. The model also assumes initial conditions with some initial fore-aft velocity while the robot trials all start from a resting state. The addition of a Buehler-clock enabled the SLIP model to stably accelerate from rest [73], suggesting a route for future work which might inform how to stably progress from a resting state to dynamic climbing. A failure from the dynamics during such a transition could also prevent the study of steady-state climbing in the robot.

The SLAP model also makes the assumption that the feet of the system have negligible mass relative to the total system mass. The RCM ankle and feet mechanisms presented here for aligning the adhesive with the surface add 4 grams to the total system mass and represent more than one quarter of the total system mass. To gain a better understanding of the effect of non-negligible foot mass on system dynamics, a simple model of the robot using a spring-mass-damper system (Figure 5.14a) was developed to explain the maximum climbing velocity dependence on surface angle observed in Figure 5.11b. We assume that at the instant one tripod leaves the ground, the second tripod is traveling towards the surface with some initial velocity, $\dot{x}_o$, with the mass of robot, m, and stiffness and damping, k and c representing the overall stiffness and damping of the transmission and legs. Using $\tau = \frac{k}{c}t$, $\hat{x} = k^2/gc^2$, $\dot{\hat{x}} = \frac{k}{gc}\dot{x}$ and $\ddot{\hat{x}} = \frac{1}{g}\ddot{x}$ to non-dimensionalize the terms, this system can be described by the following ODE:

$$\ddot{\hat{x}} = -\frac{c^2}{km}\hat{x} - \frac{c^2}{km}\dot{\hat{x}} + cos(\theta) \tag{5.1}$$

Once solved, this reveals the well-known damped oscillation seen in Figure 5.14b. Of importance for dynamic climbing is the point of maximum outward force on the mass system caused by the robot "bouncing" off the wall. This maximum outward force increases monotonically with the initial inward velocity of the mass, $\dot{x}_o$, which is correlated with the overall running speed. If this maximum outward force overcomes the maximum normal adhesion of the feet, they will detach from the wall and the robot will fall. Thus, as the robot velocity

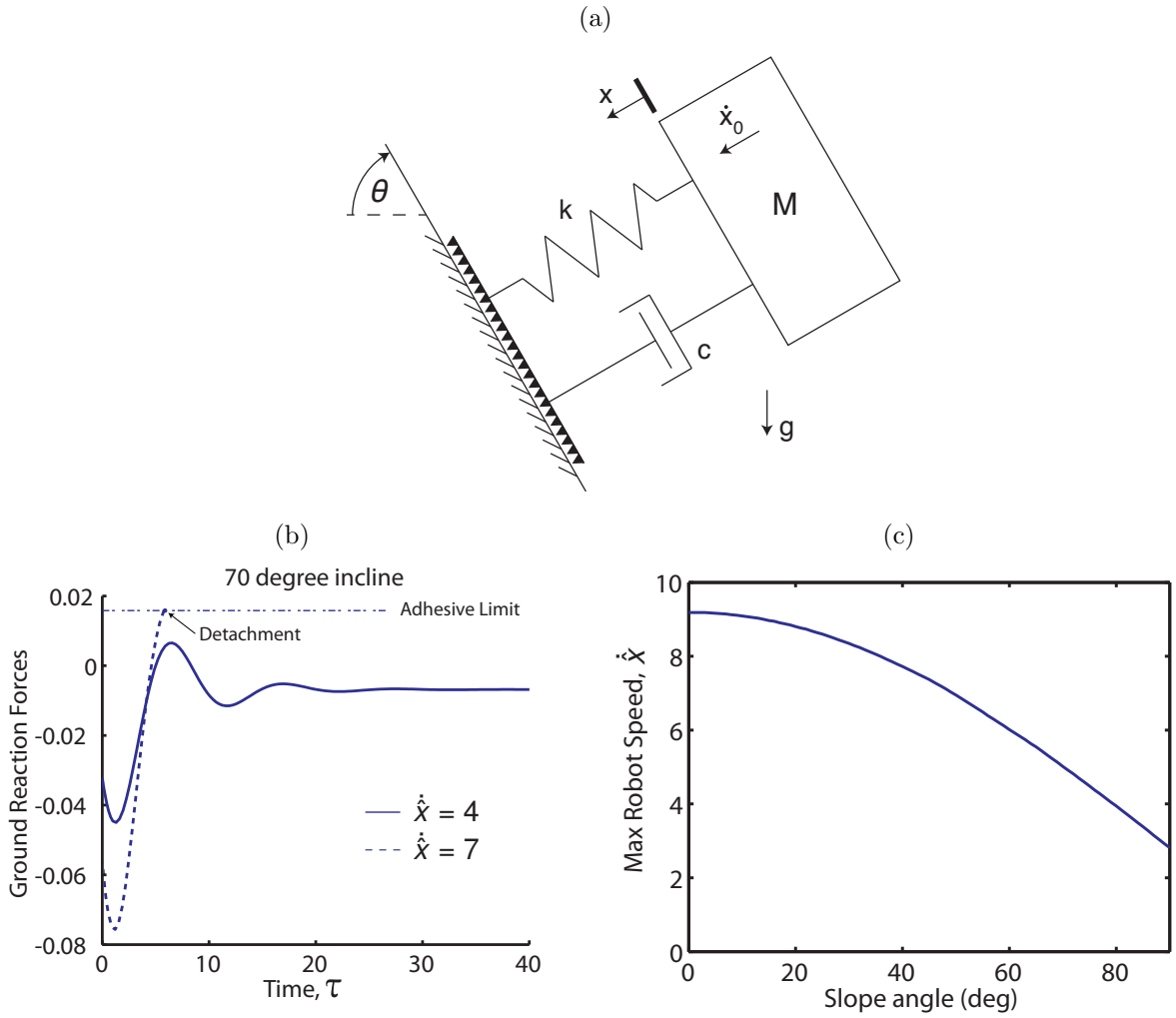

Figure 5.14: (a) Model used showing robot mass, m, and leg stiffness and damping, k and c, at the instant a tripod contacts the ground. (b) Non-dimensionalized impact forces upon touchdown for two different running speeds, with one resulting in loss of contact. (c) Given a certain maximum adhesive force, the climbing velocity, $\hat{x}$, must decrease as slope increases to maintain contact with the wall.

increases at a given angle, it will reach a threshold where the robot will bounce and fall off the wall. For the above analysis, a maximum normal adhesive is given by the product of the body weight with the normal-to-shear ratio $\tan\alpha = 0.4$ found from the data of Figure 5.9.

This threshold is less critical at lower angles, where the component of gravity into the surface is large, and helps to maintain foot contact with the wall. However, as the slope angle increases, the contribution from gravity is reduced, and the threshold is reached at a lower velocity. Figure 5.14c shows that given a certain maximum adhesive force, the climbing velocity must decrease as surface angle increases to maintain contact with the wall.

This model also shows the importance of tuning the robot stiffness and damping. If the robot is too stiff or underdamped, the wall reaction forces become much larger, and the adhesive limit is overcome at much lower velocities. The stiffness parameters here are fundamentally the same as those used in the SLAP model presented in Chapter 2 and could be combined in a climbing model with adhesive feet with non-negligible mass.

5.5 Conclusions

Although measured foot adhesion forces should theoretically be great enough to prevent detachment from the wall under ideal conditions (Figure 5.9), it is possible that the normal adhesion is not great enough to prevent pitch-back of the robot during vertical running, as evidenced during running experiments. Our analysis describes one such possible failure, where the impact velocity causes the foot to rebound off the surface. Since higher adhesive strength may prevent this, future foot designs will concentrate on improving the normal force capability of the adhesive. Increased adhesive strength has also been suggested to increase the space of leg stiffnesses which result stable climbing gaits in SLAP.

Another possible failure mechanism may be that the dynamics of high-speed running cause alterations in the gait which prevent the feet from properly engaging. Moving a massive foot on a compliant leg with intermittent ground reaction forces introduces unmodeled deviations from the unloaded quasi-static foot trajectories. This is a more challenging problem that may require more careful tuning of the foot-leg mechanism and more precise tracking data.

In addition to the failure to prevent pitch-back, CLASH could either fail to climb vertically due to either a power limitation or a shear force limitation, although there is evidence against both. The ability of CLASH to rapidly climb vertical loose cloth (Chapter 4) and magnetic surfaces (Appendix A) shows that the robot is not limited by the available power. Also, it does not appear that CLASH is limited by the available shear force. When single feet are mounted to a controlled stage, shear forces approach 1N, more than five times the weight of the robot (Figure 5.10a). When integrated into a climbing robot, the feet generate large shear forces when they rapidly arrest the falling robot on a near-vertical surface. The rapid arrest stretches the latex strip, reducing the instantaneous load on the adhesive and often keeping the load within the force limits. The ability of the latex to stretch during loading may also allow load-sharing between the feet, similar to the load sharing within a single foot demonstrated by Asbeck *et al* [2].

CLASH exhibits several interesting behaviors during climbing. CLASH is observed to be stable in yaw; CLASH repeatedly orients itself after a misstep introduces a yaw perturbation. CLASH was designed with most of the mass located toward the rear of the system, including the motor, battery, and electronics to create a stable body pendulum [17]. Serial compliance in the transmission allows the legs to quickly advance their phase and regain purchase if one tripod loses contact suddenly. This occurs because the forces on the feet load the serial compliance in the transmission, effectively creating a phase lag between the motor position

and actual leg position. A sudden loss of shear load releases the stored energy and accelerates the legs forward quickly and engages the next tripod sooner than otherwise.

This compliance also has the effect of reducing the stride length as the shear load due to gravity increases with increased incline. This variable stride length may explain why the velocity increases at a faster rate than the motor frequency as incline decreases (Figure 5.11); with a fixed stride length, they should increase at the same rate.

CLASH has an aerial phase during climbing at inclines up to 70 degrees. Aerial phases are not observed in other climbing robots, including DynoClimber and ROCR which largely ignore motions in the sagittal plane. When CLASH is tuned and adapted to vertical surfaces, it is expected to maintain an aerial or pseudo-aerial phase similar to those seen in geckos [3].

The limitations on stride frequency and thus climbing velocity from the model proposed in Figure 5.14c shows a strong behavioral correlation with the observed climbing velocity limitations in Figure 5.11b. The actual robot performance does not reach the limitations suggested by the model, likely due to unmodeled phenomena such as transmission dynamics, perturbations from missteps, or asynchronous foot touchdown or pull off. Also, there is an increasing risk associated with loss of contact as the incline increases for which the model does not account. At or near vertical, a failure due to a foot rebounding off of the surface will cause the robot to fail. A foot rebound at lower angles results in intermittent contact and less positive work on the system but is not catastrophic in the same sense.

The coauthors of this work created the gecko-inspired adhesive used for this climbing system, developed the apparatus required to perform simulated steps and record force data during those steps, and contributed to the design process and assembly of feet used by in the climbing experiments. The coauthors also generated figures used here showing the performance of the ankle design presented in this chapter.

Chapter 6

Conclusion

This work has explored the challenges of dynamic climbing with non-neglible dynamics in the sagittal plane through numerical dynamic models as well as through meso-scale robots. We developed the Spring-Loaded Adhesive Pendulum (SLAP) model, which builds upon the SLIP model by incorporating a clock-driven foot position that adds energy to the system and two different adhesive foot models. Climbing speed and body dynamics are explored for the different foot models, and the system is shown to be passively stable when climbing vertical surfaces. The SLAP model also exhibits dynamic running on an inverted surface. A clock-driven feed-forward position control exhibits passive stability when running on an inverted surface.

A novel meso-scale legged robotic platform is created to enable dynamic climbing on cloth and smooth acrylic. The CLASH platform uses a single DC motor to drive all six legs in a sprawled alternating tripod. The low profile of the system reduces pitching moments, and the internal dynamics were engineered to minimize out-of-plane accelerations to relax the loads on the adhesive. A passive spine foot was presented that generates sustainable tension during stance but disengages easily when retracted at the desired liftoff angle. This foot enables CLASH to climb loose and rigidly-backed cloth at speeds comparable to the fastest legged climbing robots when normalized to body-length. A remote-center-of-motion ankle with a synthetic gecko adhesive loaded via elastic tendon is presented and is shown to conform to a range of angles while maintaining nearly ideal performance of the adhesive. With this foot, CLASH was able to climb 70° acrylic at 10 cm/s while exhibiting significant sagittal-plane dynamics.

Prior to the work presented in this dissertation, all dynamic legged climbing models and dynamically climbing robots were designed to remove sagittal-plane dynamics from the design challenge. These models and systems have contributed greatly to the understanding of climbing dynamics, but ultimately robots that must navigate and climb obstacles in unstructured environments will not often encounter planar surfaces. Legged systems that use SLIP-like dynamics during horizontal locomotion may be able to modify their existing dynamics to scale vertical surfaces as well. For these systems or for those systems which must climb over uneven terrain, the understanding of sagittal-plane dynamics will be necessary

for success.

6.1 Future Work

Despite the progress presented in this dissertation toward generating robust climbing systems, further work is needed to create a foundation for future systems and models upon which further understanding and performance can be achieved when rapidly navigating surfaces with adhesive feet.

6.1.1 SLAP Development

The SLAP model of Chapter 2 is a new framework for furthering the understanding of sagittal-plane dynamics with locomotion modes that require adhesion for stable gaits, but its morphology is fundamentally similar to the SLIP and CT-SLIP models for horizontal locomotion. As such, some of the recent advances in the understanding of SLIP may be applicable to the SLAP model. The introduction of a Buehler clock to the SLIP model increased the range of stable operation and showed stability through transition from resting [73]. The inclusion of a Buehler clock to the SLAP model could bring the duty factor closer to 50% without significantly impacting the stance dynamics, making the system more directly comparable to available data on dynamic climbing in organisms. Adding mass to the feet or adding more detailed foot models might enhance the model's fidelity, although the added complexity would change the nature of the model from a low-dimensional template. The model could also be considered in parallel with the F-G model in a manner similar to that which brought together the ideas of SLIP and LLS for horizontal locomotion [75]. The incorporation of pitch dynamics using a variable-center-of-pressure method similar to work done on LLS could be applied as well [51].

6.1.2 Anchoring the SLAP Model

A method of achieving high-performance dynamic climbing would be to create a physical system that anchors the SLAP model [25], as has been done with the Full-Goldman template through the Dynoclimber system [55]. To anchor the SLAP model with the clock-driven release foot model, an early anchor could leverage controllable adhesives such as thin films of electrostatic adhesives or gripping feet on easily-grasped surfaces such as carpet or stiff wire mesh. An understanding of pitch dynamics or designing the system to be independent of pitch would be necessary. The physical anchor could then be used to explore the implementation of future control algorithms and provide feedback to the SLAP template as well as studies of dynamic behavior in animals.

6.1.3 Continued Development of Vertical Climbing

Although the minimally-actuated CLASH platform presented in Chapter 4 and Chapter 5 was able to rapidly climb challenging surfaces, improvements to climbing speed and demonstrations of climbing robustness can be better explored. Improved release of cloth would improve climbing performance and predictability. Reduced foot mass to mitigate ground reaction forces at touchdown on hard surfaces and enhancements to the gecko-inspired adhesive appear to be the most straightforward approaches to improving performance on hard, smooth surfaces. Dynamic tuning, guided by further analysis of the SLAP model, could yield climbing speed and robustness improvements while also providing further validation of the model.

6.1.4 Multimodal Systems

The ultimate goal of a highly-mobile robot is to achieve all-terrain mobility. It is well established that sagittal-plane dynamics impart efficiencies and stability to legged systems while running horizontally, and the SLAP model shows passive stability from sagittal dynamics when climbing and running on an inverted surface. Creating a system that can take advantage of such COM motions during horizontal, vertical, and even inverted locomotion would represent a large increase in performance over any current climbing robot.

6.1.5 Testing Biological Hypotheses with Robotic Platforms

The meso-scale robotic platform presented in this work is easily modified and controlled. Different legs are shown to be interchangeable on the same chassis to enable climbing on different surfaces, but the leg strokes and general morphology can also be easily changed with the SCM process leveraged in the designs presented here [38]. This makes the robot an excellent, adaptable platform for those working at the intersection of integrative biology and robotics to quickly and inexpensively test hypotheses about animal locomotion.

It is a sincere hope that the work presented in this dissertation will provide the inspiration as well as design tools and insight to lead future engineers and scientists to create the high-performance, all-terrain robotic platforms that remain just outside of our current abilities.

Bibliography

[1] R. Altendorfer, U. Saranli, H. Komsuoglu, D. Koditschek, J. Brown, H.Benjamin, M. Buehler, N. Moore, D. McMordie, and R. Full, "Evidence for Spring Loaded Inverted Pendulum Running in a Hexapod Robot," in *Experimental Robotics VII*. Springer Berlin Heidelberg, 2001, vol. 271, pp. 291–302.

[2] A. T. Asbeck, S. Kim, M. R. Cutkosky, W. R. Provancher, and M. Lanzetta, "Scaling hard vertical surfaces with compliant microspine arrays," *International Journal of Robotics Research*, vol. 25, no. 12, pp. 1165–1179, 2006.

[3] K. Autumn, S. T. Hsieh, D. M. Dudek, J. Chen, C. Chitaphan, and R. J. Full, "Dynamics of geckos running vertically," *Journal of Experimental Biology*, vol. 209, no. 2, pp. 260–272, 2006.

[4] K. Autumn, "Properties, principles, and parameters of the gecko adhesive system," in *Biological Adhesives*, A. Smith and J. Callow, Eds. Springer Berlin Heidelberg, 2006, pp. 225–256. [Online]. Available: http://dx.doi.org/10.1007/978-3-540-31049-5_12

[5] J. Berengueres, K. Tadakuma, T. Kamoi, and R. Kratz, "Compliant distributed magnetic adhesion device for wall climbing," in *IEEE International Conference on Robotics and Automation (ICRA)*, April 2007, pp. 1256 –1261.

[6] P. Birkmeyer, A. G. Gillies, and R. S. Fearing, "CLASH: Climbing vertical loose cloth," in *IEEE/RSJ International Conference on Intelligent Robots and Systems (IROS)*, Sept. 2011, pp. 5087 –5093.

[7] P. Birkmeyer, A. Gillies, and R. Fearing, "Dynamic climbing of near-vertical smooth surfaces," in *Intelligent Robots and Systems (IROS), 2012 IEEE/RSJ International Conference on*, 2012, pp. 286–292.

[8] P. Birkmeyer, K. Peterson, and R. Fearing, "DASH: A dynamic 16g hexapedal robot," in *IEEE/RSJ International Conference on Intelligent Robots and Systems (IROS)*, 2009, pp. 418–419.

[9] R. Blickhan, "The spring-mass model for running and hopping," *Journal of Biomechanics*, vol. 22, pp. pp. 1217– 1227, 1989.

[10] R. Blickhan and R. J. Full, "Similarity in multilegged locomotion: Bouncing like a monopode," *Journal of Comparative Physiology A: Neuroethology, Sensory, Neural, and Behavioral Physiology*, vol. 173, no. 5, pp. 509–517, 1993.

[11] T. Bretl, S. Rock, and J.-C. Latombe, "Motion planning for a three-limbed climbing robot in vertical natural terrain," in *IEEE International Conference on Robotics and Automation (ICRA)*, vol. 3, 2003, pp. 2946–2953.

[12] T. Bretl, S. Rock, J.-C. Latombe, B. Kennedy, and H. Aghazarian, "Free-Climbing with a Multi-Use Robot," in *International Symposium on Experimental Robotics*, 2004.

[13] L. Briones, P. Bustamante, and M. Serna, "Wall-climbing robot for inspection in nuclear power plants," in *IEEE International Conference on Robotics and Automation (ICRA)*, vol. 2, 1994, pp. 1409–1414.

[14] G. A. Cavagna, N. C. Heglund, and C. R. Taylor, "Mechanical work in terrestrial locomotion: two basic mechanisms for minimizing energy expenditure," *American Journal of Physiology - Regulatory, Integrative and Comparative Physiology*, vol. 233, no. 5, pp. R243–R261, 1977. [Online]. Available: http://ajpregu.physiology.org/content/233/5/R243.abstract

[15] J. G. Cham, S. A. Bailey, and M. R. Cutkosky, "Robust Dynamic Locomotion Through Feedforward-Preflex Interaction," in *ASME IMECE Proceedings*, November 2000.

[16] J. Clark, D. Goldman, P. Lin, G. Lynch, T. Chen, H. Komsuoglu, R. Full, and D. Koditschek, "Design of a Bio-inspired Dynamical Vertical Climbing Robot," in *Proceedings of Robotics: Science and Systems*, Atlanta, GA, USA, June 2007.

[17] J. E. Clark, D. I. Goldman, T. S. Chen, R. J. Full, and D. Koditschek, "Toward a Dynamic Vertical Climbing Robot," in *Proceedings of the 9th International Conference on Climbing and Walking Robots (CLAWAR)*, 2006.

[18] K. A. Daltorio, T. E. Wei, A. D. Horchler, L. Southard, G. D. Wile, R. D. Quinn, S. N. Gorb, and R. E. Ritzmann, "Mini-Whegs Climbs Steep Surfaces Using Insect-inspired Attachment Mechanisms," *International Journal of Robotics Research*, vol. 28, no. 2, pp. 285–302, 2009.

[19] A. Degani, H. Choset, and M. Mason, "DTAR - A Dynamic, Tube-Ascending Robot," *Robotics, IEEE Transactions on*, vol. 27, no. 2, pp. 360–364, 2011.

[20] A. Degani, H. Choset, and M. T. Mason, "DSAC - Dynamic, Single Actuated Climber: Local stability and bifurcations," in *IEEE International Conference on Robotics and Automation (ICRA)*, 2010, pp. 2803–2809.

[21] A. Degani, S. Feng, H. Brown, K. Lynch, H. Choset, and M. T. Mason, "The ParkourBot - a dynamic BowLeg climbing robot," in *IEEE International Conference on Robotics and Automation (ICRA)*, 2011, pp. 795–801.

[22] A. Frigon and S. Rossignol, "Experiments and models of sensorimotor interactions during locomotion," *Biological Cybernetics*, vol. 95, no. 6, pp. 607–627, 2006. [Online]. Available: http://dx.doi.org/10.1007/s00422-006-0129-x

[23] R. J. Full, R. Blickhan, and T. L.H., "Leg design in hexapedal runners," *Journal of Experimental Biology*, vol. 158, pp. 369–390, 1991.

[24] R. J. Full and M. Tu, "Mechanics of rapid running insects: two-, four-, and six-legged locomotion," *Journal of Experimental Biology*, vol. 156, pp. 215–231, 1991.

[25] R. Full and D. Koditschek, "Templates and anchors: neuromechanical hypotheses of legged locomotion on land," *Journal of Experimental Biology*, vol. 202, no. 23, pp. 3325–3332, 1999. [Online]. Available: http://jeb.biologists.org/content/202/23/3325.abstract

[26] H. Geyer, A. Seyfarth, and R. Blickhan, "Spring-mass running: simple approximate solution and application to gait stability," *Journal of Theoretical Biology*, vol. 232, no. 3, pp. 315 – 328, 2005. [Online]. Available: http://www.sciencedirect.com/science/article/pii/S0022519304003881

[27] R. Ghigliazza, R. Altendorfer, P. Holmes, and D. Koditschek, "A simply stabilized running model," *SIAM Journal on Applied Dynamical Systems*, vol. 2, no. 2, pp. 187–218, 2003. [Online]. Available: http://epubs.siam.org/doi/abs/10.1137/S1111111102408311

[28] D. I. Goldman, T. S. Chen, D. M. Dudek, and R. J. Full, "Dynamics of rapid vertical climbing in cockroaches reveals a template," *The Journal of Experimental Biology*, vol. 209, pp. 2990–3000, May 2006.

[29] N. Gravish, M. Wilkinson, and K. Autumn, "Frictional and elastic energy in gecko adhesive detachment." *Journal of the Royal Society, Interface*, vol. 5, no. 20, pp. 339–48, Mar. 2008.

[30] J. Guckenheimer and P. Holmes, *Nonlinear Oscillations, Dynamical Systems, and Bifurcations of Vector Fields*. New York: Springer-Verlag, 1990.

[31] D. Haldane, K. Peterson, F. G. Bermudez, and R. Fearing, "Animal-Inspired Design and Aerodynamic Stabilization of a Hexapedal Millirobot," in *IEEE International Conference on Robotics and Automation (ICRA)*, May 2013.

[32] E. W. Hawkes, J. Ulmen, N. Esparza, and M. Cutkosky, "Scaling walls: Applying dry adhesives to the real world," in *IEEE/RSJ International Conference on Intelligent Robots and Systems (IROS)*, 2011, pp. 5100–5106.

[33] E. Hawkes, E. Eason, A. Asbeck, and M. Cutkosky, "The Gecko's Toe: Scaling Directional Adhesives for Climbing Applications," *IEEE/ASME Transactions on Mechatronics*, vol. 18, no. 2, pp. 518–526, 2013.

[34] G. C. Haynes, A. Khripin, G. Lynch, J. Amory, A. Saunders, A. A. Rizzi, and D. E. Koditschek, "Rapid pole climbing with a quadrupedal robot," in *Proceedings of the IEEE International Conference on Robotics and Automation*, 2009.

[35] S. Hirose and H. Tsutsumitake, "Disk Rover: A Wall-Climbing Robot Using Permanent Magnets Disks," in *IEEE/RSJ International Conference on Intelligent Robots and Systems (IROS)*, vol. 3, 1992, pp. 2074–2079.

[36] P. Holmes, R. J. Full, D. Koditschek, and J. Guckenheimer, "The dynamics of legged locomotion: Models, analyses, and challenges," *SIAM Review*, vol. 48, no. 2, pp. 207–304, 2006.

[37] A. Hoover, S. Burden, X.-Y. Fu, S. Sastry, and R. Fearing, "Bio-inspired design and dynamic maneuverability of a minimally actuated six-legged robot," in *Biomedical Robotics and Biomechatronics (BioRob), 2010 3rd IEEE RAS and EMBS International Conference on*, Sept. 2010, pp. 869 –876.

[38] A. Hoover and R. Fearing, "Fast scale prototyping for folded millirobots," *IEEE International Conference on Robotics and Automation (ICRA)*, pp. 886–892, May 2008.

[39] A. J. Ijspeert, A. Crespi, D. Ryczko, and J.-M. Cabelguen, "From Swimming to Walking with a Salamander Robot Driven by a Spinal Cord Model," *Science*, vol. 315, no. 5817, pp. 1416–1420, 2007. [Online]. Available: http://www.sciencemag.org/content/315/5817/1416.abstract

[40] S. Jensen-Segal, S. Virost, and W. Provancher, "ROCR: Dynamic vertical wall climbing with a pendular two-link mass-shifting robot," in *IEEE International Conference on Robotics and Automation (ICRA)*, 2008, pp. 3040 –3045.

[41] M. Journee, X. Chen, J. Robertson, M. Jermy, and M. Sellier, "An investigation into improved non-contact adhesion mechanism suitable for wall climbing robotic applications," in *IEEE International Conference on Robotics and Automation (ICRA)*, 2011, pp. 4915–4920.

[42] A. Jusufi, D. I. Goldman, S. Revzen, and R. J. Full, "Active tails enhance arboreal acrobatics in geckos," *Proceedings of the National Academy of Sciences*, vol. 105, no. 11, pp. 4215–4219, 2008. [Online]. Available: http://www.pnas.org/content/105/11/4215.abstract

[43] S. Kim, A. Asbeck, M. Cutkosky, and W. Provancher, "SpinybotII: climbing hard walls with compliant microspines," July 2005, pp. 601 –606.

[44] S. Kim, J. E. Clark, and M. R. Cutkosky, "iSprawl: Design and tuning for high-speed autonomous open-loop running," *International Journal of Robotics Research*, vol. 25, no. 9, pp. 903–912, 2006.

[45] S. Kim, M. Spenko, S. Trujillo, B. Heyneman, D. Santos, and M. Cutkosky, "Smooth Vertical Surface Climbing With Directional Adhesion," *IEEE Transactions on Robotics*, vol. 24, no. 1, pp. 65 –74, Feb. 2008.

[46] J.-S. Koh and K.-J. Cho, "Omegabot: Crawling robot inspired by Ascotis Selenaria," in *IEEE International Conference on Robotics and Automation (ICRA)*, 2010, pp. 109–114.

[47] K. H. Koh, R. Kuppan Chetty, and S. G. Ponnambalam, "Modeling and Simulation of Electrostatic Adhesion for Wall Climbing Robot," in *IEEE International Conference on Robotics and Biomimetics (ROBIO)*, 2011, pp. 2031–2036.

[48] R. Kukillaya, J. Proctor, and P. Holmes, "Neuromechanical models for insect locomotion: Stability, maneuverability, and proprioceptive feedback," *Chaos: An Interdisciplinary Journal of Nonlinear Science*, vol. 19, no. 2, p. 026107, 2009. [Online]. Available: http://link.aip.org/link/?CHA/19/026107/1

[49] A. D. Kuo, J. M. Donelan, and A. Ruina, "Energetic consequences of walking like an inverted pendulum: Step-to-step transitions," in *Exercise and Sport Sciences Reviews*, vol. 33, 2005, pp. 88–97.

[50] M. K. Kwak, C. Pang, H.-E. Jeong, H.-N. Kim, H. Yoon, H.-S. Jung, and K.-Y. Suh, "Towards the Next Level of Bioinspired Dry Adhesives: New Designs and Applications," *Advanced Functional Materials*, vol. 21, no. 19, pp. 3606–3616, Oct. 2011. [Online]. Available: http://doi.wiley.com/10.1002/adfm.201100982

[51] J. Lee, A. Lamperski, J. Schmitt, and N. Cowan, *Task-Level Control of the Lateral Leg Spring Model of Cockroach Locomotion*, ser. Lecture Notes in Control and Information Sciences. Springer Berlin / Heidelberg, 2006, vol. 340.

[52] J. Lee, R. S. Fearing, and K. Komvopoulos, "Directional adhesion of gecko-inspired angled microfiber arrays," *Applied Physics Letters*, vol. 93, no. 19, pp. 191 910 –191 910–3, nov. 2008.

[53] J. Lee, C. Majidi, B. Schubert, and R. S. Fearing, "Sliding-induced adhesion of stiff polymer microfibre arrays. I. Macroscale behaviour." *Journal of the Royal Society, Interface*, vol. 5, no. 25, pp. 835–44, Aug. 2008. [Online]. Available: http://rsif.royalsocietypublishing.org/cgi/content/abstract/5/25/835

[54] G. Lynch, J. Clark, and D. Koditschek, "A self-exciting controller for high-speed vertical running," in *IEEE/RSJ International Conference on Intelligent Robots and Systems*, October 2009, pp. 631–638.

[55] G. Lynch, "Dynamic Vertical Climbing: Bioinspiration, Design, and Analysis," Ph.D. dissertation, University of Pennsylvania, 2011.

[56] C. McKenzie and A. Parness, "Video summary of D.R.O.P. the Durable Reconnaissance and Observation Platform," in *IEEE International Conference on Robotics and Automation (ICRA)*, 2012, pp. 3535–3536.

[57] B. Miller, J. Schmitt, and J. E. Clark, "Quantifying disturbance rejection of SLIP-like running systems," *The International Journal of Robotics Research*, 2012. [Online]. Available: http://ijr.sagepub.com/content/early/2012/03/27/0278364912439613.abstract

[58] J. M. Morrey, B. Lambrecht, A. D. Horchler, R. E. Ritzmann, and R. D. Quinn, "Highly mobile and robust small quadruped robot," in *Proceedings of the 2003 IEEE/RSJ International Conference on Intelligent Robots and Systems, Las Vegas, NV*, 2003, pp. 82–87.

[59] M. P. Murphy, C. Kute, Y. Menguc, and M. Sitti, "Waalbot II: Adhesion recovery and improved performance of a climbing robot using fibrillar adhesives," *The International Journal of Robotics Research*, vol. 30, no. 1, pp. 118–133, 2011. [Online]. Available: http://ijr.sagepub.com/content/30/1/118

[60] A. Parness, M. Frost, N. Thatte, and J. King, "Gravity-independent mobility and drilling on natural rock using microspines," in *IEEE International Conference on Robotics and Automation (ICRA)*, 2012, pp. 3437–3442.

[61] A. Parness, D. Soto, N. Esparza, N. Gravish, M. Wilkinson, K. Autumn, and M. Cutkosky, "A microfabricated wedge-shaped adhesive array displaying gecko-like dynamic adhesion, directionality and long lifetime." *Journal of the Royal Society, Interface*, vol. 6, no. 41, pp. 1223–32, Dec. 2009. [Online]. Available: http://rsif.royalsocietypublishing.org/cgi/content/abstract/rsif.2009.0048v1

[62] K. Peterson, "Running with flapping wings," Master's thesis, EECS Department, University of California, Berkeley, May 2010. [Online]. Available: http://www.eecs.berkeley.edu/Pubs/TechRpts/2010/EECS-2010-76.html

[63] H. Prahlad, R. Pelrine, S. Stanford, J. Marlow, and R. Kornbluh, "Electroadhesive robots - wall climbing robots enabled by a novel, robust, and electrically controllable adhesion technology," in *IEEE International Conference on Robotics and Automation (ICRA)*, 2008, pp. 3028–3033.

[64] W. R. Provancher, J. E. Clark, B. Geisler, and M. R. Cutkosky, "Towards Penetration-Based Clawed Climbing," in *Proceedings of the International Conference on Climbing and Walking Robots (CLAWAR)*, 2004.

[65] W. Provancher, S. Jensen-Segal, and M. Fehlberg, "ROCR: An Energy-Efficient Dynamic Wall-Climbing Robot," *Mechatronics, IEEE/ASME Transactions on*, vol. 16, no. 5, pp. 897–906, 2011.

[66] F. Qian, T. Zhang, chen Li, A. Hoover, P. Masarati, P. Birkmeyer, A. Pullin, R. Fearing, and D. Goldman, "Walking and running on yielding and fluidizing ground," in *Proceedings of Robotics: Science and Systems*, Sydney, Australia, July 2012.

[67] L. Righetti and A. Ijspeert, "Pattern generators with sensory feedback for the control of quadruped locomotion," in *IEEE International Conference on Robotics and Automation (ICRA)*, 2008, pp. 819–824.

[68] G. L. Rosa, M. Messina, G. Muscato, and R. Sinatra, "A low-cost lightweight climbing robot for the inspection of vertical surfaces," *Mechatronics*, vol. 12, no. 1, pp. 71 – 96, 2002. [Online]. Available: http://www.sciencedirect.com/science/article/pii/S0957415800000465

[69] U. Saranli, M. Buehler, and D. E. Koditschek, "RHex: A simple and highly mobile hexapod robot," *International Journal of Robotics Research*, vol. 20, no. 7, pp. 616 – 631, July 2001.

[70] J. Schmitt and S. Bonnono, "Dynamics and stability of lateral plane locomotion on inclines," *Journal of Theoretical Biology*, vol. 261, no. 4, pp. 598 – 609, 2009. [Online]. Available: http://www.sciencedirect.com/science/article/B6WMD-4X2DD79-4/2/fa73720938da5af21f577b31681d1f95

[71] J. Schmitt and P. Holmes, "Mechanical Models for insect locomotion: dynamics and stability in the horizontal plane II. Application," *Biol. Cybern.*, vol. 83, no. 6, pp. 517–527, 2000.

[72] J. Schmitt and P. J. Holmes, "Mechanical Models for insect locomotion: dynamics and stability in the horizontal plane I. Theory," *Biol. Cybern.*, vol. 83, no. 6, pp. 501–515, 2000.

[73] J. Seipel and P. Holmes, "A simple model for clock-actuated legged locomotion," *Regular and Chaotic Dynamics*, vol. 12, no. 5, pp. 502–520, 2007. [Online]. Available: http://dx.doi.org/10.1134/S1560354707050048

[74] J. Seipel and P. J. Holmes, "Three-dimensional Translational Dynamics and Stability of Multi-legged Runners," *The International Journal of Robotics Research*, vol. 25, no. 9, pp. 889–902, 2006. [Online]. Available: http://ijr.sagepub.com/content/25/9/889.abstract

[75] J. E. Seipel and P. Holmes, "Running in Three Dimensions: Analysis of a Point-mass Sprung-leg Model," *The International Journal of Robotics Research*, vol. 24, no. 8, pp. 657–674, 2005. [Online]. Available: http://ijr.sagepub.com/content/24/8/657.abstract

[76] J. E. Seipel, P. J. Holmes, and R. J. Full, "Dynamics and stability of insect locomotion: a hexapedal model for horizontal plane motions," *Biol. Cybern.*, vol. 91, no. 2, pp. 76–90, 2004.

[77] A. Seyfarth, H. Geyer, M. Günther, and R. Blickhan, "A movement criterion for running," *Journal of Biomechanics*, vol. 35, pp. 649–655, 2002.

[78] M. Sitti, "High aspect ratio polymer micro/nano-structure manufacturing using nanoembossing, nanomolding and directed self-assembly," in *IEEE/ASME International Conference on Advanced Intelligent Mechatronics (AIM)*, vol. 2. IEEE, 2003, pp. 886–890. [Online]. Available: http://ieeexplore.ieee.org/xpl/articleDetails.jsp?arnumber=1225459

[79] M. J. Spenko, G. C. Haynes, J. A. Saunders, M. R. Cutkosky, A. A. Rizzi, R. J. Full, and D. E. Koditschek, "Biologically inspired climbing with a hexapedal robot," *Journal of Field Robotics*, vol. 25, no. 4-5, pp. 223–242, 2008.

[80] E. E. Steltz, "Redesign of the micromechanical flying insect in a power density context," Ph.D. dissertation, EECS Department, University of California, Berkeley, May 2008.

[81] Y. Tian, N. Pesika, H. Zeng, K. Rosenberg, B. Zhao, P. McGuiggan, K. Autumn, and J. Israelachvili, "Adhesion and friction in gecko toe attachment and detachment," *Proceedings of the National Academy of Sciences*, vol. 103, no. 51, pp. 19 320–19 325, 2006. [Online]. Available: http://www.pnas.org/content/103/51/19320.abstract

[82] O. Unver, A. Uneri, A. Aydemir, and M. Sitti, "Geckobot: a gecko inspired climbing robot using elastomer adhesives," in *IEEE International Conference on Robotics and Automation (ICRA)*, 2006, pp. 2329–2335.

[83] M. Varenberg, A. Peressadko, S. N. Gorb, E. Arzt, and S. Mrotzek, "Advanced testing of adhesion and friction with a microtribometer," *Review of Scientific Instruments*, vol. 77, no. 6, p. 066105, 2006. [Online]. Available: http://link.aip.org/link/?RSI/77/066105/1

[84] N. Wiltsie, M. Lanzetta, and K. Iagnemma, "A controllably adhesive climbing robot using magnetorheological fluid," in *IEEE International Conference on Technologies for Practical Robot Applications (TePRA)*, 2012, pp. 91–96.

[85] R. Wood, S. Avadhanula, R. Sahai, E. Steltz, and R. Fearing, "Microrobot design using fiber reinforced composites," *Journal of Mechanical Design*, vol. 130, p. 052304, 2008.

[86] A. Yamamoto, T. Nakashima, and T. Higuchi, "Wall-Climbing Mechanisms Using Electrostatic Attraction Generated by Flexible Electrodes," in *International Symposium on Micro-NanoMechatronics and Human Science*, 2007, pp. 389–394.

[87] G. Zong, X. Pei, J. Yu, and S. Bi, "Classification and type synthesis of 1-DOF remote center of motion mechanisms," *Mechanism and Machine Theory*, vol. 43, no. 12, pp. 1585 – 1595, 2008. [Online]. Available: http://www.sciencedirect.com/science/article/pii/S0094114X08000050

Appendix A

Magnetic Climbing

Magnetic feet simplify engagement and allow CLASH to rapidly climb a vertical surface to study climbing dynamics and the effects of kinematics and transmission design on the dynamics. It was previously shown that the SCM transmissions of robots such as CLASH and DASH contribute significant forces on the body while climbing and thus have significant impact on body dynamics [6, 62].

The magnet foot design is similar to that seen in [5], with six 0.012 g 3 mm diameter neodymium magnets oriented in a hexagonal pattern within a rubber flap. This is attached on the front edge of the foot to create a peeling motion during liftoff. The hexagonal pattern has a single magnet near the base of the flap; when the peel begins, it must overcome the attractive force of a single magnet, resulting in a smoother peel [5]. The peeling crack propagates along the flap until it terminates with a single magnet. This minimizes the final pull-off force and the impulse associated with the final release of the foot. Because a magnet does not have the controllable shear-induced normal adhesion exhibited by the gecko-inspired synthetic adhesive, the peeling release reduces the instantaneous pull-off force to keep the total normal load under the available adhesion.

Unlike the gecko-inspired adhesive foot, the magnetic foot is designed to be planar. Thus, the RCM ankle is not necessary for this foot and instead has a revolute joint designed within the plane of the foot. The magnetic foot is designed to use the parallel four-bar leg design seen in Figure 5.2.

For the magnetic foot trials, the robot was equipped with four magnetic feet on the front and middle legs and non-magnetic frictional feet on the rear legs. In these trials, CLASH was able to climb vertical surfaces at 18 centimeters second^{-1} with stride frequencies between 5 or 6 Hz (Figure A.2), making it the fastest legged climbing robot relative to body length. At higher frequencies, the body dynamics cause one of the magnetic feet to peel prematurely, causing the robot to roll about foot still in contact, which prevents future touchdowns and leads to complete loss of contact. With these feet, CLASH is also able to climb up the underside of a magnetic surface inclined at 60 degrees above horizontal (Figure A.3).

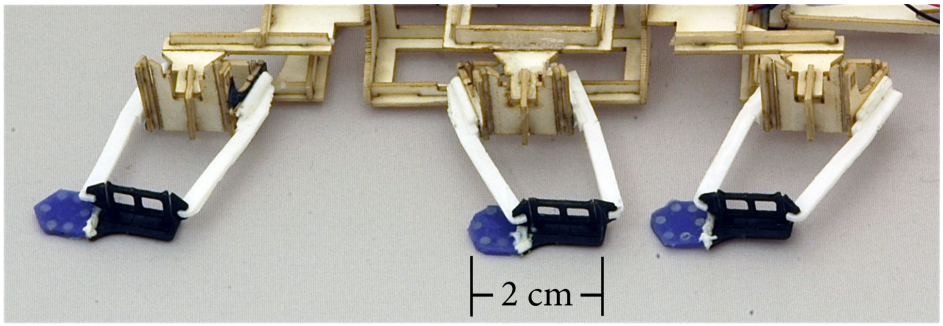

Figure A.1: Closeup of magnet feet on CLASH.

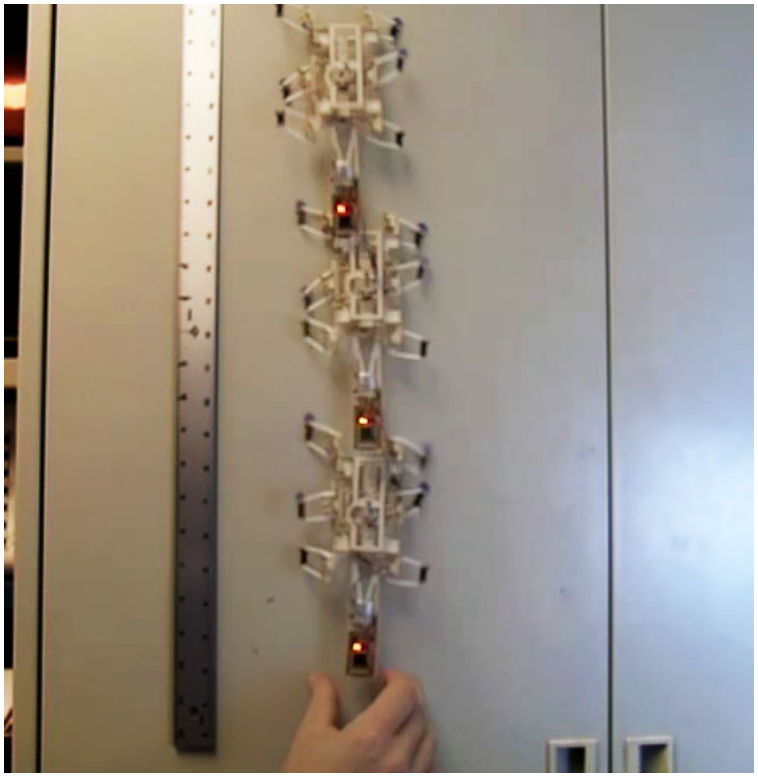

Figure A.2: Superimposed frames of CLASH climbing a vertical metal cabinet at 18 cm second $^{-1}$.

(a) t = 0s

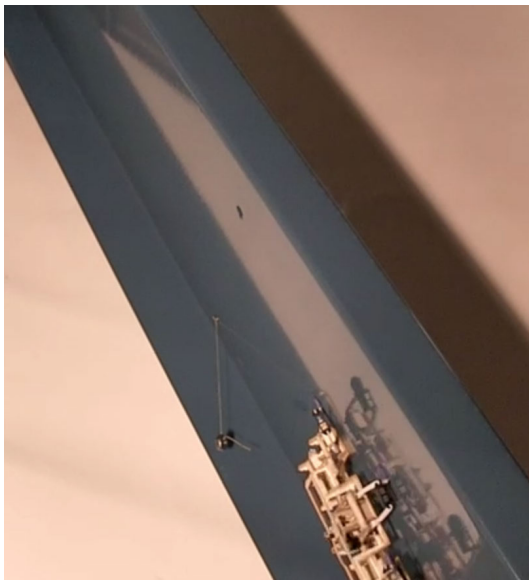

(b) t = 2.27s

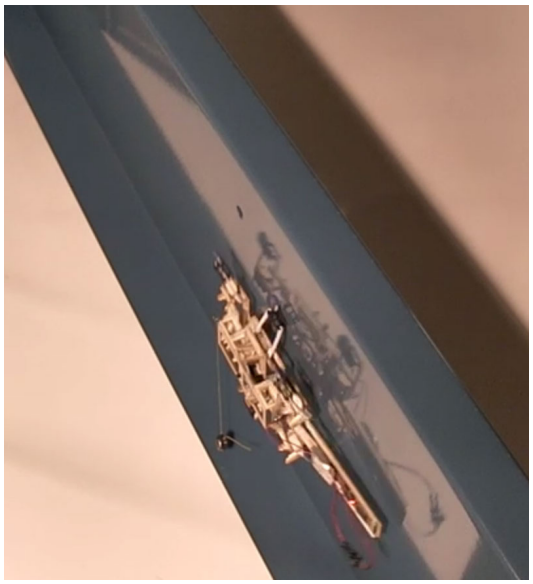

(c) t = 4.63s

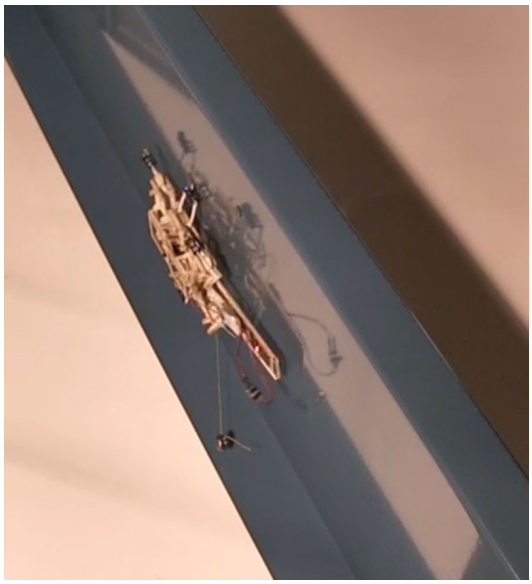

(d) t = 7.2s

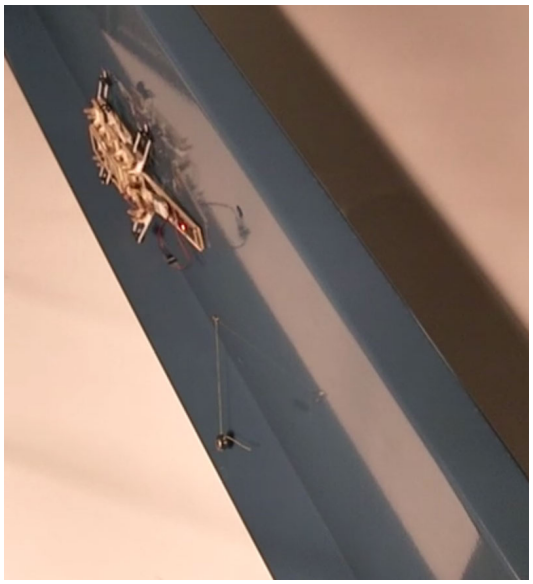

Figure A.3: A sequence of frames from a video showing CLASH climbing an inverted metal surface 60° above horizontal using the magnetic feet.